UNIVERSITÀ DEGLI STUDI DI PALERMO

Dottorato Internazionale in Fisica Applicata
Dipartimento di Fisica e Chimica
Settore Scientifico Disciplinare FIS/03

DISSIPATIVE DYNAMICS OF MULTI-STATE BISTABLE QUANTUM SYSTEMS

DINAMICA DISSIPATIVA DI SISTEMI QUANTISTICI BISTABILI A MOLTI STATI

DOTTORE
Luca Magazzù

COORDINATORE
Prof. Bernardo Spagnolo

TUTOR
Dott. Davide Valenti

CO TUTOR
Prof. Alexander A. Dubkov
Prof. Gennady. F. Efremov

CICLO XXV
ANNO CONSEGUIMENTO TITOLO 2015

UNIVERSITÀ DEGLI STUDI DI PALERMO

Contents

Chapter 1

Introduction

Every physical system S that we study as an individual entity is usually just a sufficiently isolated part of a larger *universe* which we divide, more or less arbitrarily, into the system S itself and the remaining part, the so-called environment E. The fact that these two parts interact is at the basis of the phenomenon of *dissipation* affecting S. The archetypical model of dissipation is the damped harmonic oscillator in which S is a point mass which loses its initial energy due to the friction exerted by the surrounding environment. The effect of the environment is introduced through a viscous term, proportional to the velocity $\dot{x}$ of the particle, in the differential equation describing the point mass dynamics

$$M\ddot{x}(t) + kx(t) + \gamma\dot{x}(t) = 0,$$

where γ is the damping coefficient.

There are limiting cases, as for example that of a heavy body moving in absence of external atmosphere, where the dissipative effects of the surrounding environment (other objects in contact with the body, the electromagnetic field etc.) can be safely neglected for all practical purposes. However in general this is not the case. For example, in the opposite limit of a very light classical particle suspended in a fluid, the mere introduction of a viscous term in the Newton equation is not sufficient to account for the particle's motion. As the particle is sufficiently light to be sensitive to the collisions with the individual constituents of its environment, the granular nature of the fluid emerges and the particle's trajectory manifest itself as a random process. The description of such a motion can only be given statistically, unless one keeps track of the individual degrees of freedom of the environment. The behavior of the suspended particle is called Brownian motion. In the one-dimensional case it is mathematically described by the Langevin *stochastic* differential equation [1]

$$M\ddot{x}(t) + \gamma\dot{x}(t) = \xi(t). \tag{1.1}$$

The term $\xi(t)$ is a stochastic force modeling a delta correlated noise source i.e. $\langle\xi(t)\rangle = 0$ and $\langle\xi(t)\xi(t')\rangle = 2\gamma k_B T\delta(t-t')$.

If we consider a quantum system, the presence of a dissipative environment has even deeper consequences in that, not only implies the relaxation to equilibrium, but also prevents the assignment of a well defined quantum state to the system once it has become entangled with the environment. Indeed, even if we require that at a certain initial time t_0 S and E are uncorrelated, at a successive time t the overall state of $S + E$ will be

non-separable or *entangled*. Mathematically this is expressed by

$$|\Psi(t_0)\rangle = |\psi^S\rangle|\phi^E\rangle \quad \rightarrow \quad |\Psi(t)\rangle = \sum_{i,j} c_{ij}|i^S\rangle|j^E\rangle, \tag{1.2}$$

where $|\psi^S\rangle = \sum_i a_i|i^S\rangle$, in some basis $\{|i\rangle\}$ of the Hilbert space of S.

It follows that the trace over the environmental degrees of freedom of the full density matrix $\rho(t) = |\Psi(t)\rangle\langle\Psi(t)|$ gives a mixed reduced density matrix for S, which means that we can describe the state of S only as a probabilistic mixture of quantum states, with probability p_i associated to the outcome A_i in a measurement of the observable $\hat{A}$, such that $\hat{A}|i\rangle = A_i|i\rangle$ [2]. Tracing out the environment, the reduced density matrix of the system S describes the mixed state

$$\rho^S(t) = Tr_E\{\rho(t)\} = \sum_i p_i|i^S\rangle\langle i^S|. \tag{1.3}$$

This is because, in taking the trace over E, we discard an essential part of the information about the quantum state of the global system $S + E$ which has become a unique system described by the overall density matrix $\rho(t) = |\Psi(t)\rangle\langle\Psi(t)|$, with $|\Psi(t)\rangle$ given by Eq. (1.2).

The entanglement between S and E is at the basis of the *decoherence*, a peculiar feature of dissipation in Quantum Mechanics, which consist in the loss of the relative phases in the superposition of basis states defining a specific quantum state of S. This can be seen by comparing the initial state $|\psi^S\rangle$ of S with the mixture weighted by classical probabilities given by Eq. (1.3)

Every quantum mechanical system is subject to the interaction with the surrounding environment. The very act of observing the system, however protected from the uncontrolled degrees of freedom of a noisy environment, perturbs it as implies the interaction with a large *classical* system which is the measurement apparatus.

A large system, such as the measurement apparatus or uncontrolled noisy environment, is ultimately made by its microscopic constituents which obey the quantum mechanical laws. The way the classical behavior emerges from a large ensemble of quantum object constituting the ordinary classical systems is a problem of the foundations of Quantum Mechanics which has been and is still actively investigated [3–6].

However, independently of these interpretational issues, the interaction of a system S with a large, even macroscopic, environment can always be understood as the sum of the contributions of the interactions between S and a multitude of microscopic quantum objects. This observation make it possible to formulate the problem of the dissipation in quantum mechanics in terms of the Hamiltonian formalism by considering the unitary evolution of the global *closed* system and tracing out the environment degrees of freedom, as shown above.

The predictions obtained by taking into account the quantum nature of dissipation coincide with those of classical mechanics only in the limit $\hbar \rightarrow 0$ (i.e. high temperature) and differ substantially whereas the quantum effects cannot be neglected [7–9].

1.1 Quantum systems for computation

The field of quantum hardware for computation is an area of investigation where much theoretical and experimental effort has been devoted in studying and limiting the detrimental effects of dissipation.

The idea of quantum computation can be traced back to the end of the fifties when Richard Feynman had the intuition that the use of hardware obeying the laws of Quantum Mechanics would have a potential beyond the possibilities of "classical" hardware[1].

It soon became clear that quantum hardware could open new possibilities in information processing and simulation of quantum mechanical systems. Indeed, using classical machines, tasks like the simulation of quantum systems present formidable difficulties even for quite small systems and turns out to be hopeless as soon as the number of degrees of freedom becomes moderately large ($N \sim 100$), not to speak of macroscopic many body ensembles.

At the basis of the exorbitant amount of resources required for a classical computer to simulate a many body quantum system is the fact that the system's Hilbert space grows exponentially with the number of degrees of freedom involved. On the other hand, this the reason underlying the potential of quantum mechanical systems as computation resources.

The elementary unit of information that can be stored in a quantum system is called the quantum bit or *qubit*. It differs from the classical bit in that, while the latter can be in one of the two mutually exclusive states 0 or 1, a qubit can be in one of an infinite number of states given by the superposition of the two classical states. Specifically a qubit state is the state of a two-state quantum system (without any reference to its practical realization) whose Hilbert space is spanned by the *computational* basis set which we denote by $\{|0\rangle, |1\rangle\}$

$$|\psi\rangle = c_0|0\rangle + c_1|1\rangle, \tag{1.4}$$

where $|c_0|^2 + |c_1|^2 = 1$ [2, 10]. So, the specification of a qubit state requires two complex numbers with the constraint of probability conservation and up to an irrelevant global phase factor, which amounts to two real numbers that can be identified with the angles defining a point on the surface of a unit sphere called *Bloch sphere*. In principle an infinite amount of information can be encoded for example in the relative phase between the two orthogonal basis states of a single qubit [11], but this doesn't work in practice because it would require an infinite precision in writing or reading the information.

In passing from one qubit to multiple qubit states the wired features of quantum mechanics become evident. The Hilbert space of a two qubit system has dimension four and a generic state can be written as

$$|\psi\rangle = c_{00}|00\rangle + c_{01}|01\rangle + c_{10}|10\rangle + c_{11}|11\rangle \tag{1.5}$$

Take for example the so-called Bell state

$$|\psi\rangle = \frac{1}{\sqrt{2}}\left(|00\rangle + |11\rangle\right).$$

This entangled state state has the nonlocal feature that if we measure the first qubit and we obtain $|0\rangle$ ($|1\rangle$), a measure on the second qubit will give with certainty the result $|0\rangle$ ($|1\rangle$), even if the measurements are two space-like separated events.

A N-qubit state in the computational basis reads

$$|\psi\rangle = \sum_{i=1}^{2^N} c_i|x_i\rangle, \tag{1.6}$$

[1] Richard Feynman talk "There is plenty of room at the bottom", 1959.

where $|x_i\rangle$ is a state of the computational basis of the N qubit Hilbert space. The number of amplitudes required to specify the state of Eq. (1.6) is 2^N. This means that it is impossible to store in any conceivable classical device the information required to define a N qubit state as $N \sim 100$, which explains the impossibility to simulate large quantum system with classical computer, as discussed above. However, an ensemble of N two-level quantum system can be realized and prepared in an arbitrary state, in principle even for large N. Moreover the linearity of Quantum Mechanics can be exploited to perform operations on the quantum superposition defining the state in Eq. (1.6), which amounts to perform the operation on each of the basis states $|x_i\rangle$ at the same time. This feature, named *quantum parallelism*, produces the speedup theoretically allowing quantum computers to perform tasks which are out of the reach of classical computers. An example is the factorization of large numbers using the Shor algorithm [12].

Every practical realization of quantum computing has to satisfy a number of criteria [13] which include scalability (the possibility to build large scale system) and a coherence time larger than that required to perform the operations (the quantum gates) and to perform error correcting protocols [14].

In one of the first realizations the qubits are nuclear spins of molecules in a magnetic field, manipulated using nuclear magnetic resonance techniques (liquid-state NMR) [15]. By this technique a twelve qubit system has been demonstrated [16], but liquid-state NMR presents scalability problems due to the difficulties in distinguishing singular spin when the size of the system grows [17].

Other physical realizations include trapped ions [18], in which the information is encoded in some internal degree of freedom of the ion or in collective motional degrees of freedom of an ensemble of ions, quantum dots, which are solid state systems with electrons or holes trapped in potential wells with discrete energy levels [19], atoms in cavity QED [20] and photons in circuits with linear optical elements [21].

1.1.1 Superconducting qubits

Superconducting qubits represent a viable technology for the realization of quantum computing systems [17, 22–30] and for the simulation of quantum systems (e.g. atoms) in a controlled fashion [31]. The key element of superconducting circuits is the Josephson junction, consisting in a thin layer of insulator between two superconducting electrodes. This element introduces the nonlinearity necessary for obtaining non-equally spaced energy levels, so that a couple of levels (usually the two lowest) with a well defined and unique transition frequency can be isolated and associated to the computational basis of the qubit. The supercurrent tunnels across the junction and a phase difference φ is associated to the collective wave function of the Cooper pairs on the two sides of the junction $\psi(x,t) = |\psi(x,t)| \exp(i\varphi(x,t))$. The phase φ is related to the potential energy of the junction by

$$V(\varphi) = -E_J(\cos\varphi - 1).$$

The Josephson energy E_j is defined by $E_j = \Phi_0 I_J$, where I_J is the critical current and the quantity $\Phi_0 = \hbar/2e$ is the flux quantum. The quantization of the magnetic flux in the superconducting circuit derives from the requirement that the wave function ψ be single-valued.

The Hamiltonian of the Josephson junction, with the charge Q in the capacitance C_J associated to the junction and the phase φ promoted to (canonically conjugate) operators

$([\hat{\varphi}, \hat{Q}/2e] = i)$, reads

$$\hat{H} = \frac{\hat{Q}^2}{2C_J} - E_j \cos\hat{\varphi}.$$

The Josephson relation is obtained by the Heisenberg equation of motion $\dot{\hat{\varphi}} = i[\hat{H}, \hat{\varphi}]/\hbar$

$$\frac{d\hat{\varphi}}{dt} = \frac{\hat{Q}}{\Phi_0 C_J}$$

Similarly we get, for the current/phase relation of the junction, the equation

$$\frac{d\hat{Q}}{dt} = \frac{E_J}{\Phi_0} \sin\hat{\varphi}.$$

A superconducting qubit can be in a variety of configurations corresponding to different circuit designs. There are three basic configurations, according to which couple of variable is chosen as the conjugate dynamical variables: the charge qubit, the phase qubit and the flux qubit (see Fig. 1.1). There are in addition a variety of hybrid configurations. Here

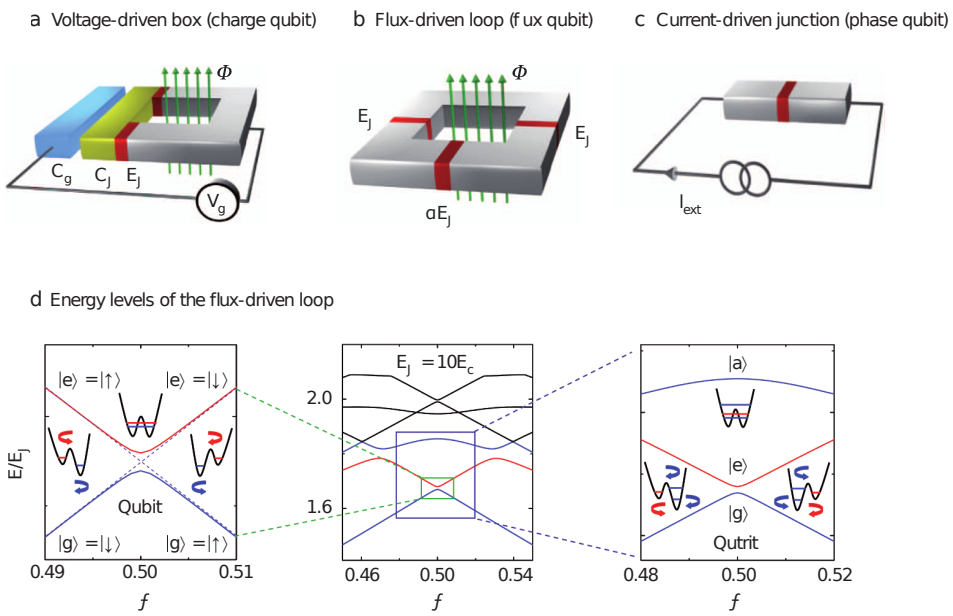

Figure 1.1: $(a$ - $c)$ The three basic realizations of superconducting qubits. The Josephson junctions are indicated by the red stripes. Notice that in the flux qubit (panel (b)) there are two identical junctions with energy E_j and a third with energy αE_j. (d) Energy levels of the flux qubit as functions of the applied bias flux f (figure from J. You and F. Nori, Nature **474**, 589 (2011)).

we consider in some detail only the flux qubit. The flux qubit Hamiltonian is

$$\hat{H} = \frac{\hat{Q}^2}{2C_J} + \frac{\hat{\Phi}^2}{2L} - E_J \cos\left[\frac{\hat{\Phi}}{\Phi_0} - \frac{\Phi_{\rm ext}}{\Phi_0}\right], \tag{1.7}$$

where $\Phi_{\rm ext}$ is an external control flux and L is the ring inductance. Notice that the external flux acts as a bias, the potential being symmetric for $\Phi_{\rm ext} = \Phi_0/2$.

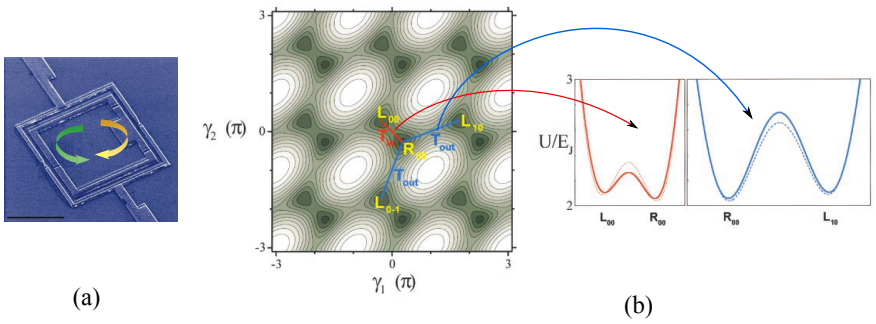

Figure 1.2: (*a*) Actual configuration of a three junction flux qubit. The arrows indicate the two opposite directions of the circulating supercurrent, giving the $|L/R\rangle$ states (figure from J. Clarke and F. K. Wilhelm, Nature **453**, 1031 (2008)). (*b*) Potential energy as a function of the two gauge invariant phases across the identical Josephson junctions and potential energy along the red and blue trajectories. The phase at the remaining junction is fixed by the requirement of ψ being single valued (figure from J. Mooij et al., Science **285**, 1036 (1999)).

In terms of the energy eigenstates $|g\rangle$ and $|e\rangle$, the ground state and the first excited state given by the Hamiltonian in Eq. (1.7), the *localized basis* $|R/L\rangle$, which is the basis of states localized in one of the two wells, reads

$$\begin{aligned} |R\rangle &= \cos\frac{\phi}{2}|g\rangle + \sin\frac{\phi}{2}|e\rangle \\ |L\rangle &= \sin\frac{\phi}{2}|g\rangle - \cos\frac{\phi}{2}|e\rangle, \end{aligned} \tag{1.8}$$

where ϕ depends on the control parameter Φ_{ext}. In particular, for zero bias one has $\phi = \pi/2$ and Eq. (1.8) becomes $|R/L\rangle = (|g\rangle \pm |e\rangle)/\sqrt{2}$. In this basis, using the Pauli spin matrices $\sigma_z = |R\rangle\langle R| - |L\rangle\langle L|$ and $\sigma_x = |R\rangle\langle L| + |L\rangle\langle R|$, the qubit Hamiltonian can be written as

$$\hat{H} = -\frac{\hbar}{2}(\Delta\sigma_x + \epsilon\sigma_z). \tag{1.9}$$

The frequency Δ is called *tunneling element* and ϵ the *bias*. Diagonalizing the Hamiltonian of Eq. (1.9) one finds $\tan(\phi) = \Delta/\epsilon$. In Fig. 1.3 is depicted the potential in the biased case with energy levels, tunneling element and bias factor. In the working regime the system can transfer its state from an anti-clockwise circulating current state $|L\rangle$ to a clockwise one $|R\rangle$, by tunneling through the effective potential barrier. This phenomenon takes the name of *macroscopic quantum tunneling* (MQT). The quantum state of the qubit can be a superposition of the two above current states as, for example, $|g\rangle$ or $|e\rangle$.

A major obstacle to the realization of quantum operations is constituted by the environmental noise sources causing the loss of quantum coherence and, on larger time scales, the system relaxation. To these processes are associated two characteristic times, the relaxation time T_1 and the decoherence time T_2.

The theoretical modeling of the dissipative qubit dynamics is based on the introduction of an Hamiltonian in an enlarged Hilbert space, which includes, along with the qubit Hamiltonian of Eq. (1.9), a reservoir of harmonic oscillators linearly interacting with the

system, modeling the quantum noise source, and a classical noise source of $1/f$ noise [32, 33]. This last noise source is attributable to the impurities present in the junctions, behaving as effective two-level systems, and represent a serious limitation on the system's coherence. However, in the following we limit to the study of the quantum noise only, as it represents an ubiquitous dissipation mechanism in a variety of quantum system, both natural and manufactured.

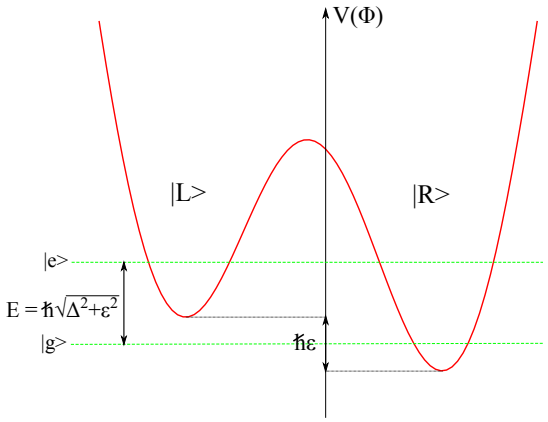

Figure 1.3: Potential energy as a function of the flux threading the superconducting loop realizing the flux qubit. The localized states $|R/L\rangle$ are given by Eq. (1.8) and are associated to the current moving in the anti-clockwise and clockwise directions.

1.1.2 Single-molecule magnets

Another class of physical systems displaying quantum tunneling dynamics at low temperature is that of single-molecule magnets (SMM), hi-spin molecules ($s = 10$) in which the total spin tunnels through an effective potential barrier due to the molecular field creating two states of opposite spin, which we can indicate as $|\downarrow\rangle$ and $|\uparrow\rangle$. Their state can be manipulated by an external applied magnetic field [34–36]. Their slow relaxation time at the temperature of few K makes these composites suitable as hi density storage devices and possible resources for classical and quantum computing [37, 38]. Indeed quantum coherence has been recently demonstrated in Fe_8 single-molecule magnets with coherence time of ~ 700 ns at $T = 1.3\ K$ [39].

The effective Hamiltonian of the system can be put in the form [36]

$$\hat{H} = \hat{H}' - D\hat{S}_z^2 - A\hat{S}_z^4 - g_z\mu_B H_z \hat{S}_z \tag{1.10}$$

where the last three terms are a quartic potential in the spin variable $\hat{S}_z$ with asymmetry given by the external (magnetic) bias field H_z and $[\hat{S}_z, \hat{H}'] \neq 0$.

Performing a sweep with the magnetic field H_z from negative to positive values, the magnetization shows an hysteresis loop with steps corresponding to the resonant tunneling, occurring as the couples of energy levels associated to the potential become nearly degenerate. In figure 1.4 is shown the potential in the unbiased and biased case, with tunneling transitions occurring via the levels indicated by arrows, and energy levels as functions of the external bias.

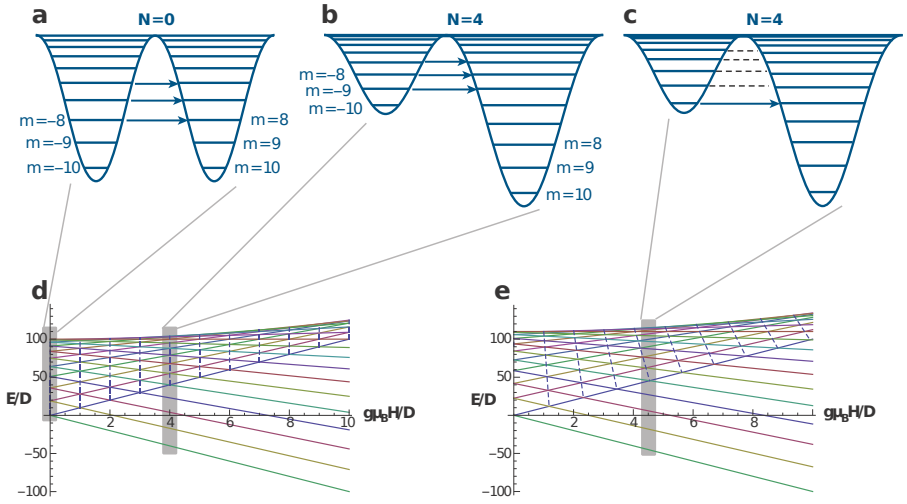

Figure 1.4: (a) Potential with zero bias and energy levels associated to the spin projections. Biased case without (b) and with (c) the fourth order term in the Hamiltonian Eq. (1.10). Tunneling transitions indicated by arrows. $N = 4$ refers to the step in the hysteresis loop at a certain temperature for a given (positive) external field H_z. (d) Energies of the spin operator eigenstates as a function of the external field without and (e) with the quartic term in the Hamiltonian. In the latter case at different field strength different couples of levels are in resonance (figure from J. R. Friedman and M. P. Sarachik, Annu. Rev. Condens. Matter Phys. **1**, 109 (2010)).

The SMM are another example of dissipative quantum system with an environment at a certain temperature, which can be modeled as a reservoir with degrees of freedom linearly interacting with the system.

1.2 Caldeira-Leggett model of dissipation in quantum mechanics

The model of dissipation considered throughout this thesis is the so-called Caldeira-Leggett model [40–42]. It allows for a *microscopic* derivation of dissipation which emerges once we consider the reduced dynamics of the system in interaction with the environment. This is in contrast with the classical case, where noise terms whose statistical properties are fixed a priori, are phenomenologically introduced into the dynamical equations.

The system, a particle of mass M and coordinates $\hat{q}$ and $\hat{p}$ subject to a potential V_0, is linearly coupled to the environment, a reservoir of N independent quantum harmonic oscillators of masses m_j, frequencies ω_j and coordinates $\hat{x}_j$ and $\hat{p}_j$. The reservoir is also called, in the thermodynamical limit $N \to \infty$, bosonic *heat bath* (bosonic since its excitations obey the Bose statistics).

The full Hamiltonian is the sum of a free system term, a free reservoir term and a

system-reservoir interaction term

$$\begin{aligned}\hat{H} =&\hat{H}_S + \hat{H}_R + \hat{H}_I \\ =&\frac{\hat{p}^2}{2M} + V_0(\hat{q}) + \sum_{j=1}^{N} \frac{1}{2}\left[\frac{\hat{p}_j^2}{m_j} + m_j\omega_j^2\hat{x}_j^2\right] - \sum_{j=1}^{N} c_j\hat{x}_j\hat{q}\end{aligned} \tag{1.11}$$

The interaction of the particle with the individual degrees of freedom of the bath is defined by the set of constants c_j and is proportional to the inverse of the reservoir's volume [9]. Thus, for a macroscopic environment, the coupling with the individual oscillators is weak, which justifies the linear coupling assumption. As a consequence we can consider the bare system energy levels unaffected by the reservoir. The collective effect of the reservoir on the system level structure can be assumed to be a *frictional level broadening*. Nevertheless, since the number of degrees of freedom coupled to the system is very large for a macroscopic reservoir, such as that surrounding a superconducting device [40], the overall effective system-bath coupling can be strong (see Sec. 1.4.1).

The effective potential energy to which the system is subject is $V_{\text{eff}}(\hat{q}, \hat{x}_j) = V_0(\hat{q}) + \Delta V(\hat{q}, \hat{x}_j)$ where

$$\Delta V(\hat{q}, \hat{x}_j) = \sum_{j=1}^{N}\left(-c_j\hat{x}_j\hat{q} + \frac{1}{2}m_j\omega_j^2\hat{x}_j^2\right).$$

The minima surface of V_{eff}, with respect to the reservoir coordinates at fixed $\hat{q}$, is at $\hat{x}_j^{\min} = c_j\hat{q}/(m_j\omega_j^2)$. The corresponding $\hat{q}$-dependent offset in the potential felt by the particle is

$$\Delta V(\hat{q})_{\hat{x}_j^{\min}} = -\sum_{j=1}^{N}\frac{c_j^2}{2m_j\omega_j^2}\hat{q}^2.$$

This term can be large and modify qualitatively the potential V_0. To have a purely dissipative environment and get rid of this additional potential term we add a renormalization term $-\Delta V(\hat{q})_{\hat{x}_j^{\min}}$ to the Hamiltonian. The new renormalized Hamiltonian can be rewritten as

$$\hat{H} = \frac{\hat{p}^2}{2M} + V_0(\hat{q}) + \sum_{j=1}^{N}\frac{1}{2}\left[\frac{\hat{p}_j^2}{m_j} + m_j\omega_j^2\left(\hat{x}_j - \frac{c_j}{m_j\omega_j^2}\hat{q}\right)^2\right]. \tag{1.12}$$

The model described by Eq. (1.12) is the Caldeira-Leggett model.

1.3 Quantum Langevin equation

The derivation of dissipation on a microscopic basis, within the Caldeira-Leggett model, can be carried out using the density matrix formalism or deriving a quantum version of the Langevin equation for the particle's position operator $\hat{q}$ in the Heisenberg picture. This latter approach, though not easily manageable in practice for predicting the actual time evolution of the system, has the advantage to allow for a clear comparison with the classical case.

The density matrix formalism, within the path integral representation of quantum mechanics, will be used in the next chapters for studying the time evolution of bistable systems in various dissipation regimes.

Taking the time derivative of the Heisenberg equations of motion for $\hat{q}(t)$ and $\hat{x}_j(t)$, the following two second order differential equations are obtained

$$M\ddot{\hat{q}}(t) + \frac{dV(\hat{q}(t))}{d\hat{q}(t)} + \hat{q}(t)\sum_{j=1}^{N}\frac{c_j^2}{m_j\omega_j^2} = \sum_{j=1}^{N} c_j\hat{x}_j(t) \tag{1.13}$$

and

$$m_j\ddot{\hat{x}}_j(t) + m_j\omega_j^2\hat{x}_j(t) = c_j\hat{q}(t). \tag{1.14}$$

In Laplace space Eq. (1.14) reads

$$\tilde{x}_j(\lambda) = \frac{\lambda}{\lambda^2+\omega_j^2}x_j(0) + \frac{\omega_j}{\lambda^2+\omega_j^2}\frac{\dot{x}_j(0)}{\omega_j} + \frac{c_j}{\omega_j m_j}\frac{\omega_j}{\lambda^2+\omega_j^2}\tilde{q}(\lambda).$$

Transforming back to the time domain we get the solution

$$\hat{x}_j(t) = \hat{x}_j(0)\cos(\omega_j t) + \frac{\hat{p}_j(0)}{m_j\omega_j}\sin(\omega_j t) + \frac{c_j}{m_j\omega_j}\int_0^t dt' q(t')\sin[\omega_j(t-t')]. \tag{1.15}$$

Substituting Eq. (1.15) into Eq. (1.13) we obtain the following *generalized Langevin equation* for the particle's position operator

$$M\ddot{\hat{q}}(t) + M\int_0^t dt'\gamma(t-t')\frac{d}{dt'}\hat{q}(t') + \frac{dV(\hat{q}(t))}{d\hat{q}(t)} = -M\gamma(t)\hat{q}(0) + \hat{\zeta}(t), \tag{1.16}$$

where

$$\gamma(t) = \Theta(t)\frac{1}{M}\sum_{j=1}^{N}\frac{c_j^2}{m_j\omega_j^2}\cos(\omega_j t) \tag{1.17}$$

and

$$\hat{\zeta}(t) = \sum_{j=1}^{N} c_j\left[\hat{x}_j(0)\cos(\omega_j t) + \frac{\hat{p}_j(0)}{m_j\omega_j}\sin(\omega_j t)\right] \tag{1.18}$$

are respectively the memory-friction kernel and the bath force operator.

Suppose the bath is in the thermal state

$$\rho_{\rm th}^R = \frac{e^{-\beta\hat{H}_R}}{Z}, \tag{1.19}$$

then the expectation value of the bath force operator and the bath force autocorrelation are

$$\langle\hat{\zeta}(t)\rangle_R = Tr_R\left[\rho_{th}^R\hat{\zeta}(t)\right] = 0 \qquad \text{and}$$
$$\langle\hat{\zeta}(t)\hat{\zeta(0)}\rangle_R = Tr_R\left[\rho_{th}^R\hat{\zeta}(t)\hat{\zeta}(0)\right] = \sum_{j=1}^{N}\frac{\hbar c_j^2}{2m_j\omega_j}\left[\coth\left(\frac{\hbar\omega_j\beta}{2}\right)\cos(\omega_j t) - i\sin(\omega_j t)\right], \tag{1.20}$$

respectively.

In the classical limit ($\hbar \to 0$) the bath force correlation function is

$$\lim_{\hbar\to 0}\langle\hat{\zeta}(t)\hat{\zeta(0)}\rangle_R = \frac{1}{\beta}\sum_{j=1}^{N}\frac{c_j^2}{m_j\omega_j^2}\cos(\omega_j t) = Mk_BT\gamma(t), \tag{1.21}$$

where we used $\coth(\beta\hbar\omega_j/2) \sim 2(\beta\hbar\omega_j)^{-1}$ for $\hbar \to 0$. Therefore the two relations in Eq. (1.20), in the continuum limit ($N \to \infty$), describe a stochastic force which in turn reproduce, in the classical limit, a classical colored noise source.

Note that in the quantum Langevin equation (1.16) a term appears in the RHS which is dependent on the initial condition $\hat{q}(0)$. This term vanishes at long time due to the interference of the quasi continuum of spectral components of $\gamma(t)$, and is ascribable to the fact that we have implicitly assumed a factorized initial condition with the reservoir in the canonical equilibrium.

Consider a different preparation, e.g. with the particle held fixed at the position q_0 from $t = -\infty$ to $t = t_0$: the reservoir starts in a *shifted* thermal condition. Focusing on the jth oscillator, for times $t < t_0$ it can be considered as a particle in a potential dependent on q_0 with Hamiltonian

$$\begin{aligned}\hat{H}_R^j(q_0) =& Tr_S\left[|q_0\rangle\langle q_0|\hat{H}_{RI}^j\right] \\ =& \frac{\hat{p}_j^2}{2m_j} + V(\hat{x}_j, q_0) = \frac{\hat{p}_j^2}{2m_j} + \frac{1}{2}m_j\omega_j^2\left(\hat{x}_j - \frac{c_j}{m_j\omega_j^2}\hat{q}_0\right)^2 .\end{aligned} \tag{1.22}$$

Setting $X_j := \omega_j/\Omega_j(\hat{x}_j - c_j q_0/m_j\omega_j^2)$ we have that the new free reservoir Hamiltonian is

$$\hat{H}_R(q_0) = \sum_{j=1}^{N}\left(\frac{\hat{p}_j^2}{2m_j} + \frac{1}{2}m_j\Omega_j^2\hat{X}_j^2\right) = \sum_{j=1}^{N}\hbar\Omega_j\left(\hat{b}_j^\dagger\hat{b}_j + \frac{1}{2}\right). \tag{1.23}$$

Now consider the RHS of Eq. (1.16). We define a new modified bath force operator $\hat{\xi}(t)$ which includes the term dependent on the initial particle's position. By the definition in Eq. (1.18), we get

$$\begin{aligned}\hat{\xi}(t) =& \hat{\zeta}(t) - M\gamma(t)q_0 \\ =& \sum_{j=1} c_j\left[\hat{X}_j(0)\cos(\omega_j t) + \frac{\hat{p}_j(0)}{m_j\omega_j}\sin(\omega_j t)\right].\end{aligned} \tag{1.24}$$

It follows immediately that the new force has the properties (1.20) and (1.21) if the averages are taken with respect to the shifted thermal density matrix of the reservoir

$$\rho_R^{\text{th}}(q_0) = \frac{e^{-\beta\hat{H}_R(q_0)}}{Z(q_0)}. \tag{1.25}$$

The new initial condition, with the particle held fixed at q_0 and the reservoir thermalized in interaction with the particle, gives to the quantum Langevin equation a close correspondence with the classical version, featuring the single stochastic force term $\xi(t)$,

$$M\ddot{\hat{q}}(t) + M\int_0^t dt'\gamma(t-t')\frac{d}{dt'}\hat{q}(t') + \frac{dV(\hat{q}(t))}{d\hat{q}(t)} = \hat{\xi}(t), \tag{1.26}$$

It is to notice that this kind of preparation is actually realized for a large class of experimental settings.

1.4 Spectral density function

In this section we introduce the bath spectral density function, which describes the frequency distribution of the reservoir (or thermal bath) and the coupling of each oscillator with the particle

$$J(\omega) = \frac{\pi}{2}\sum_{j=1}^{N}\frac{c_j^2}{m_j\omega_j}\delta(\omega-\omega_j). \tag{1.27}$$

Note that $J(\omega)$ has the dimension of a mass times a frequency. By comparing Eq. (1.17) and Eq. (1.27) one can see that the bath spectral density function and the memory damping kernel are related by the equation

$$\gamma(t) = \Theta(t)\frac{1}{M}\frac{2}{\pi}\int_0^\infty d\omega\frac{J(\omega)}{\omega}\cos(\omega t). \tag{1.28}$$

To relate $J(\omega)$ to $\tilde{\gamma}(\omega)$, the Fourier transform of the memory damping kernel $\gamma(t)$, we have to express the latter in the frequency space. The Laplace transform of $\gamma(t)$ (see Eq. (1.17)) is

$$\hat{\gamma}(\lambda) = \frac{1}{M}\sum_{j=1}^{N}\frac{c_j^2}{m_j\omega_j^2}\frac{\lambda}{\lambda^2+\omega_j^2}. \tag{1.29}$$

The Fourier transform is related to the Laplace transform through the relation $\tilde{\gamma}(\omega) = \lim_{\epsilon\to 0^+}\hat{\gamma}(\lambda = -i\omega+\epsilon)$, so that in Fourier space $\gamma(t)$ reads

$$\tilde{\gamma}(\omega) = \lim_{\epsilon\to 0^+}\frac{1}{M}\sum_{j=1}^{N}\frac{c_j^2}{m_j\omega_j^2}\frac{i\omega}{\omega^2-\omega_j^2+2i\epsilon\omega}. \tag{1.30}$$

The real part of $\tilde{\gamma}(\omega) = \tilde{\gamma}'(\omega) + \tilde{\gamma}''(\omega)$ is

$$\tilde{\gamma}'(\omega) = \frac{1}{M}\frac{\pi}{2}\sum_{j=1}^{N}\frac{c_j^2}{m_j\omega_j^2}\delta(\omega-\omega_j). \tag{1.31}$$

As a result the real part of the Fourier transform of the damping kernel is related to the spectral density function through the relation

$$J(\omega) = M\tilde{\gamma}'(\omega)\omega. \tag{1.32}$$

Already for a moderate number of reservoir oscillators, the periodicity in the time evolution of the system, given by the Poincarè recurrence time, is practically lost so that the continuum or thermodynamical limit $N\to\infty$ of the reservoir is usually considered. In this case the coupling constant c_j, the masses m_j and the frequencies of the bath's oscillators ω are continuous functions $c(\omega)$, $m(\omega)$ and ω, respectively. The special case of frequency independent (Ohmic) damping $\tilde{\gamma}'(\omega) = \gamma$, Eq. (1.32) gives $J(\omega) = M\gamma\omega$.

However, allowing this linear behavior to arbitrarily high frequency gives non-physical results as, for example, the divergence of the renormalization term

$$-\Delta V(\hat{q})_{\hat{x}_j^{\min}} = 2\gamma M q_0^2\pi\int_0^\infty d\omega = \infty \tag{1.33}$$

in the Hamiltonian Eq. (1.12).

To avoid this kind of difficulties a cut-off is introduced on the memory time of the kernel at a finite time $\tau_D = \omega_D^{-1}$, the inverse of the (Drude) frequency ω_D. The friction memory kernel with Drude cut-off reads

$$\tilde{\gamma}(t) = \Theta(t)\gamma\omega_D \exp(-\omega_D t). \tag{1.34}$$

This exponential cut-off corresponds to an algebraic cut-off on the spectral density function. Indeed

$$\hat{\gamma}(\lambda) = \frac{\gamma\omega_D}{\lambda + \omega_D} \tag{1.35}$$

and, using the relation $\tilde{\gamma}(\omega) = \lim_{\epsilon\to 0^+} \hat{\gamma}(\lambda = -i\omega + \epsilon)$,

$$\tilde{\gamma}'(\omega) + i\tilde{\gamma}''(\omega) = \frac{\gamma}{1 + (\omega/\omega_D)^2} + i\frac{\gamma\omega/\omega_D}{1 + (\omega/\omega_D)^2}. \tag{1.36}$$

The corresponding spectral density is

$$J(\omega) = M\tilde{\gamma}'(\omega)\omega = \frac{M\gamma\omega}{1 + (\omega/\omega_D)^2} \tag{1.37}$$

The physical consequences of the introduction of the cut-off is that the system behaves like being in contact with an Ohmic environment on time scales longer than τ_D. At shorter times the higher frequencies are coupled to the system according to Eq. (1.37). So the cut-off corresponds to a coarse grained model for the system dynamics. What is the effect of the high frequency modes of the reservoir on the coarse grained dynamics?

To answer this question we consider a general cut-off $f(\omega_c)$ at a characteristic frequency ω_c and take into account the high frequency part ($\omega > \omega_c$) of the reservoir by writing the spectral density as the sum [9]

$$J(\omega) = J_{\rm lf}(\omega)f(\omega_c) + J_{\rm hf}(\omega)[1 - f(\omega_c)]. \tag{1.38}$$

Comparing the definition of $J(\omega)$ in Eq. (1.27) with the expression in Eq. (1.30), we get

$$\tilde{\gamma}(\omega) = \lim_{\epsilon\to 0^+} \frac{2}{M\pi}\int_0^\infty d\omega' \frac{J(\omega')}{\omega'} \frac{i\omega}{\omega^2 - \omega'^2 + 2i\epsilon\omega}. \tag{1.39}$$

At $\omega \ll \omega_c$ we have

$$\tilde{\gamma}(\omega \ll \omega_c) \sim \frac{J_{\rm lf}(\omega)}{M\omega} - i\frac{\omega}{M}\Delta_{\rm hf}, \tag{1.40}$$

where $\Delta_{\rm hf} = 2/\pi \int_0^\infty d\omega' J_{\rm hf}(\omega')/\omega'^3$. Inserting this expression into the Fourier transform of the quantum Langevin equation (Eq. (1.16)) we have

$$i\omega(M + \Delta_{\rm hf})q_0 + \mathcal{F}[V'(\hat{q})] = \zeta(-i\omega), \tag{1.41}$$

which makes clear that, at sufficiently long times ($t \gg \omega_c^{-1}$), the effect of the high frequency spectral density function consists in dressing the particle's bare mass by the high frequency modes of the bath. In the coarse grained description, once the mass has been redefined, one can consider only the low frequency part of the spectral density function and drop the suffix "*lf*".

In the general case of continuous bath the spectral density function is modeled as a power law, characterized by the exponent s with respect to ω, with an exponential cutoff at ω_c

$$J(\omega) = M\gamma_s\omega_{\rm ph}^{1-s}\omega^s e^{-\omega/\omega_c}. \tag{1.42}$$

The bath is said sub-Ohmic for $0 < s < 1$ and super-Ohmic for $s > 1$. The *phonon* frequency $\omega_{\rm ph}$ is introduced for γ_s to mantain the dimension of a frequency also in the non-Ohmic case ($s \neq 1$).

1.4.1 Coupling with the individual bath oscillators in the Ohmic case

Having introduced the bath spectral density function $J(\omega)$ and its continuous limit, it is now possible to extrapolate the frequency dependence of the coupling of the system with the individual bath oscillators for frequencies $\ll \omega_c$. The general expression for the spectral density is

$$J(\omega) = \frac{\pi}{2} \sum_{j=1}^{N} \frac{c_j^2}{m_j \omega_j} \delta(\omega - \omega_j). \tag{1.43}$$

If the n-th coupling coefficient is given by

$$c_n = \left(\gamma \frac{2Mm}{\pi n} \omega_n^3 \right)^{1/2}, \tag{1.44}$$

then, substituting in Eq. (1.43) with $\omega_n/n =: \Delta\omega_n$, we get

$$\begin{aligned} J(\omega) =& M\gamma \sum_{j=1}^{N_\Omega} \Delta\omega_j \omega_j \delta(\omega - \omega_j) \\ \xrightarrow{N \gg 1}& M\gamma \int_0^\infty d\omega' \omega' \delta(\omega - \omega') = M\gamma\omega, \end{aligned} \tag{1.45}$$

and we obtain the Ohmic spectral density in the continuous limit.

The result (1.44) shows that if the environment is a large collection of oscillators, one can have strong dissipation, quantified by γ, and still a weak coupling with the individual oscillators, as anticipated in Sec. 1.2.

1.5 Outline of the thesis

In this thesis the dissipative dynamics of bistable quantum systems, as those described in the previous sections, is studied within the path integral (PI) approach. This approach is particularly effective in the presence of nonlinear potentials, such as those involved in tunneling dynamics and escape problems in the quantum regime [8, 9, 43, 44].

Being inherently non-perturbative in the coupling with the environment, the PI approach is suited for treating the dissipation in the weak to strong coupling regime, whereas the traditional Born-Markov master equation techniques, perturbative in the coupling [42, 45], are confined to the weak coupling case. Moreover, the PI techniques have the further advantage of being flexible, as they allow for different approximate treatments in the various dissipation regimes.

The Hamiltonian model used throughout the thesis is the Caldeira-Leggett model, introduced in Sec. 1.2. The results shown are obtained for Ohmic dissipation in the thermodynamical limit, i.e. considering a quasi-continuum of bath spectral components with spectral density given by Eq. (1.42) with $s = 1$.

In Chapter 2 a brief description of the path integral representation of Quantum Mechanics is given, with a detailed description of the approach for *discrete variable* systems. In particular, as an exemplification, the dynamics of a free two-level system is obtained by the PI approach and compared to the standard result as given by the Sroödinger equation.

In the second part of the chapter a PI picture of dissipation is introduced by deriving the Feynman-Vernon (FV) influence functional from the trace over the environment

degrees of freedom in the PI representation of the full density matrix, along the lines of Ref. [9]. The FV influence functional multiplies the amplitude associated to a path of the isolated system, accounting for the effects brought by the environment. Further, it incorporates the effects exerted by the motion of the particle on the reservoir of harmonic oscillators constituting the environment. This last feature gives a hint of how this approach describes the non-Markovoian character of the dynamics in open systems. Using the FV formalism, a formally exact expression for the propagator of the system reduced density matrix is obtained. However this exact expression is too intricate in the general case and of little practical use, unless suitable approximations are introduced.

In Chapter 3 the main approximations to the FV influence are introduced and applied to the the so-called spin-boson model, a two-level system coupled the bosonic heat bath of the Caldeira-Leggett model. A generalized master equation is derived for the populations, the diagonal elements of the system reduced density matrix in the $\{|L\rangle, |R\rangle\}$ basis, starting from their PI expressions. The kernels of the master equation are taken within approximation schemes designed to deal with different coupling strengths and temperatures.

In Chapter 4 the techniques developed in Chapter 3 are applied to a bistable system beyond the two-level system approximation. The energy levels in the strongly non-linear potential considered are arranged in doublets. If k_BT is of the order of the inter-doublet spacing or the initial condition involves energy states beyond the first doublet of energy state, a description in terms of two-level system is inappropriate and the physical system has to be describes as a multi-state system. Specifically, the so-called double-doublet system is considered. By the combined use of the Bloch-Redfield perturbative approach and of the PI techniques, a phase diagram showing the various dynamical and dissipative regimes of the double-doublet system is established. Examples of time evolution of the populations in a spatially localized basis are shown in various coupling/temperature regimes.

Chapter 5 deals with the general case of biased multi-state system in the strong coupling regime, possibly driven by a high-frequency oscillating force. Using a Markov-approximated version of the generalized master equation for these multi-state systems, a systematic study is performed on the transient and stationary properties of the dynamics as functions of the driving parameters. The role of the temperature and the damping is investigated. Within the same approach the problem of the escape from a metastable state with nonequilibrium initial condition, in the presence of strong dissipation, is also considered in the static case. This dynamical approach to escape dynamics allows to take in consideration a broader class of initial preparations, with the particle possibly not in the quasi-stationary state, at the bottom of the metastable well. This is motivated by the role played in the corresponding classical problem by the initial condition. The nonmonotonic behavior of the escape time as a function of the noise intensity, found in the classical context, takes the name of noise enhanced stability (NES). The study of the corresponding quantum problem is aimed at determining if a similar effect is present once the tunneling is involved.

Chapter 2

Path integral approach for discrete variable systems

In this chapter the path integral representation of Quantum Mechanics is introduced and the expression for the propagator of the state vector for a closed system is derived in the position representation. The corresponding expression for a closed system with finite Hilbert space (of dimension D) is derived in the eigenbasis $\{|k_j\rangle\}$ of some operator $\hat{K}$. This general expression is specialized to the free two-level system. The propagator for the density matrix of a discrete variable system with D-dimensional Hilbert space is obtained along the same lines.

In the second part of the chapter the path integral approach to dissipation is introduced for a general open quantum system. The trace over the environment in the path integral expression of the full density matrix leads to the introduction of the Feynman-Vernon (FV) influence functional. The discrete variable version of the FV functional is obtained through a suitable parametrization for the step-like paths of the reduced density matrix (RDM) of the open system. The formalism and the notation introduced here are applied to the dissipative two-level system in Chap. 3 and to the dissipative double-doublet system in Chap. 4.

2.1 Path integral representation of Quantum Mechanics

In this section a brief outline of the path integral expression of the propagator for a generic closed quantum system is given following the derivation in [46, 47].

The probability amplitude for a quantum mechanical system, described by the (time independent) Hamiltonian $\hat{H} = T(\hat{p}) + V(\hat{q})$, to be in the eigenstate $|q\rangle$ of the position operator $\hat{q}$ at time t is given by

$$\langle q|\psi(t)\rangle = \langle q|U(t-t')|\psi(t')\rangle = \int dq' \langle q|U(t-t')|q'\rangle\langle q'|\psi(t')\rangle, \tag{2.1}$$

where $U(t) = \exp(-i\hat{H}t/\hbar)$ is the time evolution operator, solution of the Schrödinger equation $i\hbar\dot{U}(t) = \hat{H}U(t)$, which satisfies the composition law $U(t-t') = U(t-t'')U(t''-t')$ (where $t' < t'' < t$).

The function

$$G(q,t;q',t') \equiv \langle q|U(t-t')|q'\rangle \tag{2.2}$$

is the *propagator* for the quantum state of the system from the state $|q'\rangle$ at time t' to the state $|q\rangle$ at time t.

Dividing the time interval $t-t'$ in $N \gg 1$ intervals $\Delta t = (t-t')/N$ and using the Trotter splitting formula

$$e^{-i(\hat{T}+\hat{V})(t-t')/\hbar} = \left(e^{-i(\hat{T}+\hat{V})\Delta t/\hbar}\right)^N = \lim_{N\to\infty}\left(e^{-i\hat{T}\Delta t/\hbar}e^{-i\hat{V}\Delta t/\hbar}\right)^N, \tag{2.3}$$

the propagator can be put in the form

$$\begin{aligned} G(q,t;q',t') &\simeq \langle q|\prod_{n=1}^{N} e^{-i\hat{T}\Delta t/\hbar}e^{-i\hat{V}\Delta t/\hbar}|q'\rangle \\ &= \prod_{n=1}^{N}\int dq_n dp_n \langle q_n|p_n\rangle\langle p_n|e^{-i\hat{T}\Delta t/\hbar}e^{-i\hat{V}\Delta t/\hbar}|q_{n-1}\rangle\delta(q_N-q)\delta(q_0-q') \\ &= \prod_{n=1}^{N}\int dq_n \frac{dp_n}{2\pi\hbar} e^{-\frac{i}{\hbar}\Delta t\left[p_n^2/2M+V(q_{n-1})-p_n\frac{q_n-q_{n-1}}{\Delta t}\right]}\delta(q_N-q)\delta(q_0-q'). \end{aligned} \tag{2.4}$$

Here the identity operator $\mathbb{I} = \int dq_n \int dp_n |q_n\rangle\langle q_n|p_n\rangle\langle p_n|$ has been introduced N times in passing from the first to the second line and the scalar product $\langle q_n|p_n\rangle = \exp(iq_np_n/\hbar)/\sqrt{2\pi\hbar}$ has been used.

Performing the gaussian integrals over p_n (using the result $\int dp \exp(-ap^2+bp) = \sqrt{\pi/a}\exp(b^2/4a)$) and taking the limit $N\to\infty$, the path integral representation of the propagator is obtained

$$G(q,t;q',t') = \int_{q(t')=q'}^{q(t)=q} \mathcal{D}q e^{\frac{i}{\hbar}S[q]}. \tag{2.5}$$

The functional $S[q] = \int_{t'}^{t} dt'' L(q,\dot{q})$ is the classical action functional associated to the Lagrangian $L(q,\dot{q}) = M\dot{q}^2/2 - V(q)$. The integration symbol is defined as

$$\int \mathcal{D}q = \lim_{N\to\infty}\sqrt{\frac{M}{i2\pi\hbar\Delta t}}\prod_{n=1}^{N-1} dq_n. \tag{2.6}$$

The meaning of Eq. (2.5) is that the propagator is the sum of the amplitudes $\exp(iS[q(\tau)]/\hbar)$ over all possible paths $q(\tau)$ with fixed extrema (the values of the function $q(\tau)$ at t' and t).

2.2 Propagator for a discrete variable system

There are quantum system with no classical analogues, as for example two-state systems like a spin 1/2 particle, for which the classical action is not defined. Nevertheless the path integral expression for the propagator can be constructed as follows.

Consider a system with a finite Hilbert space of dimension D, spanned by some basis set $\mathcal{B} = \{|K_1\rangle, \ldots, |K_D\rangle\}$. The probability amplitude for the system to be in the state $|k_f\rangle \in \mathcal{B}$ at time t_f is the discrete analogous of Eq. (2.1), i.e.

$$\langle k_f|\psi(t_f)\rangle = \sum_{k_i=K_1}^{K_D} G(k_f,t_f;k_i,t_0)\langle k_i|\psi(t_0)\rangle. \tag{2.7}$$

Splitting the time interval $t - t'$ in $N \gg 1$ small Δt, the propagator can be written as

$$\begin{aligned} G(k_f, t_f; k_i, t_0) &= \langle k_f | \prod_{j=1}^{N} e^{-i\hat{H}\Delta t/\hbar} | k_i \rangle \\ &\simeq \delta_{k_N k_f} \delta_{k_0 k_i} \prod_{j=1}^{N} \sum_{k_j} \langle k_j | \mathbf{1} - \frac{i}{\hbar} \hat{H} \Delta t | k_{j-1} \rangle. \end{aligned} \tag{2.8}$$

In passing from the first to the second line of Eq. (2.8) the identity $\mathbb{I} = \sum_{j=1}^{M} |K_j\rangle\langle K_j|$ has been introduced $N+1$ times. Moreover, due to the small Δt, the time evolution operator from time t_{j-1} to time t_j has been taken in the linearized form, i.e. to the first order in Δt. As the limit $N \to \infty$ of Eq. (2.8) is taken, the path integral expression for G is obtained, but before doing the limit it is necessary to perform other intermediate steps.

The propagator in Eq. (2.8) is the sum of the amplitudes relative to all of the possible paths with $n < N$ transitions. If, for some path, $k_j = k_{j-1}$, then no transitions occur in the time interval $t_{j+1} - t_{j-1}$. As a consequence, even if N is very large there are paths with few or even zero transitions. It is convenient to express the propagator as the sum over the propagators G_n with fixed number n of transitions

$$G(k_f, t_f; k_i, t_0) = \sum_{n=0}^{\infty} G_n(k_f, t_f; k_i, t_0), \tag{2.9}$$

and then to take the limit $N \to \infty$, as in Ref. [48].

The propagator with zero transitions doesn't vanish only if initial and final state are the same ($k_f = k_i$). It reads

$$\begin{aligned} G_0(k_f, t_f; k_i, t_0) &= \lim_{N\to\infty} \delta_{k_N k_f} \prod_{j=1}^{N} \sum_{k_j} \langle k_j | \mathbf{1} - \frac{i}{\hbar} \hat{H} \Delta t | k_{j-1} \rangle \delta_{k_j k_{j-1}} \\ &= \lim_{N\to\infty} \delta_{k_f k_i} \left(1 - \frac{i}{\hbar} H_{k_f k_i} \frac{t_f - t_0}{N} \right)^N \\ &\equiv \delta_{k_f k_i} e^{-iE_{fi}(t_f - t_0)}. \end{aligned} \tag{2.10}$$

Hereinafter the Hamiltonian $\hat{H}$ in the $\{|k\rangle\}$ representation is decomposed into its diagonal and off-diagonal parts

$$\begin{aligned} E_{nm} &= \delta_{nm} \langle k_n | \hat{H} | k_m \rangle / \hbar \\ \Delta_{nm} &= (1 - \delta_{nm}) \langle k_n | \hat{H} | k_m \rangle / \hbar. \end{aligned} \tag{2.11}$$

The one-transition propagator is different from zero if $k_f \neq k_i$. Suppose that the unique

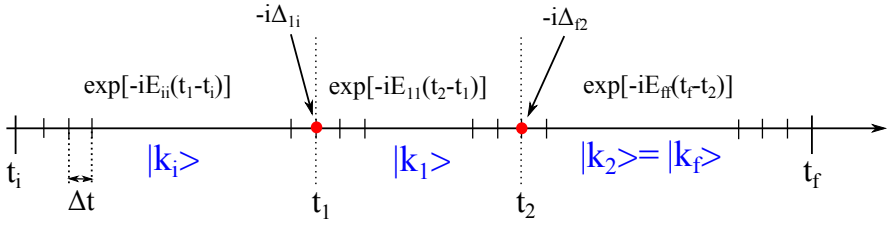

Figure 2.1: Example of a path with two transitions at times t_1 and t_2. The factors that form the amplitude for this path are indicated in the upper part of the figure. See the last line of Eq. (2.13) for comparison.

transition occurs at time t_L, where L runs between 1 and $N-1$, then

$$\begin{aligned} G_1(k_f,t_f;k_i,t_0) &= \lim_{N\to\infty} \delta_{k_N k_f}\delta_{k_0 k_i} \sum_{L=1}^{N-1} \prod_{j=L+1}^{N} \sum_{k_j} \langle k_j|\mathbf{1} - \frac{i}{\hbar}\hat{H}\Delta t|k_{j-1}\rangle \delta_{k_j k_{j-1}} \\ &\quad \times \sum_{k_L} \langle k_L| - \frac{i}{\hbar}\hat{H}\Delta t|k_{L-1}\rangle \prod_{j=1}^{L-1} \sum_{k_j} \langle k_j|\mathbf{1} - \frac{i}{\hbar}\hat{H}\Delta t|k_{j-1}\rangle \delta_{k_j k_{j-1}} \\ &= \lim_{N\to\infty} \sum_{L=1}^{N-1} \Delta t \left(1 - iE_{ff}\frac{t_f - t_L}{N-L}\right)^{N-L} (-i\Delta_{fi}) \left(1 - iE_{ii}\frac{t_L - t_0}{L}\right)^{L} \\ &= -i\int_{t_0}^{t_f} dt_1 \Delta_{fi} e^{-i[E_{ff}(t_f - t_1) + E_{ii}(t_1 - t_0)]}. \end{aligned} \tag{2.12}$$

Notice that the sum over the intermediate state collapses because the target state of the transition has to be the final (fixed) state.

By a similar construction the two-transition propagator G_2 is obtained. For $n \geq 2$ the propagator is nonzero for any pair of initial and final states. In the $n = 2$ case the target state of the first transition and the starting state of the second transition have to be the same, which implies that only one of the sums over the intermediate states survives. Assume that the first transition to take place at time t_R and the second at time t_L with $0 < R < L < N$. The resulting $n = 2$ propagator reads

$$\begin{aligned} G_2(k_f,t_f;k_i,t_0) &= \lim_{N\to\infty} \sum_{L=2}^{N-1} \Delta t \left(1 - iE_{ff}\frac{t_f - t_L}{N-L}\right)^{N-L} \sum_{k_R} (-i\Delta_{fR}) \\ &\quad \times \sum_{R=1}^{L-1} \Delta t \left(1 - iE_{RR}\frac{t_L - t_R}{L-R}\right)^{L-R} (-i\Delta_{Ri}) \left(1 - iE_{ii}\frac{t_R - t_0}{R}\right)^{R} \\ &= (-i)^2 \int_{t_0}^{t_f} dt_2 \int_{t_0}^{t_2} dt_1 \sum_{k_1} \Delta_{f1}\Delta_{1i} e^{-i[E_{ff}(t_f - t_2) + E_{11}(t_2 - t_1) + E_{ii}(t_1 - t_0)]} \end{aligned} \tag{2.13}$$

In Fig. 2.1 is sketched an example of two-transition path. The factors constituting the amplitude are indicated in correspondence of the stationary parts and of the transitions.

The three-transition propagator G_3, obtained with the same procedure as that used above for G_2, results in a series of three nested integrals over the transition times t_j (with

$j = 1, 2, 3$). The sum over the intermediate states is for the first and second transition, since the third is fixed by the fact that the target state has to be $|k_f\rangle$. The resulting expression is

$$G_3(k_f, t_f; k_i, t_0) = (-i)^3 \int_{t_0}^{t_f} dt_3 \int_{t_0}^{t_3} dt_2 \int_{t_0}^{t_2} dt_1 \sum_{k_1,k_2} e^{-iE_{ff}(t_f-t_3)} \prod_{j=1}^{3} \Delta_{jj-1} e^{-iE_{jj-1}(t_j-t_{j-1})} \tag{2.14}$$

We are now in the position to generalize the result for the n-transition propagator which reads

$$G_n(k_f, t_f; k_i, t_0) = (-i)^n \int_{t_0}^{t_f} \mathcal{D}\{t\}_n e^{-iE_{ff}(t_f-t_n)} \prod_{j=1}^{n} \Delta_{jj-1} e^{-iE_{jj-1}(t_j-t_{j-1})}, \tag{2.15}$$

where

$$\int_{t_0}^{t_f} \mathcal{D}\{t\}_n = \int_{t_0}^{t_f} dt_n \int_{t_0}^{t_n} dt_{n-1} \ldots \int_{t_0}^{t_2} dt_1 \sum_{k_1,\ldots,k_{n-1}} . \tag{2.16}$$

Notice that in the energy basis $\{|E_j\rangle\}$ the propagator assumes a very simple form because the Hamiltonian is diagonal in this basis: every term but the first (G_0) vanishes as, by the definition in Eq. (2.11), the factors Δ_{jj-1} vanish. In the energy basis

$$G(E_f, t_f; E_i, t_0) = \delta_{E_f E_i} e^{-iE_{fi}(t_f-t_0)}. \tag{2.17}$$

2.2.1 Propagator for the free two-level system

The simplest nontrivial example of a quantum system with finite Hilbert space is that of a two-level system (TLS). As an illustrative example, I give the path integral expression of the propagator in the *localized* basis $\{|L\rangle, |R\rangle\}$, introduced in Sec 1.1.1 (Eq. (1.8)). In this basis the Hamiltonian reads

$$\hat{H}_{TLS} = -\frac{\hbar}{2}(\Delta\sigma_x + \epsilon\sigma_z), \tag{2.18}$$

where $\sigma_z = |R\rangle\langle R| - |L\rangle\langle L|$ and $\sigma_x = |R\rangle\langle L| + |L\rangle\langle R|$. In terms of the tunneling (Δ) and bias (ϵ) factors the energy splitting between the ground and the excited states is $E \equiv E_e - E_g = \hbar\sqrt{\Delta^2 + \epsilon^2}$ (see Fig. 1.3).

Suppose that the system is in the localized state $|L\rangle$ at time $t = 0$. The probability amplitude for the system to be in the state $|L\rangle$ at time t is easily calculated using Eq. (2.7) in the energy eigenbasis, with the propagators given by Eq. (2.17), which gives

$$\langle L|\psi(t_f)\rangle = \cos\left(\frac{Et}{2\hbar}\right) + i\frac{\hbar\epsilon}{E}\sin\left(\frac{Et}{2\hbar}\right), \tag{2.19}$$

where I used Eq. (1.8) and $\tan\phi = \Delta/\epsilon$. The *survival probability* in the state $|L\rangle$ is thus

$$|\langle L|\psi(t_f)\rangle|^2 = \frac{\hbar^2\epsilon^2}{E^2} + \frac{\hbar^2\Delta^2}{E^2}\cos^2\left(\frac{Et}{2\hbar}\right). \tag{2.20}$$

Let's move to the path integral expression in the localized basis. The probability amplitude $\langle L|\psi(t_f)\rangle$, as given by Eq. (2.7) in the localized basis, coincides with the propagator

$G(L,t;L,0)$ itself. The initial and final state are fixed by the definition of the propagator but, contrary to the $D>2$ case in the TLS there is no sum over the internal states, since the path can only alternate between $|L\rangle$ and $|R\rangle$.

Specializing to the TLS case, the matrix elements of the Hamiltonian are $E_{jj}=\pm\epsilon/2$ and $\Delta_{jk}=-\Delta/2$ (see Eq. (2.18)). Recognizing that, if the starting and final states are the same, each contributing path must have an even number $2n$ of transitions, the sum (2.9) of general term (2.15) becomes

$$\begin{aligned} G(L,t;L,0) &= \sum_{n=0}^{\infty}\int_0^t dt_{2n}\ldots\int_0^{t_2}dt_1\left(-\frac{\Delta^2}{4}\right)^n\prod_{j=0}^{n}e^{-i\epsilon(t_{2j+1}-t_{2j})/2}\prod_{j=1}^{n}e^{i\epsilon(t_{2j}-t_{2j-1})/2} \\ &= \sum_{n=0}^{\infty}\int_0^t d\sigma_0\int_0^{t-\sigma_0}d\tau_1\ldots\int_0^{t-\ldots\tau_{n-1}-\sigma_{n-1}}d\tau_n\left(-\frac{\Delta^2}{4}\right)^n\prod_{j=0}^{n}e^{-i\epsilon\sigma_j/2}\prod_{j=1}^{n}e^{i\epsilon\tau_j/2}, \end{aligned} \tag{2.21}$$

where I introduced the $n+1$ odd time intervals $\sigma_j=t_{2j+1}-t_{2j}$ and the n even time intervals $\tau_j=t_{2j}-t_{2j-1}$. The Laplace transform of Eq. (2.21) reads

$$\begin{aligned} G(L,\lambda;L,0) &= \sum_{n=0}^{\infty}\left(-\frac{\Delta^2}{4}\right)^n\prod_{j=0}^{n}\frac{1}{\lambda+i\epsilon/2}\prod_{j=1}^{n}\frac{1}{\lambda-i\epsilon/2} \\ &= \frac{1}{\lambda+i\epsilon/2}\sum_{n=0}^{\infty}\left(-\frac{\Delta^2/4}{\lambda^2+\epsilon^2/4}\right) \\ &= \frac{\lambda-i\epsilon/2}{\lambda^2+E^2/4\hbar^2}. \end{aligned} \tag{2.22}$$

The inverse Laplace transform is performed using the Bromwich integral

$$G(L,t;L,0)=\mathcal{L}^{-1}\{G(L,\lambda;L,0)\}(t)=\frac{1}{2\pi i}\int_{c-i\infty}^{c+i\infty}d\lambda e^{\lambda t}G(L,\lambda;L,0), \tag{2.23}$$

where, by convention, a counterclockwise oriented integration contour is used with $c\in\mathbb{R}>\Re\{\text{poles of } G(L,\lambda;L,0)\}$. The integral is evaluated calculating the residues at the poles $\lambda=\pm iE/2\hbar$. The result is

$$G(L,t;L,0)=\cos\left(\frac{Et}{2\hbar}\right)+i\frac{\hbar\epsilon}{E}\sin\left(\frac{Et}{2\hbar}\right), \tag{2.24}$$

which coincides with the amplitude in Eq. (2.19) obtained in the energy basis.

2.3 Propagator for the density matrix of a discrete variable system

As shown in the previous sections, the calculation of the propagator for a free system is straightforward in the energy basis. However the path integral construction in different basis (e.g. position eigenstates) demonstrates its usefulness in the presence of a (possibly strong) interaction with the environment as in the Caldeira-Leggett model. As the environment is the large thermal reservoir with uncontrollable degrees of freedom such as that introduced in Sec. 1.2, the formalism suited for describing the system dynamics is that of

the density matrix. Therefore, in view of the applications to the dissipative case, in this section I construct a path integral expression for the propagator of the density matrix of the discrete variable system considered in Sec. 2.2, which has a D-dimensional Hilbert space spanned by the basis $\{|K_j\rangle\}$ $(j = 1, \ldots, D)$. It turns out that the propagator assumes the form of a double discretized path integral. The construction is along the same lines as the one performed in Sec. 2.2.

The density matrix element k_f, k'_f at time t_f is given by

$$\begin{aligned}\rho_{k_f,k'_f} &= \langle k_f|\rho(t_f)|k'_f\rangle = \langle k_f|U(t_f,t_0)|\rho(t_0)|U^\dagger(t_f,t_0)|k'_f\rangle \\ &= \sum_{k_i,k'_i=K_1}^{K_D} \rho_{k_i,k'_i}(t_0) G(k_f,k'_f,t_f;k_i,k'_i,t_0),\end{aligned} \tag{2.25}$$

where the propagator for the density matrix is defined as

$$G(k_f,k'_f,t_f;k_i,k'_i,t_0) = \langle k_f|U(t_f,t_0)|k_i\rangle\langle k'_i|U^\dagger(t_f,t_0)|k'_f\rangle. \tag{2.26}$$

Dividing the time interval into N sub-intervals and proceeding as for the quantum state propagator in Sec. 2.2 we have

$$G(k_f,k'_f,t_f;k_i,k'_i,t_0) = f \sum_{k_j,k'_j=K_1}^{K_D} \prod_{j=1}^{N} \langle k_j|U(t_j,t_{j-1})|k_{j-1}\rangle\langle k'_{j-1}|U^\dagger(t_j,t_{j-1})|k'_j\rangle, \tag{2.27}$$

where $f = \delta_{k_0,k_i}\delta_{k'_0,k'_i}\delta_{k_N,k_f}\delta_{k'_N,k'_f}$ fixes the states at initial and final time. Again, it is convenient to express the propagator as a sum over the number of transitions of propagators with fixed number n of transitions, i.e.

$$G(k_f,k'_f,t_f;k_i,k'_i,t_0) = \sum_{n=0}^{\infty} G_n(k_f,k'_f,t_f;k_i,k'_i,t_0). \tag{2.28}$$

The difference with the quantum state propagator is that now n is the sum of the number of left and right coordinate transitions.

The propagator with zero transitions doesn't vanish only if $k_f = k_i$ and $k'_f = k'_i$. It is given by

$$\begin{aligned}G_0(k_f,k'_f,t_f;k_i,k'_i,t_0) = \lim_{N\to\infty} f \prod_{j=1}^{N} \sum_{k_j,k'_j} &\langle k_j|\mathbf{1} - \frac{i}{\hbar}\hat{H}\Delta t_j|k_{j-1}\rangle \\ &\times \langle k'_{j-1}|\mathbf{1} + \frac{i}{\hbar}\hat{H}\Delta t_j|k'_j\rangle\delta_{k_{j+1},k_j}\delta_{k'_{j+1},k'_j} \\ =&\delta_{k_f,k_i}\delta_{k'_f,k'_i}\exp\{-i\epsilon_i(t_f - t_0)\},\end{aligned} \tag{2.29}$$

where I have introduced

$$\epsilon_j = E_{jj} - E'_{jj} = \frac{1}{\hbar}\left(\langle k_j|\hat{H}|k_j\rangle - \langle k'_j|\hat{H}|k'_j\rangle\right). \tag{2.30}$$

Notice that ϵ_j vanishes if the system is in a diagonal configuration $(k_j = k'_j)$. Indeed the so-called *bias factor* $\exp(-i\epsilon_j\Delta t)$ gives the probability amplitude to be in the off-diagonal state (k_j, k'_j) during the time Δt.

The one-transition propagator is obtained with a procedure similar to that in Eq. (2.12) and we eventually obtain

$$G_1(k_f,k'_f,t_f;k_i,k'_i,t_0) = -is_1\Delta_1\int_{t_0}^{t_f} dt_1 e^{-i\left[\epsilon_f(t_f-t_1)+\epsilon_i(t_1-t_0)\right]}, \tag{2.31}$$

where $s_1=+1$ (-1) if the unique transition, occurring at time t_1, is in the left [unprimed] (right [primed]) coordinate. Accordingly, the factor Δ_1 is defined as Δ_{k_1,k_0} $(\Delta_{k'_1,k'_0})$ (see Eq. (2.11)). Also in this case there is no sum over the internal transition as the target state is fixed by the final state of the coordinate that makes the transition.

In the two-transition propagator, with transitions occurring at times t_1 and t_2, we sum over the intermediate configurations $\{(k_1,k'_1),(k_2,k'_2)\}$ denoted by $\{k_j,k'_j\}_2$. The $n=2$ propagator is

$$G_2(k_f,k'_f,t_f;k_i,k'_i,t_0) = \int_{t_0}^{t_f} dt_2\int_{t_0}^{t_2} dt_1 \sum_{\{k_j,k'_j\}_2} e^{-i\epsilon_i(t_1-t_i)}\prod_{j=1}^{2}(-is_j\Delta_j)\,e^{-i\epsilon_j(t_{j+1}-t_j)}. \tag{2.32}$$

According to Eq. (2.28), the full propagator is the sum over the number of transitions of the n-transition propagators and reads

$$G(k_f,k'_f,t_f;k_i,k'_i,t_0) = \sum_{n=0}^{\infty}\int_{t_0}^{t_f}\mathcal{D}\{t\}_n e^{-i\epsilon_i(t_1-t_0)}\prod_{j=1}^{n}(-is_j\Delta_j)\,e^{-i\epsilon_j(t_{j+1}-t_j)}, \tag{2.33}$$

where

$$\int_{t_0}^{t_f}\mathcal{D}\{t_j\}_n = \int_{t_0}^{t_f} dt_n\int_{t_0}^{t_n} dt_{n-1}\ldots\int_{t_0}^{t_2} dt_1\sum_{\{k_j,k'_j\}_n}.$$

In Chapter 3 this general path integral expression for a D-state system is specialized to the free TLS and then used in the dissipative case.

2.4 Path integral and dissipation: the Feynman-Vernon influence functional

Due to its close resemblance to the classical Langevin equation for a particle subject to a stochastic force, the quantum Langevin equation gives a clear insight into the physics described by the Caldeira-Leggett model. However, for practical calculations beyond the weak coupling approximation, it is more convenient to use the path integral representation of the reduced dynamics.

Consider the system described by the full Hamiltonian $\hat{H}$ in Eq. (1.12) plus a possible external driving term of the type $f(t)\hat{q}(t)$. The full (system plus reservoir) density matrix at the initial time is $\mathcal{W}(t_0)$ and evolves according to

$$\mathcal{W}(t) = U(t,t_0)\mathcal{W}(t_0)U^{\dagger}(t,t_0), \tag{2.34}$$

where the time evolution operator, in the general case of a time dependent driving acting on the particle, is

$$U(t,t_0) = \mathcal{T}\exp\left(-\frac{i}{\hbar}\int_{t_0}^{t} dt'\hat{H}(t')\right). \tag{2.35}$$

The position eigenvalues of the bath oscillators are collectively denoted by $\mathbf{x} := (x_1, \ldots, x_N)$. In the position representation the matrix elements of $\mathcal{W}(t)$ are given by

$$\begin{aligned}\langle q_f, \mathbf{x}_f|\mathcal{W}(t)|q_f', \mathbf{x}_f'\rangle = \int dq_0 dq_0' d\mathbf{x}_0 d\mathbf{x}_0' \langle q_f, \mathbf{x}_f|U(t,t_0)|q_0, \mathbf{x}_0\rangle \\ \times \langle q_0, \mathbf{x}_0|\mathcal{W}(t_0)|q_0', \mathbf{x}_0'\rangle \langle q_0', \mathbf{x}_0'|U^\dagger(t,t_0)|q_f', \mathbf{x}_f'\rangle.\end{aligned} \tag{2.36}$$

Here I have used Eq. (2.34) and inserted two times the identity operator $\int dq_0 d\mathbf{x}_0 |q_0, \mathbf{x}_0\rangle\langle q_0, \mathbf{x}_0|$, before and after $\mathcal{W}(t_0)$. The transition amplitude for the full system in the path integral representation reads

$$\langle q_f, \mathbf{x}_f|U(t,t_0)|q_0, \mathbf{x}_0\rangle = \int_{q_0,\mathbf{x}_0}^{q_f,\mathbf{x}_f} \mathcal{D}q(t)\mathcal{D}\mathbf{x}(t) \exp\left(\frac{i}{\hbar} S[q(t), \mathbf{x}(t)]\right), \tag{2.37}$$

where $S[q(t), \mathbf{x}(t)]$ is the classical action for the full system's path $q(t), \mathbf{x}(t)$ with fixed extrema $(q_0, \mathbf{x}_0)$ at time t_0 and $(q, \mathbf{x})$ at time t

$$S[q(t), \mathbf{x}(t)] = \int_{t_0}^{t} dt' \mathcal{L}(q(t'), \dot{q}(t'), \mathbf{x}(t'), \dot{\mathbf{x}}(t'), t').$$

For brevity, from now on I omit the time dependencies of the coordinates where there is no ambiguity. The classical Lagrangian function for the full system is

$$\mathcal{L}(q, \dot{q}, \mathbf{x}, \dot{\mathbf{x}}, t) = \mathcal{L}_S(q, \dot{q}, t) + \sum_{j=1}^{N} \mathcal{L}_R^j(q, \dot{q}, x_j, \dot{x}_j, t), \tag{2.38}$$

where the bare system Lagrangian is

$$\mathcal{L}_S(q, \dot{q}, t) = \frac{M\dot{q}^2}{2} - V(q) - f(t)q \tag{2.39}$$

and the Lagrangian of the j-th oscillator under the influence of the external time-dependent force exerted by the particle is

$$\mathcal{L}_{RI}^j(q, \dot{q}, x_j, \dot{x}_j) = \frac{\dot{x}_j^2}{2m_j} - \frac{m_j\omega_j^2}{2}\left(x_j - \frac{c_j}{m_j\omega_j^2}q(t)\right)^2. \tag{2.40}$$

The choice of merging the interaction term and the free-bath Lagrangian is motivated by the circumstance that the path integral for a driven harmonic oscillator is exactly resolvable. Instead, in most of the interesting applications, such as the dissipative tunneling dynamics, the strong non-linearity of the potential prevents an exact calculation of the path integral for the bare system, even in the non-driven case.

2.4.1 Factorized initial condition: the Feynman-Vernon influence functional

Suppose that the interaction starts at time t_0 and that the bath is in the unperturbed thermal state of Eq. (1.19). The full density matrix at initial time is then in the factorized form

$$\mathcal{W}(t_0) = \rho(t_0) \otimes \rho_{\text{th}}^R. \tag{2.41}$$

From Eqs. (2.36) and (2.37), the RDM at time t, obtained by tracing out the bath's degrees of freedom, has the formal expression

$$\begin{aligned}\langle q_f|\rho(t)|q'_f\rangle &= \int d\mathbf{x}\langle q_f,\mathbf{x}_f|\mathcal{W}(t)|q'_f,\mathbf{x}_f\rangle \\ &= \int dq_0 dq'_0\langle q_0|\rho(t_0)|q'_0\rangle \int_{q_0}^{q_f}\mathcal{D}q\int_{q'_0}^{q'_f}\mathcal{D}^*q' e^{\frac{i}{\hbar}(S_S[q]-S_S[q'])}\mathcal{F}_{FV}[q,q'],\end{aligned} \tag{2.42}$$

where $S_S[q]$ is the classical action given by the Lagrangian $\mathcal{L}_S$ of the bare system defined in Eq. (2.39). The functional $\mathcal{F}_{FV}$ is the so called *Feynman-Vernon influence functional* whose explicit expression is

$$\mathcal{F}_{FV}[q,q'] = \int d\mathbf{x}_0 d\mathbf{x}'_0\langle \mathbf{x}_0|\rho^R_{\rm th}|\mathbf{x}'_0\rangle \int d\mathbf{x}\int_{\mathbf{x}_0}^{\mathbf{x}_f}\mathcal{D}\mathbf{x}\int_{\mathbf{x}'_0}^{\mathbf{x}_f}\mathcal{D}^*\mathbf{x}' e^{\frac{i}{\hbar}(S_{RI}[\mathbf{x},q]-S_{RI}[\mathbf{x}',q'])}, \tag{2.43}$$

where, using Eq. (2.40),

$$S_{RI}[q,\mathbf{x}] = \sum_{j=1}^{N}\int_{t_0}^{t} dt'\mathcal{L}^j_{RI}(q,\dot{q},x_j,\dot{x}_j). \tag{2.44}$$

Since the bath oscillators are mutually independent, the amplitude for a path of the reservoir under the influence of the particle factorizes as the product of the amplitudes for the single oscillators as follows

$$\int_{\mathbf{x}_0}^{\mathbf{x}_f}\mathcal{D}\mathbf{x}e^{\frac{i}{\hbar}S_{RI}[\mathbf{x},q]} = \prod_{j=1}^{N}\int_{x_{j,0}}^{x_{j,f}}\mathcal{D}x_j e^{\frac{i}{\hbar}S^j_R[x_j,q]}. \tag{2.45}$$

Also the matrix elements of the thermal density matrix, describing the state of the bath at initial time, factorize as the product

$$\langle \mathbf{x}_0|\rho^R_{\rm th}|\mathbf{x}'_0\rangle = \prod_{j=1}^{N}\frac{1}{Z_j}\langle x_{j,0}|e^{-\beta\hat{H}^j_R}|x'_{j,0}\rangle, \tag{2.46}$$

where

$$Z_j = \sum_{n_j=0}^{\infty}\langle n_j|e-\beta\hbar\omega_j\hat{n}_j|n_j\rangle = \frac{1}{1-e^{-\beta\hbar\omega_j}} = \frac{1}{2\sinh(\beta\hbar\omega_j/2)}. \tag{2.47}$$

The path integral for the harmonic oscillator in the presence of a time-dependent potential $V(t)$ is solved in [49]. The solution for the j-th oscillator, in the product on the RHS of Eq. (2.45), is

$$\int_{x_{j,0}}^{x_{j,f}}\mathcal{D}x_j e^{\frac{i}{\hbar}S^j_R[x_j,q]} = \sqrt{\frac{m_j\omega_j}{2\pi i\hbar\sin\left(\omega_j(t-t_0)\right)}}\exp\left(\frac{i}{\hbar}S[x^{\rm Cl}_j(t)]\right), \tag{2.48}$$

where $S[x^{\rm Cl}_j(t)]$ is the action for the classical path $x^{\rm Cl}_j(t)$. This path is the solution of the Euler-Lagrange equation of motion with the Lagrangian function given in Eq. (2.40) and

boundary conditions $x_j(t_0) = x_{j,0}$ and $x_j(t) = x_j$. Explicitly

$$\begin{aligned} S[x_j^{\rm Cl}(t)] =& \frac{m_j\omega_j}{2\sin\left(\omega_j(t-t_0)\right)}\left[(x_{j,0}^2+x_{j,f}^2)\cos\left(\omega_j(t-t_0)\right) - 2x_{j,0}x_{j,f}\right] \\ &+\frac{x_{j,0}c_j}{\sin\left(\omega_j(t-t_0)\right)}\int_{t_0}^{t} dt' \sin\left(\omega_j(t-t')\right) q(t') \\ &+\frac{x_{j,f}c_j}{\sin\left(\omega_j(t-t_0)\right)}\int_{t_0}^{t} dt' \sin\left(\omega_j t'\right) q(t') - \frac{c_j^2}{2m_j\omega_j^2}\int_{t_0}^{t} dt' q^2(t') \\ &-\frac{c_j^2}{m_j\omega_j\sin\left(\omega_j(t-t_0)\right)}\int_{t_0}^{t} dt' \int_{t_0}^{t'} dt'' \sin\left(\omega_j(t-t')\right)\sin\left(\omega_j t''\right) q(t')q(t'') \end{aligned} \tag{2.49}$$

Eq. (2.48) is the path integral expression for the transition amplitude

$$\langle x_{j,0}|e^{-\frac{i}{\hbar}\int_{t_0}^{t} dt' \hat{H}_R^j(t')}|x_{j,f}\rangle \tag{2.50}$$

where $\hat{H}_R^j$ is the Hamiltonian operator of the driven j-th harmonic oscillator, i.e.

$$\hat{H}_R^j(t) = \frac{\hat{p}_j^2}{2m_j} + \frac{m_j\omega_j^2}{2}\left(\hat{x}_j - \frac{c_j}{m_j\omega_j^2}q(t)\right)^2. \tag{2.51}$$

At this point we note the formal identity of the j-th term of the product defining the canonical thermal equilibrium of the bath (Eq. (2.46)) and the transition amplitude of Eq. (2.51). It follows that the solution of the path integral expression for Eq. (2.51), given by Eq. (2.48), represents also the state of the j-th bath's oscillator in the canonical equilibrium state (non-normalized), provided that we express it i) in imaginary time $t = -i\hbar\beta$, ii) with $c_j = 0$ (because the interaction starts at $t > t_0$) and iii) with different endpoints. From Eq. (2.48) and Eq. (2.49), the matrix elements of the product (2.46) are given by

$$\begin{aligned} \langle x_{j,0}|e^{-\beta\hat{H}_R^j}|x'_{j,0}\rangle =& \sqrt{\frac{m_j\omega_j}{2\pi\hbar\sinh(\beta\hbar\omega_j)}} \\ &\times\exp\left\{-\frac{m_j\omega_j}{2\hbar\sinh(\beta\hbar\omega_j)}\left[(x_{j,0}^2+x'^2_{j,0})\cosh(\beta\hbar\omega_j) - 2x_{j,0}x'_{j,0}\right]\right\}. \end{aligned} \tag{2.52}$$

Putting everything together and setting

$$\mathcal{F}_{FV} = \exp(-\Phi_{FV}), \tag{2.53}$$

the influence phase functional Φ_{FV} takes the form

$$\begin{aligned} \Phi_{FV}[y,x] =& \frac{1}{\hbar^2}\int_{t_0}^{t} dt' \int_{t_0}^{t'} dt'' y(t')\left[L'(t'-t'')y(t'') + iL''(t'-t'')x(t'')\right] \\ &+ i\frac{\mu}{2\hbar^2}\int_{t_0}^{t} dt' x(t')y(t'), \end{aligned} \tag{2.54}$$

where I have introduced the relative and center of mass coordinates

$$y(t) = q(t) - q'(t) \quad \text{and} \quad x(t) = q(t) + q'(t), \tag{2.55}$$

and used the the bath correlation function $L(t)$, whose expression is (cf. Eqs. (1.20) and (1.27))

$$L(t) = L'(t) + iL''(t) = \frac{\hbar}{\pi}\int_0^\infty d\omega J(\omega)\left(\coth\frac{\hbar\omega\beta}{2}\cos\omega t - i\sin\omega t\right). \tag{2.56}$$

Performing the time integrations in Eq. (2.54) by parts, with care in exchanging the integrations variables, the Feynman-Vernon influence phase functional can be put in a form convenient in view of working with discrete variables (see below)

$$\begin{aligned}\Phi_{FV}[x,y] = &-\int_{t_0}^t dt'\int_{t_0}^{t'} dt''\Big[\dot y(t')Q'(t'-t'')\dot y(t'') + i\dot y(t')Q''(t'-t'')\dot x(t'')\Big]\\ &+ y(t)\int_{t_0}^t dt'\left[\dot y(t')Q'(t-t') + i\dot x(t')Q''(t-t')\right]\\ &+ y(t_0)\left[y(t)Q'(t-t_0) - \int_{t_0}^t dt'\dot y(t')Q'(t'-t_0)\right]\\ &+ x(t_0)\left[y(t)Q''(t-t_0) - \int_{t_0}^t dt'\dot y(t')Q''(t'-t_0)\right].\end{aligned} \tag{2.57}$$

The function

$$Q(t) = Q'(t) + iQ''(t) = \frac{1}{\pi\hbar}\int_0^\infty d\omega\frac{J(\omega)}{\omega^2}\left[\coth\frac{\hbar\omega\beta}{2}\Big(1-\cos\omega t\Big) + i\sin\omega t\right] \tag{2.58}$$

is related to the bath force correlation function by $L(t)/\hbar^2 = d^2Q(t)/dt^2$ (see Eq. (2.56)).

Substituting in Eq. (2.58) the bath spectral density function in the general continuous limit form given in Sec. 1.4

$$J(\omega) = M\gamma_s\omega_{\rm ph}^{1-s}\omega^s e^{-\omega/\omega_c}, \tag{2.59}$$

the integral can be performed and yields [9]

$$\begin{aligned}Q(t) = &\frac{M\gamma_s}{\pi\hbar}\left(\frac{\omega_c}{\omega_{\rm ph}}\right)^{s-1}\Gamma(s-1)\Big\{1-(1+i\omega_c t)^{1-s} + 2(\hbar\beta\omega_c)^{1-s}\zeta(s-1,1+\kappa)\\ &-(\hbar\beta\omega_c)^{1-s}\left[\zeta(s-1,1+\kappa+i\kappa\omega_c t) + \zeta(s-1,1+\kappa-i\kappa\omega_c t)\right]\Big\},\end{aligned} \tag{2.60}$$

where the dimensionless quantity $\kappa = (\hbar\beta\omega_c)^{-1}$ is a measure of the ratio between the temperature and the cutoff frequency. The function $\zeta(z,q)$ is the Hurwitz zeta function, related to the Riemann zeta function $\zeta(z)$ by $\zeta(z) \equiv \zeta(z,1)$, and $\Gamma(z)$ is the Euler gamma function.

The limit $s \to 1$ of Eq. (2.60) gives $Q(t)$ in the Ohmic case

$$Q(t) = \frac{M\gamma}{\pi\hbar}\ln\left(\frac{\kappa^{-1}\Gamma^2(1+\kappa)}{\Gamma(\kappa+i\kappa\omega_c t)\Gamma(1+\kappa-i\kappa\omega_c t)}\right). \tag{2.61}$$

At finite temperature and assuming a high frequency cutoff $\omega_c \gg \omega_0$ i.e. in the limit $\kappa \ll 1$, the function $Q(t)$ has the form

$$Q(t) = \frac{M\gamma}{\pi\hbar}\ln\left(\sqrt{1+\omega_c^2t^2}\frac{\sinh(\pi\kappa\omega_c t)}{\pi\kappa\omega_c t}\right) + i\frac{M\gamma}{\pi\hbar}\arctan(\omega_c t). \tag{2.62}$$

The long time or high temperature limit ($\kappa\omega_c t \gg 1$) of Eq. (2.62) has a linear dependence on time

$$Q(t) \simeq \frac{M\gamma}{\pi\hbar}\left[\frac{\pi}{\hbar\beta}t - \ln\left(\frac{2\pi}{\beta\hbar\omega_c}\right)\right] + i\frac{M\gamma}{2\hbar}. \tag{2.63}$$

2.5 Discrete variable representation

The exact path integral expression for the reduced dynamics (Eq. (2.42)) can be computed only in special cases. As noticed above, in the presence of nonlinear potentials, approximate solutions have to be found based on spatial discretization, which in turn is attained by restricting the Hilbert space of the open system. Specifically, based on the assumption that, given the initial condition and the damping/temperature regime, the system is not likely to visit high-energy states during its time evolution, the Hilbert space of the system is restricted to that spanned by the first D energy eigenstates. Thus the problem reduces to that of a dissipative D-state system.

The continuum of position states turns into a discrete set of states localized around a grid of D position eigenvalues $Q_1, \ldots, Q_D$, where

$$\hat{q}|Q_j\rangle = Q_j|Q_j\rangle. \tag{2.64}$$

In this picture, called discrete variable representation (DVR), the paths of the coordinates q and q' are represented by a sequence of transitions among the positions Q_j. Consider a path of the coordinate $q(\tau)$ (where $t_0 \leq \tau \leq t$) with N transitions at times $t_1, \ldots, t_N \in (t_0, t)$. In the DVR this path is parametrized by

$$\begin{aligned} q(\tau) &= \sum_{j=0}^{N-1} q_j \left[\Theta(\tau - t_j) - \Theta(\tau - t_{j+1})\right] + q_N \Theta(\tau - t_N) \\ &= q_0 \Theta(\tau - t_0) + \sum_{j=1}^{N} (q_j - q_{j-1})\, \Theta(\tau - t_j). \end{aligned} \tag{2.65}$$

As a consequence the paths of relative and center of mass coordinates read

$$\begin{aligned} y(\tau) &= \sum_{j=0}^{N} \xi_j \Theta(\tau - t_j) \\ x(\tau) &= \sum_{j=0}^{N} \chi_j \Theta(\tau - t_j), \end{aligned} \tag{2.66}$$

where, for $j \neq 0$, the quantities ξ and χ, called *charges* (for the reasons shown below), are defined by

$$\begin{aligned} \xi_j &= (q_j - q_{j-1}) - (q'_j - q'_{j-1}) \\ \chi_j &= (q_j - q_{j-1}) + (q'_j - q'_{j-1}), \end{aligned} \tag{2.67}$$

whereas $\xi_0/\chi_0 \equiv q_0 \mp q'_0$. Notice that, with this definition, the ξ-charges in a path sum up to the value $y(\tau = t)$ of the relative coordinate at the final time t

$$\begin{aligned} \sum_{j=0}^{N} \xi_j =& q_0 - q'_0 + (q_1 - q_0) - (q'_1 - q'_0) \\ &+ \cdots + (q_N - q_{N-1}) - (q'_N - q'_{N-1}) = q_N - q'_N = y_N. \end{aligned} \tag{2.68}$$

The time derivatives of the y and x coordinates, entering in the phase of the influence functional (see Eq. (2.57)), are

$$\begin{aligned} \dot{y}(\tau) &= \sum_{j=0}^{N} \xi_j \delta(\tau - t_j) \\ \dot{x}(\tau) &= \sum_{j=0}^{N} \chi_j \delta(\tau - t_j). \end{aligned} \tag{2.69}$$

2.6 Feynman-Vernon influence for the populations in the DVR

We now focus on the calculation of the populations, i.e. the diagonal elements of the RDM, in the position representation. The population $\rho_{kk}(t) \equiv \langle q_k|\rho(t)|q_k\rangle$ gives the probability of finding the particle *localized* around the position q_k at time t.

$$\rho_{kk}(t) = \int dq_0 \int dq_0' G(q_k, q_k, t; q_0, q_0', t_0) \rho_{q_0 q_0'}(t_0). \tag{2.70}$$

In the path integral approach the paths contributing to the summation which gives ρ_{kk} are those ending in a diagonal configuration at the final time t, i.e. those for which $y(\tau = t) = 0$. The Feynman-Vernon influence phase in Eq. (2.57) for these paths reduces to

$$\begin{aligned} \Phi_{FV}[x, y] = &- \int_{t_0}^{t} dt' \int_{t_0}^{t'} dt'' \left[\dot{y}(t') Q'(t' - t'') \dot{y}(t'') + i \dot{y}(t') Q''(t' - t'') \dot{x}(t'') \right] \\ &- x(t_0) \int_{t_0}^{t} dt' \dot{y}(t') Q''(t' - t_0). \end{aligned} \tag{2.71}$$

Substituting Eq. (2.69) in Eq. (2.71) we find

$$\begin{aligned} \Phi_{FV}[\xi, \chi] &= - \sum_{i=1}^{N} \sum_{j=0}^{i-1} \left(\xi_i Q'_{ij} \xi_j + i \xi_i Q''_{ij} \chi_j \right) - \chi_0 \sum_{i=0}^{N} \xi_i Q''_{j0} \\ &\simeq - \sum_{i=1}^{N} \sum_{j=0}^{i-1} \left(\xi_i Q'_{ij} \xi_j + i \xi_i Q''_{ij} \chi_j \right). \end{aligned} \tag{2.72}$$

Here the shorthand notation $Q_{ij} \equiv Q(t_i - t_j)$ it is used. The second term in Eq. (2.72) describes a transient effect which can be neglected for Ohmic damping with large ω_c. Indeed, for times $t \gtrsim 1/\omega_c$, from Eq. (2.62) we have $Q'' \sim M\gamma/2\hbar$. Thus the second term is approximated by the quantity $M\gamma/2\hbar\chi_0 \sum_{i=0}^{N} \xi_i = M\gamma/2\hbar\chi_0 y_N$ (see Eq. (2.68)), which vanishes, since y_N is equal to zero for the contributing paths in the calculation of the populations.

From Eq. (2.72) we see that the Feynman-Vernon functional couples the ξ- and χ-charges through the function $Q(t)$, called *pair interaction* [9]. This explains the name *charges*. The nature of the coupling is nonlocal in time and reflects the non-Markovian character of the general time evolution for a dissipative quantum system. This feature constitutes a major difficulty in the practical evaluation of the propagator.

Using the expression (2.33) for the amplitudes relative to the bare system and Eq. (2.72) for the phase of the Feynman-Vernon influence functions, the exact path integral expression for the propagator $G(q_k, q_k, t; q_0, q_0', t_0)$ of the dissipative D-state system is

$$\begin{aligned} G(q_k, q_k, t; q_0, q_0', t_0) = \sum_{N=0}^{\infty} \int_{t_0}^{t} \mathcal{D}_N\{t_j\} B_0(t_1 - t_0) \prod_{j=1}^{N} (-i)\, \Delta_j B_j(t_{j+1} - t_j) \\ \times \exp\left(\sum_{i=1}^{N} \sum_{l=0}^{i-1} \left(\xi_i Q_{il}' \xi_l + i \xi_i Q_{il}'' \chi_l \right) \right). \end{aligned} \tag{2.73}$$

The $N = 0$ term in this sum is $\delta_{q_0' q_0} \delta_{q_0 q_k}$. Equation (2.73) is the propagator for the populations in the DVR in the presence of dissipation. It reduces to the free case (Eq. (2.33)) if the coupling with the environment is turned off.

The q/q' transition amplitudes per unit time Δ_j in Eq. (2.73) are defined by

$$\Delta_j = \begin{cases} \frac{1}{\hbar} \langle q_j | \hat{H}_S | q_{j-1} \rangle & \text{for a } q \text{ transition} \\ -\frac{1}{\hbar} \langle q_j' | \hat{H}_S | q_{j-1}' \rangle & \text{for a } q' \text{ transition} \end{cases}, \tag{2.74}$$

and the *bias factors* by

$$B_j(t_{j+1} - t_j) = \exp\left[-i \epsilon_j (t_{j+1} - t_j) \right], \tag{2.75}$$

where

$$\epsilon_j = \frac{1}{\hbar} \left(\langle q_j | \hat{H}_S | q_j \rangle - \langle q_j' | \hat{H}_S | q_j' \rangle \right). \tag{2.76}$$

2.7 Conclusions

In this chapter the path integral approach to the dissipation in quantum Mechanics was introduced. The path integral representation of the reduced dynamics features the Feynman-Vernon influence functional. The discrete variable version of the functional was given along with the picture of interacting charges, which will be exploited for carrying out the approximations in the next chapter.

Chapter 3

The dissipative Two-Level System

[*Part of the present chapter is published in collaboration with Prof. D. Valenti*[1]*, Prof. B. Spagnolo*[1] *and Prof. M. Grifoni*[2] [50]]

Consider a quantum particle subject to a double well potential such as the one associated to a flux qubit, shown in Fig. 1.3. If the particle is initially in a superposition of the two lower energy states ($|g\rangle$ and $|e\rangle$) and the temperature is low enough, to a good approximation the system can be considered a *two-level system* (TLS) and the model in Eq. (1.12) reduces to the celebrated *spin-boson* (SB) model [51]. A picture of the TLS dynamics in terms of tunneling from one well to the other is given by the localized basis, where the left/right well states $|R/L\rangle$ are combinations of $|g\rangle$ and $|e\rangle$.

For the SB dynamics there exist various approximation schemes. When the system is weakly coupled to the heat bath (usually this is the case for quantum optical systems and qubit setups), the approach traditionally used is that of a Born-Markov master equation for the RDM [52]. It captures well the coherent tunneling dynamics, characterized by the relaxation and dephasing rates $\Gamma_{rel} = \tau_1^{-1}$ and $\Gamma_{ph} = \tau_2^{-1}$, respectively.

However, the perturbative in the coupling character of this approach makes it unsuited in situations where the coupling is not weak. In this case the real-time path integral techniques can be used to trace out the bath degrees of freedom and obtain a still exact formal expression for the RDM. This expression can, in some cases, be numerically evaluated by tensor multiplication [53] or using Monte Carlo or stochastic techniques [54**?** –56]. However, the numerical evaluation of the path integral is a hard task, especially at long times.

It is therefore convenient to have an equation for the RDM in the form of the Nakajima-Zwanzig equation [42], which captures the non-Markovian reduced dynamics of a general system plus bath model. The difficult task, in this case, is to have a reasonably simple expression for the kernel.

Starting from the real-time path integral expression for the particle's RDM, there are different approximation schemes, all yielding a generalized (integro-differential) master equation for the populations in a spatially localized representation. By tracing out the bath degrees of freedom, the amplitude associated to a path has the factorized form of a bare amplitude, relative to the free system, multiplied by the Feynman-Vernon (FV)

[1]Dipartimento di Fisica e Chimica, Università di Palermo.
[2]Theoretische Physik, Universität Regensburg, Regensburg Germany.

influence functional [57] which weights the path according to the effect exerted by the particle's motion on the bath degrees of freedom.

The FV influence introduces nonlocal in time correlations inside the paths which make the path integral expression intractable when the confining potential is anharmonic. For the SB dynamics the simplest, non-perturbative in the coupling approximation is the non-interacting blip approximation (NIBA) [51]. The NIBA scheme neglects the nonlocal part of the correlations due to an exponential cutoff in the FV functional, which is effective at high temperature and/or strong damping. This approach, while being non-perturbative in the coupling, is perturbative in the tunneling Δ.

In the opposite damping regime, the weak coupling approximation (WCA) [58], treating the coupling to the first order and Δ to all orders, is appropriate. It gives the same results as the Born-Markov approach. Finally, an approach exists which interpolates between these two extrema by considering the local correlations fully and the nonlocal ones to the first order in the coupling. This scheme is called weakly interacting blip approximation (WIBA) [59], and, by construction, also covers the intricate regime of intermediate temperatures and damping, where both the WCA and the NIBA fail.

In this chapter the three above approximation schemes are implemented in the kernels of a generalized master equation derived within the path integral approach, and their validity discussed. The predictions for the TLS dynamics obtained using these approximation schemes are shown in different dissipation regimes.

3.1 Two-level system Hamiltonian and parametrization

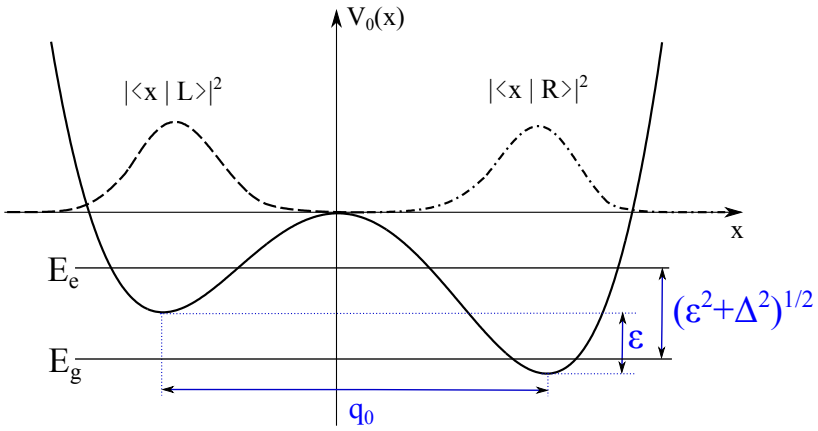

Figure 3.1: Potential and energy levels for a bistable system in the TLS approximation and probability density relative to the left and right localized states $|L/R\rangle$, defined in Eq. (1.8).

The TLS Hamiltonian in the localized basis $|R\rangle, |L\rangle$ is

$$\hat{H}_{TLS} = -\frac{\hbar}{2}(\Delta\sigma_x + \epsilon\sigma_z), \tag{3.1}$$

where Δ is the tunneling frequency, ϵ is the (static) bias. The spin operators in the localized basis are $\sigma_z = |R\rangle\langle R| - |L\rangle\langle L|$ and $\sigma_x = |R\rangle\langle L| + |L\rangle\langle R|$.

A path of the TLS consists of a sequence of alternating blips ($y \neq 0$) of length $\tau_j = t_{2j} - t_{2j-1}$ and sojourns ($y = 0$) of length $\sigma_j = t_{2j+1} - t_{2j}$. Consequently, if the system starts and ends in a sojourn, every path will have an even number $2n$ of transitions. The two ξ-charges in the same blip (say the i-th blip) are opposite in sign ($\xi_{2i} = -\xi_{2i-1}$) and the same is true for the two χ-charges in the same sojourn ($\chi_{2i+1} = -\chi_{2i}$).

A convenient parametrization for the TLS is in terms of the new charges ζ and η, scaled with q_0 and associated with blips and sojourns, respectively. They are defined by

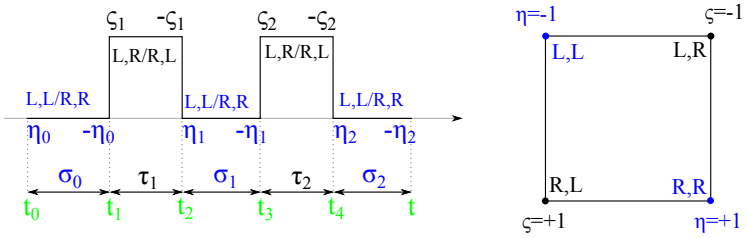

Figure 3.2: Parametrization of the TLS in terms of the sojourn and blip states η and ζ. These are related to the χ- and ξ-charges by Eq. (3.2). *Left panel* - An example of TLS path with $2n = 4$ transitions. *Right panel* - TLS states and corresponding values of η and ζ.

(see Fig. 3.2)

$$\begin{array}{l} \xi_{2j-1} = q_0\zeta_j \\ \xi_{2j} = -q_0\zeta_j \end{array} \quad j = 1, \ldots, n \qquad \text{and} \qquad \begin{array}{l} \chi_{2j} = q_0\eta_j \\ \chi_{2j+1} = -q_0\eta_j \end{array} \quad j = 0, \ldots, n \tag{3.2}$$

If the system is in the diagonal state L, L (R, R) then $\eta = -1$ $(\eta = +1)$, whereas if the system is in the blip state L, R (R, L) then $\zeta = -1$ $(\zeta = +1)$. Using this parametrization and considering the tunneling elements and the bias factor as given by the TLS Hamiltonian of Eq. (3.1), the bare system's amplitude for a path of $2n$ transitions, starting in the sojourn η_0 and ending in the sojourn state $\eta_n \equiv \eta$, reads

$$\prod_{j=1}^{n}(-i\eta_{j-1}\zeta_j)\frac{\Delta}{2}(-i\eta_j\zeta_j)\frac{\Delta}{2}\exp(-i\zeta_j\epsilon\tau_j) = \eta\eta_0\left(-\frac{\Delta^2}{4}\right)^n \exp\left(-i\sum_{j=1}^{n}\zeta_j\epsilon\tau_j\right), \tag{3.3}$$

where we used the property $\eta_j^2 = \zeta_j^2 = 1$.

3.1.1 Free TLS dynamics with the path integral approach

The general path integral expression for the populations, in the free TLS case ($F_{FV} = 1$), with the parametrization given in Eq. (3.2), becomes

$$P(\eta, t|\eta_0, t_0) = \delta_{\eta\eta_0} + \eta\eta_0 \sum_{n=1}^{\infty}\left(-\frac{\Delta^2}{4}\right)^n \sum_{\{\eta\}_{n-1}}\sum_{\{\zeta\}_n}\int_{t_0}^{t} dt_{2n}\ldots\int_{t_0}^{t_2} dt_1 \prod_{i=1}^{n}\exp\left(-i\zeta_i\epsilon\tau_i\right).$$

Consider the $|R\rangle$ $(|L\rangle)$ state population corresponding to $\eta = +1$ $(\eta = -1)$. The sum over the intermediate sojourns sates yields a factor 2^{n-1}, while the sum over the blip states ζ gives the product of the n factors $2\cos(\epsilon\tau_j)$. Changing the integration variables into the blip and sojourn times and taking the Laplace transform (as explained in Appendix **??**)

one gets a factor $1/\lambda$ for each of the $n+1$ sojourns. The resulting expression in Laplace space is

$$\begin{aligned} P(\eta,\lambda|\eta_0,t_0) =& \frac{\delta_{\eta,\eta_0}}{\lambda} - \frac{\eta\eta_0}{2\lambda} + \frac{\eta\eta_0}{2\lambda}\sum_{n=0}^{\infty}\left(-\frac{\Delta^2}{\lambda^2+\epsilon^2}\right)^n \\ =& \frac{\delta_{\eta,\eta_0}}{\lambda} - \frac{\eta\eta_0}{2\lambda} + \frac{\eta\eta_0}{2\lambda}\frac{\lambda^2+\epsilon^2}{\lambda^2+E^2/\hbar^2}, \end{aligned} \tag{3.4}$$

where $E=\hbar\sqrt{\Delta^2+\epsilon^2}$. This expression is transformed back to the time domain using the Bromwich integral

$$\mathcal{L}^{-1}\{P(\eta,\lambda|\eta_0,t_0)\} = \frac{1}{2\pi i}\int_{c-i\infty}^{c+i\infty} e^{\lambda t}P(\eta,\lambda|\eta_0,t_0). \tag{3.5}$$

We explicitly calculate the survival probability in the state $|L\rangle$ ($\eta=\eta_0=-1$). The function

$$P(-1,\lambda|-1,t_0) = \frac{1}{2\lambda}\frac{2\lambda^2+E^{2/\hbar}+\epsilon^2}{\lambda^2+E^2/\hbar^2} \tag{3.6}$$

has poles at $\lambda=0,\pm iE/\hbar$ so that, performing the inverse Laplace transform, in the time domain it reads

$$P(-1,t|-1,t_0) = \frac{\hbar^2\epsilon^2}{E^2} + \frac{\hbar^2\Delta^2}{E^2}\cos^2\left(\frac{Et}{2\hbar}\right), \tag{3.7}$$

which coincides with the result in Eq. (2.20).

3.2 Feynman-Vernon influence functions for the TLS

Now we consider the Feynman-Vernon influence function for the TLS. To this end we introduce the dimensionless functions

$$S(t) = q_0^2 Q'(t) \qquad \text{and} \qquad R(t) = q_0^2 Q''(t). \tag{3.8}$$

Using the TLS parametrization introduced above, the phase of the influence function, whose expression for a generic M-level is given in Eq. (2.72), can then be put in the form ($N=2n$)

$$\Phi_{FV}[\zeta,\eta]_n = \sum_{i=1}^{n} S_{2i,2i-1}\sum_{i=2}^{n}\sum_{j=1}^{i-1}\zeta_i\Lambda_{i,j}\zeta_j - i\sum_{i=1}^{n}\sum_{j=0}^{i-1}\zeta_i X_{i,j}\eta_j, \tag{3.9}$$

where

$$\begin{aligned} \Lambda_{i,j} &= S_{2i,2j-1} + S_{2i-1,2j} - S_{2i,2j} - S_{2i-1,2j-1} \\ X_{i,j} &= R_{2i-1,2j} + R_{2i,2j+1} - R_{2i,2j} - R_{2i-1,2j+1}. \end{aligned} \tag{3.10}$$

(see Fig. 3.3). Note that, since $R(0)=0$, the functions $X_{i,i-1}\equiv Y_{i,i-1}$ are the sum of only three non-vanishing terms

$$Y_{i,i-1} = R_{2i-1,2i-2} + R_{2i,2i-1} - R_{2i,2i-2} - \underbrace{R_{2i-1,2i-1}}_{=0}. \tag{3.11}$$

The functions Y take into account the *blip-preceding-sojourn* interactions. Rearranging the sums in Eq. (3.9)

$$\Phi_{FV}[\zeta,\eta]_n = \sum_{i=1}^{n} S_{2i,2i-1} + \sum_{j=1}^{n-1}\sum_{i=j+1}^{n}\zeta_i\Lambda_{i,j}\zeta_j - i\sum_{j=0}^{n-1}\sum_{i=j+1}^{n}\zeta_i X_{i,j}\eta_j, \tag{3.12}$$

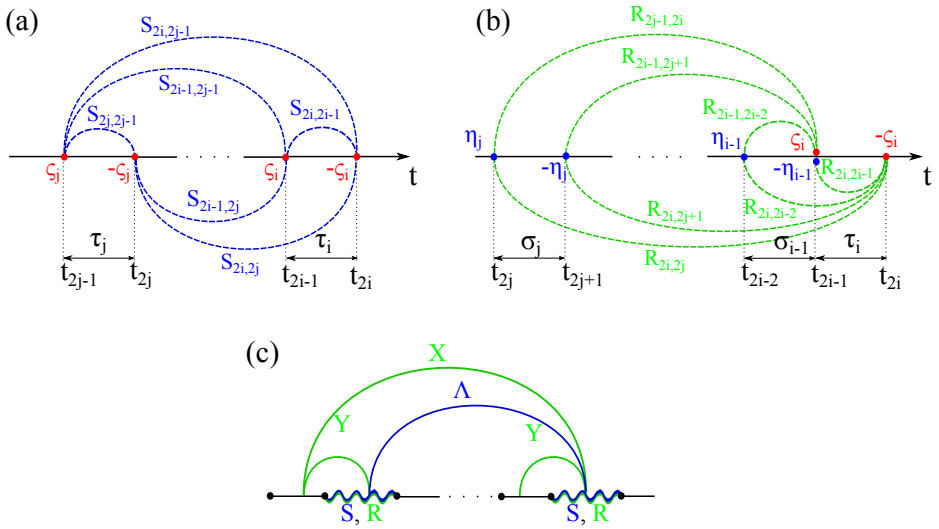

Figure 3.3: Interactions introduced by the FV influence phase in Eq. (3.12). (a) - Interactions (blue dotted lines) between a couple of blips inside a longer sequence constituting a TLS path. (b) - Interactions (green dotted lines) among a blip and pair of sojourns, one of which (the sojourn $i-1$) directly precedes the blip. Red and blue dots indicate the interacting charges. Time differences are indicated by transition time indexes. Transition times and blip/sojourn times are in the low part of the figures. (c) - Blip-blip, blip-preceding sojourn and intra-blip interactions collectively indicated by the symbols defined in Eqs. (3.10) and (3.11).

3.3 Exact path integral expressions of the conditional probabilities for the dissipative TLS

Using Eq. (3.3) and Eq. (3.9) in the general path integral expression for the system propagator we can now write the formal expression for $P(\eta, t|\eta_0, t_0)$, which is the probability of finding the system in the sojourn η at time t, given that it started in the sojourn state η_0 at time t_0 (see the left panel of Fig. 3.2). A contributing path has an even number $2n$ of transitions, with $n+1$ sojourns interrupted by n blips. The resulting general expression for the conditional probabilities is

$$P(\eta, t|\eta_0, t_0) = \delta_{\eta\eta_0} + \eta\eta_0 \sum_{n=1}^{\infty} \left(-\frac{\Delta^2}{4}\right)^n \sum_{\{\eta\}_{n-1}} \sum_{\{\zeta\}_n} \int_{t_0}^{t} dt_{2n} \ldots \int_{t_0}^{t_2} dt_1 \times \exp\left(-i \sum_{i=1}^{n} \zeta_i \epsilon \tau_i\right) \exp\left(-\Phi_{FV}[\zeta, \eta]_n\right). \tag{3.13}$$

Notice that, since the initial and final sojourns are fixed, the sum over the paths with $2n$ transitions is realized by the sum over the $n-1$ intermediate sojourn states ($\{\eta\}_{n-1} = \eta_1, \ldots, \eta_{n-1} = \pm 1$) and over the n-blip states ($\{\zeta\}_n = \zeta_1, \ldots, \zeta_n = \pm 1$).

In the influence phase (Eq.(3.12)) we isolate the $j = 0$ terms in the last sum, because

η_0 is fixed

$$-i\sum_{j=0}^{n-1}\sum_{i=j+1}^{n}\zeta_i X_{i,j}\eta_j = -i\eta_0\sum_{i=1}^{n}\zeta_i X_{i,0} - i\sum_{j=1}^{n-1}\eta_j\left(\sum_{i=j+1}^{n}\zeta_i X_{i,j}\right).$$

Performing the sum over the intermediate sojourns η in Eq. (3.13), we get

$$\begin{aligned}P(\eta,t|\eta_0,t_0) =&\delta_{\eta\eta_0} + \eta\eta_0\frac{1}{2}\sum_{n=1}^{\infty}\left(-\frac{\Delta^2}{2}\right)^n\sum_{\{\zeta_i=\pm1\}_n}\int_{t_0}^{t}dt_{2n}\ldots\int_{t_0}^{t_2}dt_1\\ &\times\exp\left(-i\sum_{i=1}^{n}\zeta_i\left(\epsilon\tau_i-\eta_0 X_{i,0}\right)\right)\exp\left(-\sum_{i=1}^{n}S_{2i,2i-1}\right)\\ &\times\exp\left(-\sum_{j=1}^{n-1}\sum_{i=j+1}^{n}\zeta_i\Lambda_{i,j}\zeta_j\right)\prod_{j=1}^{n-1}\cos\left(\sum_{i=j+1}^{n}\zeta_i X_{i,j}\right),\end{aligned} \tag{3.14}$$

where we used the formula

$$\sum_{\{\eta_j=\pm1\}_m}\prod_{j=1}^{m}\exp\left\{-i\eta_j x_j\right\} = 2^m\prod_{j=1}^{m}\cos\left(x_j\right). \tag{3.15}$$

We write the first exponential in Eq. (3.14) as $\cos(x) - i\sin(x)$. This factor is multiplied by an even function of the ζ's so that, once we perform the summation over ζ, the contribution of the sine part vanishes. Moreover we express the cosine part as $\cos(a)\cos(b) + \eta_0\sin(a)\sin(b)$. Doing this, the amplitudes in the path integral expression of Eq. (3.14) can be written as the sum of two terms, symmetric and antisymmetric in the bias ϵ:

$$\begin{aligned}P(\eta,t|\eta_0,t_0) = \delta_{\eta\eta_0}+&\eta\eta_0\frac{1}{2}\sum_{n=1}^{\infty}\left(-\frac{\Delta^2}{2}\right)^n\int_{t_0}^{t}dt_{2n}\ldots\int_{t_0}^{t_2}dt_1\\ &\times\sum_{\{\zeta_i=\pm1\}_n}\left(B_n^{(s)}F_n^{(+)}+\eta_0 B_n^{(a)}F_n^{(-)}\right)\end{aligned} \tag{3.16}$$

where we have introduced the symmetric and antisymmetric *bias factors*

$$B_n^{(s)} = \cos\left(\sum_{i=1}^{n}\zeta_i\epsilon\tau_i\right) \qquad \text{and} \qquad B_n^{(a)} = \sin\left(\sum_{i=1}^{n}\zeta_i\epsilon\tau_i\right) \tag{3.17}$$

and the *influence functions*

$$\begin{aligned}F_n^{(+)} &= G_n\prod_{j=0}^{n-1}\cos\left(\sum_{i=j+1}^{n}\zeta_i X_{i,j}\right)\\ F_n^{(-)} &= G_n\sin\left(\sum_{i=1}^{n}\zeta_i X_{i,0}\right)\prod_{j=1}^{n-1}\cos\left(\sum_{i=j+1}^{n}\zeta_i X_{i,j}\right),\end{aligned} \tag{3.18}$$

where

$$G_n = \exp\left(-\sum_{i=1}^{n}S_{2i,2i-1}\right)\exp\left(-\sum_{j=1}^{n-1}\sum_{i=j+1}^{n}\zeta_i\Lambda_{i,j}\zeta_j\right).$$

3.4 Generalized master equation for the population difference

The conditional population difference P_{η_0} is the difference between the conditional population of the $|R\rangle$ state ($\eta = +1$) and that of the $|L\rangle$ state ($\eta = -1$)

$$P_{\eta_0}(t) = P(+1, t|\eta_0, t_0) - P(-1, t|\eta_0, t_0) = 2P(+1, t|\eta_0, t_0) - 1. \tag{3.19}$$

It coincides with the expectation value of the σ_z operator, given the initial condition $P_{\pm 1}(t_0) = \pm 1$. Using Eq. (3.16) for the conditional populations of the TLS, the conditional population difference for a general initial state $\eta_0 = \pm 1$ reads

$$P_{\eta_0}(t) = \eta_0 + \sum_{n=1}^{\infty} \left(-\frac{\Delta^2}{2}\right)^n \int_{t_0}^{t} dt_{2n} \ldots \int_{t_0}^{t_2} dt_1 \sum_{\{\zeta_j = \pm 1\}_n} \left(\eta_0 B_n^{(s)} F_n^{(+)} + B_n^{(a)} F_n^{(-)}\right), \tag{3.20}$$

where we used $\delta_{+1,\eta_0} - \delta_{-1,\eta_0} = \eta_0$ and $\eta_0^2 = 1$. Notice that the stationary value of P_{η_0} doesn't depend on the initial state η_0 since the symmetric in the bias part of $P_{\eta_0}(\infty)$ vanishes (the population difference at equilibrium for the unbiased system must be zero).

In this section we obtain the exact generalized (integro-differential) master equation (GME) for P_{η_0}, and in the next sections we obtain the dynamics of the TLS by making suitable approximations on the kernels of the GME. We start by making the following general *ansatz* [60]

$$\dot{P}(\eta, t|\eta_0, t_0) = \sum_{\eta'=\pm 1} \int_{t_0}^{t} dt' K(\eta, t; \eta', t') P(\eta', t'|\eta_0, t_0), \qquad \eta = \pm 1. \tag{3.21}$$

Since, for the conservation of probability $P(+1, t|\eta_0, t_0) + P(-1, t|\eta_0, t_0) = 1$, we have $\dot{P}(+1, t|\eta_0, t_0) + \dot{P}(-1, t|\eta_0, t_0) = 0$, then $K(+1, t; \eta', t') + K(-1, t; \eta', t') = 0$, so the GME for the population difference reads

$$\dot{P}_{\eta_0}(t) = \int_{t_0}^{t} dt' \left[K^{(+)}(t, t') P_{\eta_0}(t') + K^{(-)}, (t, t')\right] \tag{3.22}$$

where

$$\begin{aligned} K^{(+)}(t, t') &= K(+1, t; +1, t') + K(-1, t; -1, t') \equiv K_{RR}(t, t') + K_{LL}(t, t'), \\ K^{(-)}(t, t') &= K(+1, t; +1, t') - K(-1, t; -1, t') \equiv K_{RR}(t, t') - K_{LL}(t, t'). \end{aligned} \tag{3.23}$$

Now we substitute Eq. (3.20) in the right hand side of Eq. (3.22) and compare the result, order by order in Δ^2, with the time derivative of Eq. (3.20), to find the kernels $K^{(\pm)}$ in terms of the influence functions $B_n^{(s/a)} F_n^{(\pm)}$. The time derivative of $P_{\eta_0}(t)$ is

$$\dot{P}_{\eta_0}(t) = \sum_{n=1}^{\infty} \left(-\frac{\Delta^2}{2}\right)^n \int_{t_0}^{t} dt_{2n-1} \ldots \int_{t_0}^{t_2} dt_1 \sum_{\{\zeta_i = \pm 1\}_n} \left\{\eta_0 B_n^{(s)} F_n^{(+)} + B_n^{(a)} F_n^{(-)}\right\}. \tag{3.24}$$

- At the first order in Δ^2

$$K^{(+)}(t,t')^{(1)} = -\frac{\Delta^2}{2}\sum_{\zeta_1=\pm1} B_1^{(s)}F_1^{(+)}(t,t'),$$
$$K^{(-)}(t,t')^{(1)} = -\frac{\Delta^2}{2}\sum_{\zeta_1=\pm1} B_1^{(a)}F_1^{(-)}(t,t').$$

- At the second order in Δ^2, using $\int_{t_0}^{t} dt' \int_{t_0}^{t'} dt'' = \int_{t_0}^{t} dt'' \int_{t''}^{t} dt'$,

$$K^{(+)}(t,t')^{(2)} = \left(-\frac{\Delta^2}{2}\right)^2 \int_{t'}^{t} dt_3 \int_{t'}^{t_3} dt_2 \sum_{\zeta_1,\zeta_2=\pm1} \tilde{B}_2^{(s)}\tilde{F}_2^{(+)}(t,t_3,t_2,t'),$$
$$K^{(-)}(t,t')^{(2)} = \left(-\frac{\Delta^2}{2}\right)^2 \int_{t'}^{t} dt_3 \int_{t'}^{t_3} dt_2 \sum_{\zeta_1,\zeta_2=\pm1} \tilde{B}_2^{(a)}\tilde{F}_2^{(-)}(t,t_3,t_2,t').$$

Here we have introduced the symmetric and antisymmetric *irreducible* influence functions of order 2. Irreducible means that they consist of the part of the original influence functions that cannot be expressed as the product of lower order, non-interacting parts. This is shown for the $n = 2$ case in Fig. 3.4.

$$\tilde{B}_2^{(s)}\tilde{F}_2^{(+)} = B_2^{(s)}F_2^{(+)} - B_1^{(s)}F_1^{(+)}B_1^{(s)}F_1^{(+)}$$
$$\tilde{B}_2^{(a)}\tilde{F}_2^{(-)} = B_2^{(a)}F_2^{(-)} - B_1^{(s)}F_1^{(+)}B_1^{(a)}F_1^{(-)}$$

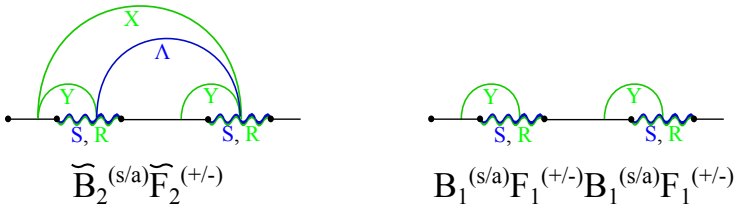

Figure 3.4: Interactions in an irreducible (left) and a reducible (right) second order kernel.

- Finally, at order n in Δ^2

$$K^{(+)}(t,t')^{(n)} = \left(-\frac{\Delta^2}{2}\right)^n \int_{t'}^{t} dt_{2n-1}\ldots\int_{t'}^{t_3} dt_2 \sum_{\{\zeta_i=\pm1\}_n} \tilde{B}_n^{(s)}\tilde{F}_n^{(+)},$$
$$K^{(-)}(t,t')^{(n)} = \left(-\frac{\Delta^2}{2}\right)^n \int_{t'}^{t} dt_{2n-1}\ldots\int_{t'}^{t_3} dt_2 \sum_{\{\zeta_i=\pm1\}_n} \tilde{B}_n^{(a)}\tilde{F}_n^{(-)},$$

where the *irreducible* influence functions of order n are given by

$$\tilde{B}_n^{(s/a)}\tilde{F}_n^{(+/-)} = B_n^{(s/a)}F_n^{(+/-)} - \sum_{j=2}^{n}(-1)^j \sum_{m_1,\ldots,m_j} B_{m_1}^{(s)}F_{m_!}^{(+)}B_{m_2}^{(s)}F_{m_2}^{(+)}\ldots B_{m_j}^{(s/a)}F_{m_j}^{(+/-)}\delta_{m_1+\cdots+m_j,n}. \tag{3.25}$$

The result for the symmetric and antisymmetric irreducible kernels is then

$$\begin{aligned} K^{(+)}(t,t') =& -\frac{\Delta^2}{2}\sum_{\xi_1=\pm1} B_1^{(s)} F_1^{(+)}(t,t') \\ &+\sum_{n=2}^{\infty}\left(-\frac{\Delta^2}{2}\right)^n \int_{t'}^{t} dt_{2n-1}\ldots\int_{t'}^{t_3} dt_2 \sum_{\{\zeta_i=\pm1\}_n} \tilde{B}_n^{(s)}\tilde{F}_n^{(+)}, \\ K^{(-)}(t,t') =& -\frac{\Delta^2}{2}\sum_{\xi_1=\pm1} B_1^{(a)} F_1^{(-)}(t,t') \\ &+\sum_{n=2}^{\infty}\left(-\frac{\Delta^2}{2}\right)^n \int_{t'}^{t} dt_{2n-1}\ldots\int_{t'}^{t_3} dt_2 \sum_{\{\zeta_i=\pm1\}_n} \tilde{B}_n^{(a)}\tilde{F}_n^{(-)}. \end{aligned} \tag{3.26}$$

Notice that the $K^{(-)}$ is antisymmetric in the bias and vanishes for $\epsilon = 0$, while $K^{(+)}$ is symmetric in ϵ.

3.4.1 GME for the free system

The free TLS dynamics is recovered setting to zero the coupling with the environment in the kernels of the GME. The only non-vanishing contribution to the irreducible kernels is the lowest order term in the symmetric kernel (the antisymmetric kernel vanishes for $\gamma = 0$, as can be checked from Eq. (3.26) with the definitions given in Eq. (3.18)) so we have

$$\begin{aligned} K_{\text{free}}^{(+)}(\tau) &= -\frac{\Delta^2}{2}\sum_{\zeta=\pm1}\exp(-i\zeta\epsilon\tau) = -\Delta^2\cos(\epsilon\tau) \\ K_{\text{free}}^{(-)}(\tau) &= 0. \end{aligned} \tag{3.27}$$

The GME for the free system is then

$$\dot{P}_{\eta_0}(t) = \int_{t_0}^{t} K_{\text{free}}^{(+)}(t-t')P_{\eta_0}(t'). \tag{3.28}$$

In this simple case it can be solved by passing to the Laplace space where the GME for the free conditional population difference reads ($P_{\eta_0}(t_0) = \eta_0$)

$$\lambda P_{\eta_0}(\lambda) - \eta_0 = -\Delta^2\frac{\lambda}{\lambda^2+\epsilon^2}P_{\eta_0}(\lambda). \tag{3.29}$$

Transforming back to the time domain by using the Bromwich integral (Eq. (3.5)), the result is

$$P_{\eta_0}(t) = \eta_0\frac{\hbar^2\epsilon^2}{E^2} + \eta_0\frac{\hbar^2\Delta^2}{E^2}\cos\left(\frac{Et}{\hbar}\right). \tag{3.30}$$

The survival probability in the left state $(1 - P_{\eta_0}(t))/2$ with $\eta_0 = -1$, obtained from Eq. (3.30), coincides with those given in Eqs. (2.20) and (3.7).

Here we introduce the *self-energies*, defined as the differences between the irreducible kernels of the GME with dissipation and in the free case [9]

$$\begin{aligned} \Sigma^{(+)}(t,t') &= K^{(+)}(t,t') - K_{\text{free}}^{(+)}(t-t'), \\ \Sigma^{(-)}(t,t') &= K^{(-)}(t,t'). \end{aligned} \tag{3.31}$$

Notice that they vanish for zero coupling with the environment.

3.5 Approximation schemes

The generalized master equation in Eq. (3.22), with the exact symmetric and antisymmetric irreducible kernels given in Eq. (3.26), gives in principle the exact dynamics of the dissipative TLS in any regime of damping/temperature compatible with the TLS approximation. However, due to the intricacies brought by the FV influence functions in practice it is not possible to compute the kernels, and approximations are required. There exist various approximation schemes, according to the dissipation regime to which the system is subject.

3.5.1 Noninteracting-blip approximation

Th simplest approximation on the influence functions consists in neglecting the nonlocal in time part of the interaction. In terms of the TLS parametrization it consists in retaining only the intra-blip interactions, represented by the wavy lines in the lower panel of Fig. 3.3. For this reason the resulting approximation scheme is called *non-interacting-blip approximation* (NIBA). This is a valid approximation at sufficiently high temperature ($T \gtrsim \hbar\Delta_b/k_B$) i.e when the cutoff operated by the real part of the Feynman-Vernon influence function occurs on time scales comparable to the average blip length. In this case one can use the long time/high temperature limit of $Q(t)$, given in Eq. (4.12). Specifically, the dimensionless functions $S(t)$ and $R(t)$ take on the linearized form and, by the definitions given in Eq. (3.10), we have

$$\Lambda_{i,j} = 0, \qquad X_{i,j\neq i-1} = 0, \qquad Y_{i,i-1} = R_{2i,2i-1} = R(\tau_i). \tag{3.32}$$

Applying to the definitions of Eq. (3.18), the approximation (3.32), the NIBA symmetric

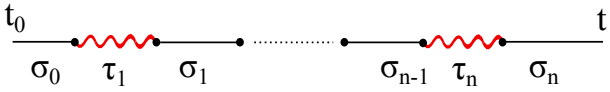

Figure 3.5: Interactions retained in the NIBA: intra-blip interactions (red wavy lines). Example of a TLS path of n transitions

and antisymmetric influence functions, in terms of the blip times, are

$$\sum_{\{\zeta_i=\pm 1\}_n} B_n^{(s)} F_n^{(+)} \simeq 2^n \prod_{i=1}^{n} e^{-S(\tau_i)} \cos(\epsilon\tau_i) \cos(R(\tau_i)) \tag{3.33}$$

and

$$\sum_{\{\zeta_i=\pm 1\}_n} B_n^{(a)} F_n^{(-)} \simeq 2^n e^{-S(\tau_i)} \sin(\epsilon\tau_1) \sin(R(\tau_i)) \prod_{i=2}^{n} e^{-S(\tau_i)} \cos(\epsilon\tau_i) \cos(R(\tau_i)), \tag{3.34}$$

respectively. Both the n-th order NIBA influence functions have the structure of the product of n first order functions. As a consequence the NIBA irreducible kernels consist solely of the first order terms in Δ^2 (see Eq. (3.26)), because the higher irreducible

influence functions vanish, as it can be easily checked from the definition of irreducible kernel in Eq. (3.25). Explicitly, the GME in the NIBA scheme is

$$\dot{P}_{\eta_0}(t) = \int_{t_0}^{t} dt' \left[K_N^{(+)}(t-t') P_{\eta_0}(t') + K_N^{(-)}(t-t') \right] \tag{3.35}$$

with the NIBA kernels given by

$$\begin{aligned} K_N^{(+)}(t) &= -\Delta^2 e^{-S(t)} \cos(\epsilon t) \cos(R(t)), \\ K_N^{(-)}(t) &= -\Delta^2 e^{-S(t)} \sin(\epsilon t) \sin(R(t)). \end{aligned} \tag{3.36}$$

The solution of the GME given in Eq. (3.35) can be obtained in principle (and also in practice, but in particular cases) by expressing it in Laplace space and solving the Bromwich integral of Eq. (3.5), once the poles are known. In terms of the self energies, defined in Eq. (3.31), the NIBA master equation in Laplace space reads ($P_{\eta_0}(t_0) = \eta_0$)

$$P_{\eta_0}(\lambda) = \frac{\eta_0 + \Sigma_N^{(-)}(\lambda)/\lambda}{\lambda + \Delta^2 \lambda/(\lambda^2 + \epsilon^2) - \Sigma_N^{(+)}(\lambda)}. \tag{3.37}$$

The result shown below are obtained by numerically integrating Eq. (3.35) rather than transforming back Eq. (3.37) to the time domain.

3.5.2 Validity of the NIBA

The NIBA scheme is non-perturbative in the coupling (the intra-blip interactions are retained at all orders in γ_s) but it is at the second order in the tunneling element Δ, so in the general case it describes correctly the dynamics only at short times $t \lesssim 1/\Delta$.

At high temperatures ($T \gtrsim \hbar\Delta_b/k_B$) it gives the correct results for the conditional populations both in the biased and in the unbiased case. For Ohmic dissipation, in the symmetric case ($\epsilon = 0$) the NIBA scheme reproduces the correct results also for weak damping at every temperature [9].

The NIBA fails for a biased ($\epsilon \neq 0$) Ohmic system at low temperature ($T \lesssim \hbar\Delta_b/\hbar$). For example, it predicts complete localization in the right well at equilibrium in the limit $T \to 0$, even for vanishingly small bias, as can be seen from Eq. (3.37), considering the limit

$$P(\infty) = \lim_{\lambda \to 0} \lambda \tilde{P}_{\eta_0}(\lambda) = -\frac{\Sigma_N^{(-)}(0)}{\Sigma_N^{(+)}(0)} = \tanh\left(\frac{\epsilon\hbar\beta}{2}\right). \tag{3.38}$$

The correct population difference at equilibrium for vanishing damping, obtained by thermodynamic considerations [9], is

$$P(\infty) = Tr[\sigma_z \rho_{eq}] = \frac{1}{Z}\left(\langle R|e^{-\beta \hat{H}_{TLS}}|R\rangle - \langle L|e^{-\beta \hat{H}_{TLS}}|L\rangle\right) = \frac{\hbar\epsilon}{E}\tanh\left(\frac{\beta E}{2}\right), \tag{3.39}$$

which shows no localization in the limit $\epsilon, T \to 0$. In Sec. 3.8 a similar expression is given for weak but finite damping using the self energies in the weak coupling approximation.

3.5.3 extended-NIBA

The convolution character of the path integral expression for the NIBA probability difference in the time domain is preserved if the *blip-preceding sojourn* interactions Y [61], discarded in the NIBA scheme, are taken fully, while the other blip-sojourn as well as the inter-blip correlations are discarded. In formulae

$$\begin{aligned} \Lambda_{i,j} =& 0, \qquad X_{i,j\neq i-1} = 0, \\ Y_{i,i-1} =& Y(\sigma_{i-1},\tau_i) = R(\sigma_{i-1}) + R(\tau_i) - R(\sigma_{i-1}+\tau_i). \end{aligned} \tag{3.40}$$

In terms of the blip and sojourn times the influence functions take the form

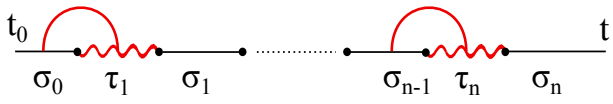

Figure 3.6: Interactions retained in the extended-NIBA: intra-blip interactions (red wavy lines) and blip-preceding sojourn interactions (red semicircles). Example of a TLS path of n transitions.

$$\sum_{\{\zeta_i=\pm 1\}_n} B_n^{(s)} F_n^{(+)} \simeq 2^n \prod_{i=1}^{n} e^{-S(\tau_i)} \cos(\epsilon\tau_i) \cos\left(Y(\sigma_{i-1},\tau_i)\right) \tag{3.41}$$

and

$$\sum_{\{\zeta_i=\pm 1\}_n} B_n^{(a)} F_n^{(-)} \simeq 2^n e^{-S(\tau_1)} \sin(\epsilon\tau_1) \sin\left(Y(\sigma_0,\tau_1)\right) \prod_{i=2}^{n} e^{-S(\tau_i)} \cos(\epsilon\tau_i) \cos\left(Y(\sigma_{i-1},\tau_i)\right). \tag{3.42}$$

As stated above the extended-NIBA preserves the convolution character of the expression for the population difference. As a result, the irreducible kernels of the extended-NIBA master equation are of the first order in Δ^2, as for the NIBA. Using the prescription (3.26) we have

$$\begin{aligned} K_{eN}^{(+)}(t,t') &= -\Delta^2 e^{-S(t-t')} \cos\big(\epsilon(t-t')\big) \cos\big(R(t') + R(t-t') - R(t)\big), \\ K_{eN}^{(-)}(t,t') &= -\Delta^2 e^{-S(t-t')} \sin\big(\epsilon(t-t')\big) \sin\big(R(t') + R(t-t') - R(t)\big). \end{aligned} \tag{3.43}$$

The resulting extended-NIBA master equation reads

$$\dot{P}_{\eta_0}(t) = \int_{t_0}^{t} dt' \left[K_{eN}^{(+)}(t,t') P_{\eta_0}(t') + K_{eN}^{(-)}(t,t') \right]. \tag{3.44}$$

For later convenience we now find the master equation satisfied by the symmetric part $P_{\eta_0}^{(+)}(t)$ of the conditional population difference in the extended-NIBA scheme

$$\dot{P}_{\eta_0,eN}^{(+)}(t) = \int_{t_0}^{t} dt' K_{eN}^{(+)}(t,t') P_{\eta_0,eN}^{(+)}(t'). \tag{3.45}$$

The path integral expression for $P_{\eta_0}^{(+)}$ is

$$P_{\eta_0,eN}^{(+)}(t) = \eta_0 + \eta_0 \sum_{n=1}^{\infty} \left(-\frac{\Delta^2}{2}\right)^n \int_0^t \mathcal{D}\{t\}_{2n} \sum_{\{\zeta_i=\pm 1\}_n} B_n^{(s)} F_n^{(+)}, \tag{3.46}$$

with $\sum B_n^{(s)} F_n^{(+)}$ given by Eq. (3.41).

3.6 Weakly-interacting blip approximation (WIBA)

While the extended-NIBA represents a small correction to the NIBA, there is a scheme, called weakly-interacting blip approximation [59] (WIBA), which is capable to give correct results in the regimes from weak to strong damping. Its results coincide with those of the weak coupling approximation (WCA [9], perturbative in γ) in the weak coupling/low temperature regime and with those of the NIBA in the opposite limit of strong coupling/high temperature. This is attained by taking at all orders in γ the *intra-blip* ('intra') and the *blip-preceding-sojourn* ('bps') parts of the influence function, as in the extended-NIBA scheme, and to the first order in the coupling strength γ the *blip-blip* ('b-b') and the *blip-sojourn* ('b-s') parts.

This scheme represents an improvement of the NIBA-like schemes in that its results coincide with those of the NIBA at high temperatures, where the nonlocal part of the interactions introduced by $\mathcal{F}_{FV}$ is efficiently suppressed by the cut-off operated through the real part of the pair interaction $S(\tau)$ so that, considering them at the first order is immaterial, even if the coupling is strong. On the other hand at low temperature the nonlocal interactions cannot be neglected and at weak coupling the WIBA gives the correct predictions for the TLS dynamics. The problematic regime is that of low temperature and strong damping because taking the nonlocal interactions at the first order in γ is not strictly correct. Nevertheless it turns out [59] that also in this regime the WIBA predictions agree quite well with those of numerically exact ab initio calculations [53].

We split the influence functions of order n in the above mentioned parts and expand the nonlocal terms $b-b$ and $b-s$ to the first order in γ

$$\begin{aligned}\mathcal{F}_{FV} &= \exp\left(\Phi_{\text{intra}}\right)\exp\left(\Phi_{\text{bps}}\right)\exp\left(\Phi_{\text{b-b}}\right)\exp\left(\Phi_{\text{b-s}}\right)\\ &\simeq \exp\left(\Phi_{\text{intra}}\right)\exp\left(\Phi_{\text{bps}}\right)\left(1+\Phi_{\text{b-b}}\right)\left(1+\Phi_{\text{b-s}}\right),\end{aligned} \tag{3.47}$$

It is convenient to restate the definitions of the influence functions (Eq. (3.18)) so as to separate the intra-blip and blip-preceding sojourn arguments from the blip-blip and intra-blip arguments. The *exact* influence functions are

$$\begin{aligned}F_n^{(+)} =& \exp\left(\phi_n^{intra}\right)\exp\left(\phi_n^{b-b}\right)\prod_{j=1}^{n}\left[\cos\left(\phi_j^{bps}\right)\cos\left(\phi_j^{b-s}\right)-\sin\left(\phi_j^{bps}\right)\sin\left(\phi_j^{b-s}\right)\right]\\ F_n^{(-)} =& \exp\left(\phi_n^{intra}\right)\exp\left(\phi_n^{b-b}\right)\left[\sin\left(\phi_1^{bps}\right)\cos\left(\phi_1^{b-s}\right)+\cos\left(\phi_1^{bps}\right)\sin\left(\phi_1^{b-s}\right)\right]\\ &\times\prod_{j=2}^{n}\left[\cos\left(\phi_j^{bps}\right)\cos\left(\phi_j^{b-s}\right)-\sin\left(\phi_j^{bps}\right)\sin\left(\phi_j^{b-s}\right)\right],\end{aligned} \tag{3.48}$$

where

$$\begin{aligned}&\phi_n^{intra} = -\sum_{i=1}^{n} S_{2i,2i-1}, \qquad \phi_j^{bps} = \zeta_j Y_{j,j-1},\\ &\phi_n^{b-b} = -\sum_{j=1}^{n-1}\sum_{i=j+1}^{n}\zeta_i\zeta_j\Lambda_{i,j} \qquad \text{and} \qquad \phi_j^{b-s} = \sum_{i=j+1}^{n}\zeta_i X_{i,j-1}.\end{aligned} \tag{3.49}$$

3.6.1 WIBA symmetric irreducible kernel

Now we calculate the symmetric irreducible kernel order by order in Δ^2. This is done, once n is fixed, by summing over ζ (using the linearized b-b and b-s terms), taking the result to the first order in γ_s and then applying the recipe (3.25). The power series in Δ^2 for the symmetric WIBA kernel is

$$K_W^{(+)}(t,t') = \sum_{n=1}^{\infty} K_W^{(+)}(t,t')^{(n)}. \tag{3.50}$$

- For n=1 the symmetric WIBA irreducible kernel coincides with the symmetric extended-NIBA irreducible kernel because, at the first order in Δ^2, the b-b and b-s contributions are absent. We have

$$K_W^{(+)}(t,t')^{(1)} = K_{eN}^{(+)}(t,t') = -\Delta^2 e^{-S(t-t')}\cos\big(\epsilon(t-t')\big)\cos\big(Y(t-t',t')\big), \tag{3.51}$$

  where

$$Y(\tau,\sigma) = R(\sigma) + R(\tau) - R(\tau+\sigma). \tag{3.52}$$

- The $n=2$ symmetric WIBA irreducible kernel is (see Appendix B)

$$\begin{aligned} K_W^{(+)}(t,t')^{(2)} =& \Delta^4 \int_0^{\tilde{t}} d\tau_1 \int_0^{\tilde{t}-\tau_1} d\tau_2 e^{-S(\tau_1)-S(\tau_2)} \sin(\epsilon\tau_1)\sin(\epsilon\tau_2)\cos(Y(\tau_2,\tilde{t}-\tau_1-\tau_2)) \\ &\times \left[X(\tilde{t},\tau_2,\sigma_0)\sin(Y(\tau_1,\sigma_0)) + \Lambda(\tilde{t},\tau_2,\tau_1)\cos(Y(\tau_1,\sigma_0))\right] \end{aligned} \tag{3.53}$$

  where $\tilde{t} = t - t'$, $\tau_2 = t - t' - \tau_1 - \sigma_1$, and $\sigma_0 = t' - t_0 = t'$, and where

$$\begin{aligned} X(\tilde{t},\tau_n,\sigma_0) &= R(\tilde{t}-\tau_n+\sigma_0) + R(\tilde{t}) - R(\tilde{t}+\sigma_0) - R(\tilde{t}-\tau_n) \\ \Lambda(\tilde{t},\tau_n,\tau_1) &= S(\tilde{t}) + S(\tilde{t}-\tau_n-\tau_1) - S(\tilde{t}-\tau_1) - S(\tilde{t}-\tau_n). \end{aligned} \tag{3.54}$$

  For reason which will be clear below, we eliminate the σ_1 dependence in $Y(\tau_2,\sigma_1) = R(\sigma_1) + R(\tau_2) - R(\tau_2+\sigma_1)$, by substituting it with the NIBA approximated form $Y(\tau_2,\sigma_1) \simeq R(\tau_2)$. It follows that

$$K_W^{(+)}(t,t')^{(2)} \simeq \int_0^{\tilde{t}} d\tau_1 \int_0^{\tilde{t}-\tau_1} d\tau_2 \mathcal{W}^{(+)}(\tilde{t},\tau_1,\tau_2,\sigma_0),$$

  where we have introduced the function

$$\begin{aligned} \mathcal{W}^{(+)}(\tilde{t},t_1,t_2,\sigma_0) =& \Delta^4 e^{-S(t_1)-S(t_2)}\sin(\epsilon t_1)\sin(\epsilon t_2)\cos(R(t_2)) \\ &\times \left[X(\tilde{t},t_2,\sigma_0)\sin(Y(t_1,\sigma_0)) + \Lambda(\tilde{t},t_2,t_1)\cos(Y(t_1,\sigma_0))\right]. \end{aligned} \tag{3.55}$$

- The $n=3$ symmetric WIBA irreducible kernel is

$$\begin{aligned} K_W^{(+)}(t,t')^{(3)} =& -\Delta^6 \int_0^{t-t'} d\tau_1 \int_0^{t-t'-\tau_1} d\sigma_1 \int_0^{t-t'-\tau_1-\sigma_1} d\tau_2 \int_0^{t-t'-\tau_1-\sigma_1-\tau_2} d\sigma_2 \\ &\times e^{-S(\tau_1)-S(\tau_2)-S(\tau_3)}\sin(\epsilon\tau_1)\cos(\epsilon\tau_2)\sin(\epsilon\tau_3)\cos(Y(\tau_3,\sigma_2))\cos(Y(\tau_2,\sigma_1)) \\ &\times \left[X(\tilde{t},\tau_3,\sigma_0)\sin(Y(\tau_1,\sigma_0)) + \Lambda(\tilde{t},\tau_3,\tau_1)\cos(Y(\tau_1,\sigma_0))\right], \end{aligned} \tag{3.56}$$

where $\tilde{t} = t - t'$, $\sigma_0 = t' - t_0 = t'$ and $\tau_3 = t - t' - \tau_1 - \sigma_1 - \tau_2 - \sigma_2$.

Similarly to the $n = 2$ case we make the change of variable $\sigma_2 \to \tau_3 = t - t' - \tau_1 - \sigma_1 - \tau_2 - \sigma_2$, and then exchange the integration order using the rule (C.2). Finally we use $Y(\sigma_2, \tau_3) \simeq R(\tau_3)$. The result is

$$K_W^{(+)}(t,t')^{(3)} \simeq \int_0^{\tilde{t}} d\tau_1 \int_0^{\tilde{t}-\tau_1} d\tau_3 \mathcal{W}^{(+)}(\tilde{t}, \tau_1, \tau_3, \sigma_0) p^{(1)}(\tilde{t} - \tau_1 - \tau_3), \tag{3.57}$$

where the first order in Δ^2 function $p^{(1)}$ is defined by

$$p^{(1)} = \eta_0 P_{\eta_0,eN}^{(+)}(t)^{(1)} = -\Delta^2 \int_0^t d\sigma_1 \int_0^{t-\sigma_1} d\tau_2 e^{-S(\tau_2)} \cos(\epsilon\tau_2) \cos(Y(\tau_2, \sigma_1)). \tag{3.58}$$

The extended-NIBA symmetric population difference $P_{\eta_0,eN}^{(+)}(t)$ is defined in Eq. (3.46) and satisfies Eq. (3.45).

- For generic $n \geq 3$, the symmetric WIBA irreducible kernel reads

$$K_W^{(+)}(t,t')^{(n)} \simeq \int_0^{\tilde{t}} d\tau_1 \int_0^{\tilde{t}-\tau_1} d\tau_n \mathcal{W}^{(+)}(\tilde{t}, \tau_1, \tau_n, \sigma_0) p^{(n-2)}(\tilde{t} - \tau_1 - \tau_n), \tag{3.59}$$

where

$$\begin{aligned} p^{(n-2)}(t) &= \eta_0 P_{\eta_0,eN}^{(+)}(t)^{(n-2)} \\ &= \left(-\Delta^2\right)^{n-2} \int_0^t d\sigma_1 \ldots \int_0^{t-\cdots-\sigma_{n-2}} d\tau_{n-1} \prod_{i=2}^{n-1} e^{-S(\tau_i)} \cos(\epsilon\tau_i) \cos(Y(\tau_i, \sigma_{i-1})). \end{aligned} \tag{3.60}$$

Here, again, we changed the last integration variable $\sigma_{n-1} \to \tau_n = t - t' - \tau_1 - \cdots - \sigma_{n-1}$, and used the approximated form $Y(\tau_n, \sigma_{n-1}) \simeq R(\tau_n)$.

Using $Y(\tau_n, \sigma_{n-1}) \simeq R(\tau_n)$, at every order ≥ 2 in Δ^2 the WIBA symmetric kernel appears as a convolution between the second order function $\mathcal{W}^{(+)}$ and $p^{(n-2)}$, where

$$p(t) = \eta_0 P_{\eta_0,eN}^{(+)}(t) \tag{3.61}$$

(the expansion of $P_{\eta,eN}^{(+)}$ in powers of Δ^2 is given in Eq. (3.46)). This feature allows us to perform the sum in Eq. (3.50). For the symmetric irreducible WIBA kernel with initial time t_0, we have

$$K_W^{(+)}(\tilde{t}, \tilde{t}') = K_{eN}^{(+)}(\tilde{t}, \tilde{t}') + \int_0^{\tilde{t}} d\tau \int_0^{\tilde{t}-\tau} d\tau' \mathcal{W}^{(+)}(\tilde{t}, \tau, \tau', \tilde{t}') p(\tilde{t} - \tau - \tau'), \tag{3.62}$$

where $\tilde{t} = t - t'$ and $\tilde{t}' = t' - t_0$.

It is important to notice that the function $p(t)$ doesn't depend on the initial condition $P_{\eta_0}(t_0) = \eta_0$. In practice it is the solution of the equation

$$\dot{p}(t) = \int_{t_0}^t dt' K_{eN}^{(+)}(t,t') p(t') \tag{3.63}$$

with initial condition $p(t_0) = \eta_0 P_{\eta_0,eN}(t_0) = 1$. The kernel $K_{eN}^{(+)}$ is given in the first of Equations (3.43).

3.6.2 WIBA antisymmetric irreducible kernel

The antisymmetric irreducible WIBA kernel is obtained carrying out the same calculations as for the symmetric kernel. The power series in Δ^2 is in this case

$$K_W^{(-)}(t,t') = \sum_{n=1}^{\infty} K_W^{(-)}(t,t')^{(n)}. \tag{3.64}$$

- For n=1 the antisymmetric kernel coincides with the corresponding on in the extended-NIBA

$$K_W^{(-)}(t,t')^{(1)} = K_{eN}^{(-)}(t,t') = -\Delta^2 e^{-S(t-t')} \sin\big(\epsilon(t-t')\big) \sin\big(Y(t-t',t')\big) \tag{3.65}$$

- The $n=2$ antisymmetric WIBA irreducible kernel is (see Appendix B)

$$\begin{aligned} K_W^{(-)}(t,t')^{(2)} \simeq & \Delta^4 \int_0^{\tilde{t}} d\tau_1 \int_0^{\tilde{t}-\tau_1} d\tau_2 e^{-S(\tau_1)-S(\tau_2)} \cos(\epsilon\tau_1)\sin(\epsilon\tau_2)\cos(R(\tau_2)) \\ & \times \big[X(\tilde{t},\tau_2,\sigma_0)\cos(Y(\tau_1,\sigma_0)) - \Lambda(\tilde{t},\tau_2,\tau_1)\sin(Y(\tau_1,\sigma_0))\big] \\ \equiv & \int_0^{\tilde{t}} d\tau_1 \int_0^{\tilde{t}-\tau_1} d\tau_2 \mathcal{W}^{(-)}(\tilde{t},\tau_1,\tau_2,\sigma_0). \end{aligned} \tag{3.66}$$

where $\tilde{t} = t-t'$, $\tau_2 = t-t'-\tau_1-\sigma_1$, and $\sigma_0 = t'-t_0 = t'$. As for the symmetric kernel we have used the approximated form $Y(\tau_2,\sigma_1) \simeq R(\tau_2)$. Here we have introduced the function

$$\begin{aligned} \mathcal{W}^{(-)}(\tilde{t},t_1,t_2,\sigma_0) = & \Delta^4 e^{-S(t_1)-S(t_2)} \cos(\epsilon t_1)\sin(\epsilon t_2)\cos(R(t_2)) \\ & \times \big[X(\tilde{t},t_2,\sigma_0)\cos(Y(t_1,\sigma_0)) - \Lambda(\tilde{t},t_2,t_1)\sin(Y(t_1,\sigma_0))\big] \end{aligned} \tag{3.67}$$

(see definitions of X and Λ in Eq. (3.54)).

- The $n=3$ antisymmetric WIBA irreducible kernel reads

$$\begin{aligned} K_W^{(-)}(t,t')^{(3)} = & -\Delta^6 \int_0^{t-t'} d\tau_1 \int_0^{t-t'-\tau_1} d\sigma_1 \int_0^{t-t'-\tau_1-\sigma_1} d\tau_2 \int_0^{t-t'-\tau_1-\sigma_1-\tau_2} d\sigma_2 \\ & \times e^{-S(\tau_1)-S(\tau_2)-S(\tau_3)} \cos(\epsilon\tau_1)\cos(\epsilon\tau_2)\sin(\epsilon\tau_3)\cos(Y(\tau_3,\sigma_2))\cos(Y(\tau_2,\sigma_1)) \\ & \times \big[X(\tilde{t},\tau_3,\sigma_0)\cos(Y(\tau_1,\sigma_0)) - \Lambda(\tilde{t},\tau_3,\tau_1)\sin(Y(\tau_1,\sigma_0))\big] \end{aligned} \tag{3.68}$$

where $\tilde{t} = t-t'$, $\sigma_0 = t'-t_0 = t'$ and $\tau_3 = t-t'-\tau_1-\sigma_1-\tau_2-\sigma_2$.

Similarly to the $n=2$ case we make the change of variable $\sigma_2 \to \tau_3 = t-t'-\tau_1-\sigma_1-\tau_2-\sigma_2$, and then exchange the integration order using the rule (C.2). Finally we use $Y(\sigma_2,\tau_3) \simeq R(\tau_3)$. The result is

$$K_W^{(-)}(t,t')^{(3)} \simeq \int_0^{\tilde{t}} d\tau_1 \int_0^{\tilde{t}-\tau_1} d\tau_3 \mathcal{W}^{(-)}(\tilde{t},\tau_1,\tau_3,\sigma_0) p^{(1)}(\tilde{t}-\tau_1-\tau_3) \tag{3.69}$$

where $\mathcal{W}^{(-)}$ and $p^{(1)}$ are defined in Eqs. (3.67) and (3.58), respectively.

- As for the symmetric one, the $n \geq 3$ irreducible antisymmetric WIBA kernel is obtained using the approximated form $Y(\tau_n, \sigma_{n-1}) \simeq R(\tau_n)$, and reads

$$K_W^{(-)}(t,t')^{(n)} \simeq \int_0^{\tilde{t}} d\tau_1 \int_0^{\tilde{t}-\tau_1} d\tau_n \mathcal{W}^{(-)}(\tilde{t},\tau_1,\tau_n,\sigma_0) p^{(n-2)}(\tilde{t}-\tau_1-\tau_n), \tag{3.70}$$

  where $p^{(n-2)}$ is defined in Eq. (3.60).

It is now possible to perform the sum in Eq. (3.64). The full antisymmetric irreducible WIBA kernel, with initial time t_0, is

$$K_W^{(-)}(\tilde{t},\tilde{t}') = K_{eN}^{(-)}(\tilde{t},\tilde{t}') + \int_0^{\tilde{t}} d\tau \int_0^{\tilde{t}-\tau} d\tau' \mathcal{W}^{(-)}(\tilde{t},\tau,\tau',\tilde{t}') p(\tilde{t}-\tau-\tau'), \tag{3.71}$$

where $\tilde{t} = t - t'$ and $\tilde{t}' = t' - t_0$. The function $p(t)$ is the solution of Eq. (3.63) with $p(t_0) = 1$.

3.6.3 Validity and features of the WIBA scheme

Some remarks are in order at this point. First, as it can be seen by inspection of Eqs. (3.59) and (3.70), the irreducible kernels of order n show a structure in which the initial sojourn and the first blip σ_0 and τ_1 are connected through the beyond NIBA interactions X and Λ to the last blip τ_n, which is the time-nonlocal feature that gives to the WIBA scheme the *non-Markovian* character. The intermediate propagation has the time-local intra-blip and blip-preceding sojourn interactions given by $p(t)$. This is exemplified in Fig.3.7.

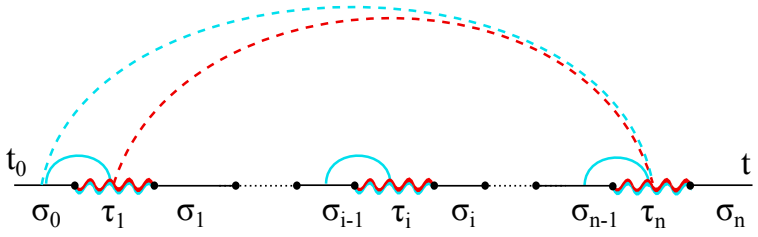

Figure 3.7: Interactions in the irreducible WIBA kernels of order n. Solid lines are the intra-blip (wavy lines) and blip-preceding sojourn interactions (semicircles). Dashed lines represent the blip-blip (red) and blip-sojourn (sky-blue) interactions taken to the first order in γ.

Secondly, the kernel $K_W^{(+)}$ is symmetric under the inversion $\epsilon \to -\epsilon$, nevertheless the beyond-NIBA correction vanishes for $\epsilon = 0$ (as obviously does the full antisymmetric kernel). This is consistent with the discussion about the validity of the NIBA scheme in Sec. 3.5.2, where it is pointed out that, for $\epsilon = 0$, the NIBA reproduces the correct results down to weak coupling in the low to high temperature regime. We also notice that the beyond-NIBA corrections in the WIBA kernels is proportional to γ, through the functions Λ and X. This means that the entity of the correction grows with γ. However it must be kept in mind that the scheme is derived under the assumption that the correction can be treated perturbatively in γ at low to intermediate temperatures, where their contribution is not made irrelevant by the cutoff exerted through $S(t)$. As a consequence, if the temperature is not high, in principle the WIBA is not valid at strong

damping. On the other hand, at high temperature it coincides with the NIBA because the functions Λ and X vanish, as $S(t)$ and $R(t)$ assume the long time/high temperature linearized form (4.12), and $Y(t) \to R(t)$. Finally, the dynamics within the WIBA scheme cannot be computed analytically so the GME (3.22) with the WIBA kernels has to be numerically integrated in order to obtain the time evolution of the population difference. The numerical scheme used to solve the GME here and in Chapter 4 is described in Appendix A.

3.7 Master Equation for the populations

In view of applying to M-states systems, with $M > 2$, the approximation schemes introduced in this chapter, we write the kernels for the conditional populations of the TLS in the basis $|R/L\rangle$ starting from the expressions of the population difference kernels $K^{(\pm)}$. Using Eq. (3.23) and the probability conservation, with no reference to any particular approximation scheme, one gets

$$\begin{aligned} K_{LR}(t,t') &= -\frac{1}{2}\left(K^{(+)}(t,t') + K^{(-)}(t,t')\right) \\ K_{RL}(t,t') &= -\frac{1}{2}\left(K^{(+)}(t,t') - K^{(-)}(t,t')\right) \\ K_{RR}(t,t') &= -K_{LR}(t,t') \\ K_{LL}(t,t') &= -K_{RL}(t,t'). \end{aligned} \tag{3.72}$$

3.7.1 NIBA and extended-NIBA kernels for the populations

Substituting Eq. (3.36) into Eq. (3.72) we obtain the irreducible NIBA kernels for the populations

$$\begin{aligned} K^N_{LR}(\tau) &= \frac{\Delta^2}{2} e^{-S(\tau)} \cos\left(\epsilon\tau - R(\tau)\right), \\ K^N_{RL}(\tau) &= \frac{\Delta^2}{2} e^{-S(\tau)} \cos\left(\epsilon\tau + R(\tau)\right) \end{aligned} \tag{3.73}$$

and analogue expressions for the extended-NIBA, with the function $Y(\tau, t')$ in place of $R(\tau)$.

3.7.2 WIBA kernels for the populations

The symmetric and antisymmetric irreducible WIBA kernels of the master equation for the population difference have the form of a extended-NIBA (eN) plus a *beyond-NIBA* (BN) contribution. The same holds for the irreducible WIBA kernels for the populations. Substituting Eqs. (3.71) and (3.62) into Eq. (3.72) we get

$$\begin{aligned} K^W_{LR}(\tilde{t},\tilde{t}') &= K^{eN}_{LR}(\tilde{t},\tilde{t}') + K^{BN}_{LR}(\tilde{t},\tilde{t}') \\ &= \frac{\Delta^2}{2} e^{-S(\tilde{t})} \cos\left(\epsilon\tilde{t} - Y(\tilde{t},\tilde{t}')\right) - \frac{\Delta^4}{2}\int_0^{\tilde{t}} d\tau \int_0^{\tilde{t}-\tau} d\tau' e^{-S(\tau)-S(\tau')} \sin(\epsilon\tau')\cos(R(\tau')) \\ &\quad \times p(\tilde{t}-\tau-\tau')\left[\Lambda(\tilde{t},\tau',\tau)\sin(\epsilon\tau - Y(\tau,\tilde{t}')) + X(\tilde{t},\tau',\tilde{t}')\cos(\epsilon\tau - Y(\tau,\tilde{t}'))\right] \end{aligned} \tag{3.74}$$

and

$$\begin{aligned} K^{W}_{RL}(\tilde{t},\tilde{t}') &= K^{eN}_{RL}(\tilde{t},\tilde{t}') + K^{BN}_{RL}(\tilde{t},\tilde{t}') \\ &= \frac{\Delta^2}{2} e^{-S(\tilde{t})} \cos\left(\epsilon\tilde{t} + Y(\tilde{t},\tilde{t}')\right) - \frac{\Delta^4}{2}\int_0^{\tilde{t}} d\tau \int_0^{\tilde{t}-\tau} d\tau' e^{-S(\tau)-S(\tau')} \sin(\epsilon\tau')\cos(R(\tau')) \\ &\quad \times p(\tilde{t}-\tau-\tau')\left[\Lambda(\tilde{t},\tau',\tau)\sin(\epsilon\tau + Y(\tau,\tilde{t}')) - X(\tilde{t},\tau',\tilde{t}')\cos(\epsilon\tau + Y(\tau,\tilde{t}'))\right], \end{aligned} \tag{3.75}$$

where $\tilde{t} = t - t'$ and $\tilde{t}' = t' - t_0$, $p(t)$ is given by Eq. (3.63), and the functions Λ and X are defined in Eq. (3.54).

3.8 Weak coupling approximation

The dynamics of P_{η_0} in the weak coupling approximation (WCA) scheme [9, 62] can be derived quite simply by the results obtained for the WIBA in Sec. 3.6. The WCA is perturbative in γ both in the inter-blip and in the intra-blip interactions and thus is an approximation scheme valid in the opposite limit with respect to the NIBA, i.e at low temperature and weak damping, where the NIBA fails in describing the biased TLS (see Sec. 3.5.2).

The WIBA interpolates between these two opposite regimes and reproduces correctly the WCA results. However at low temperatures the non-Markovian character of the dynamical evolution becomes relevant and this is reflected by an increase of the memory time of the WIBA kernels which, in turn, makes the numerical solution of the GME increasingly harder. On the other hand the WCA allows for an analytical solution which can be used as a check for other approximation schemes in the weak coupling and low temperature regime.

We start from the expressions (3.62) and (3.71) for the symmetric and antisymmetric WIBA kernels and expand every function of γ to the first order. The result is

$$\begin{aligned} K^{(+)}_{WCA}(\tilde{t},\tilde{t}') &= K^{(+)}_{\text{free}}(\tilde{t}) + \Sigma^{(+)}_{WCA}(\tilde{t},\tilde{t}') \\ K^{(-)}_{WCA}(\tilde{t},\tilde{t}') &= \Sigma^{(-)}_{WCA}(\tilde{t},\tilde{t}'), \end{aligned} \tag{3.76}$$

where $K^{(+)}_{\text{free}}(t) = -\Delta^4\cos(\epsilon t)$ is the kernel of the GME for the free system (see Equations (3.27) and (3.31)). The self energies take the form

$$\begin{aligned} \Sigma^{(+)}_{WCA}(\tilde{t},\tilde{t}') =& \Delta^2 S(\tilde{t})\cos(\epsilon\tilde{t}) \\ &+ \Delta^4\int_0^{\tilde{t}} d\tau\int_0^{\tilde{t}-\tau} d\tau' \Lambda(\tilde{t},\tau',\tau)\sin(\epsilon\tau)\sin(\epsilon\tau')p^{\text{free}}(\tilde{t}-\tau-\tau') \\ \Sigma^{(+)}_{WCA}(\tilde{t},\tilde{t}') =& -\Delta^2 Y(\tilde{t},\tilde{t}')\sin(\epsilon\tilde{t}) \\ &+ \Delta^4\int_0^{\tilde{t}} d\tau\int_0^{\tilde{t}-\tau} d\tau' X(\tilde{t},\tau',\tilde{t}')\cos(\epsilon\tau)\sin(\epsilon\tau')p^{\text{free}}(\tilde{t}-\tau-\tau'), \end{aligned} \tag{3.77}$$

where

$$p^{\text{free}}(t) = 1 + \sum_{n=1}^{\infty}\left(-\Delta^2\right)^n \int_0^t \mathcal{D}\{t\}_{2n}\cos(\epsilon\tau_i) = \frac{\hbar^2\epsilon^2}{E^2} + \frac{\hbar^2\Delta^2}{E^2}\cos\left(\frac{Et}{\hbar}\right). \tag{3.78}$$

Expressing the self energies in Laplace space, using the spectral representation of the dimensionless pair interaction S and R, given by Eq. (2.58), and exchanging the time and frequency integrals, one obtains the expressions for $\Sigma^{(\pm)}(\lambda)$ [9, 58, 63]. Substituting these expressions in

$$P_{\eta_0}(\lambda) = \frac{\eta_0 + \Sigma^{(-)}_{WCA}(\lambda)/\lambda}{\lambda + \Delta^2\lambda/(\lambda^2+\epsilon^2) - \Sigma^{(+)}_{WCA},(\lambda)} \tag{3.79}$$

and transforming back into the time domain, the following analytical expression for the conditional population difference in the WCA is obtained

$$\begin{aligned} P_{\eta_0}(t) \simeq &\left(\eta_0\frac{\epsilon^2}{\Omega^2} - P(\infty)\right)e^{-\Gamma_r t} + P(\infty) \\ &+ \left[\eta_0\frac{\Delta^2_{\rm eff}}{\Omega^2}\cos(\Omega t) + \left(\frac{\Gamma_r\epsilon^2 + \Gamma\Delta^2_{\rm eff}}{\Omega^3} - \frac{\Gamma_r}{\Omega}P(\infty)\right)\sin(\Omega t)\right]e^{-\Gamma t}, \end{aligned} \tag{3.80}$$

where

$$\begin{aligned} \Omega^2 =& \Delta^2\left(1 - 2\Re\{u(iE/\hbar)\}\right) + \epsilon^2 \equiv \Delta^2_{\rm eff} + \epsilon^2 \\ \Gamma_r =& \gamma\frac{Mq_0^2\Delta^2_{\rm eff}}{2\hbar\Omega}\coth\left(\frac{\beta\hbar\Omega}{2}\right) \\ \Gamma =& \frac{\Gamma_r}{2} + \gamma\frac{Mq_0^2\epsilon^2}{\beta\hbar^2\Omega^2}. \end{aligned} \tag{3.81}$$

The function $u(z)$ in the definition of Ω is

$$u(z) = \gamma\frac{Mq_0^2}{2\pi\hbar}\int_0^\infty d\omega\frac{\omega e^{-\omega/\omega_c}}{\omega^2+z^2}\left[\coth\left(\frac{\hbar\beta\omega}{2}\right) - 1\right]. \tag{3.82}$$

This integral can be solved by a contour integration with residues at the two poles $\omega = \pm iz$ and at the infinite series of poles at the so-called Matsubara frequencies $\nu_n = n2\pi/\hbar\beta$. Note that increasing the damping γ the oscillation frequency Ω (which also depends on the temperature T, at low T) is decreased, which gives the frequency shift introduced by the environment. For vanishing γ one gets the free case with $\Omega \to E/\hbar$. The asymptotic population difference, entering in Eq. (3.80) is given by

$$P(\infty) = \lim_{\lambda\to 0}\lambda\tilde{P}_{\eta_0}(\lambda) = -\frac{\Sigma^{(-)}_{WCA}(0)}{\Sigma^{(+)}_{WCA}(0)} = \frac{\epsilon}{\Omega}\tanh\left(\frac{\hbar\beta\Omega}{2}\right). \tag{3.83}$$

This formula is similar to that given in Sec. 3.5.2 but takes into account (for weak coupling) the effects of the environment in determining the equilibrium values of the right/left well populations.

3.9 Examples of TLS dissipative dynamics

We show the time evolution of the conditional probability difference $P_{\eta_0} = P_{R,\eta_0} - P_{L,\eta_0} \equiv \langle\sigma_z\rangle_{\eta_0}$ in the presence of Ohmic dissipation

$$J(\omega) = M\gamma\omega e^{-\omega/\omega_c}$$

with cut-off frequency $\omega_c = 50\Delta$. The initial condition is $\eta_0 = -1$, meaning that the particle starts in the $|L\rangle$ state. Both the biased and unbiased TLS are considered at low

temperature and in the weak to strong coupling regimes. The predictions of the approximation schemes described above are shown. No noticeable difference emerges between the NIBA and the extended-NIBA results (an example is given in Fig. 3.8). On the contrary both these schemes give results significantly different from those obtained within the WIBA for the biased system in the weak to intermediate damping regime.

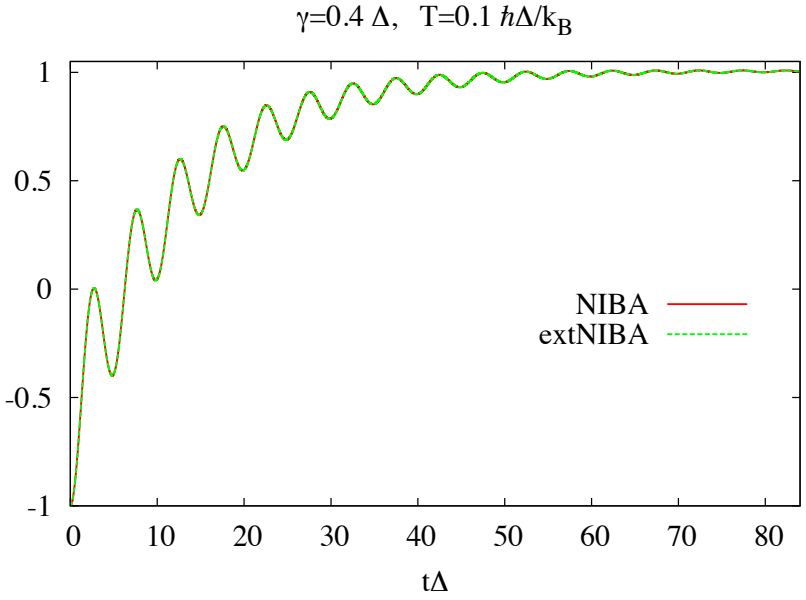

Figure 3.8: Comparison between the NIBA and the extended-NIBA schemes for the biased system ($\epsilon = 1\Delta$ and $\omega_C = 50\Delta$) in the intermediate coupling $\gamma = 0.4\Delta$ and low temperature $T = 0.1\hbar\Delta/k_B$. The two results practically coincide and both give an incorrect stationary population difference (see Fig. 3.12).

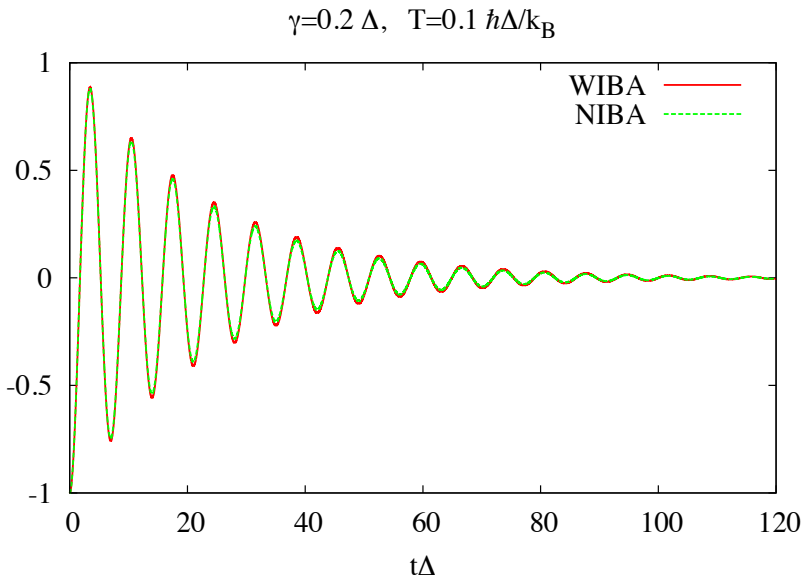

Figure 3.9: Symmetric system ($\epsilon = 0$ and $\omega_C = 50\Delta$) in the weak to intermediate coupling $\gamma = 0.2\Delta$ and low temperature temperature $T = 0.1\hbar\Delta/k_B$. The NIBA gives the correct result for the unbiased system, as confirmed by the comparison with the WIBA scheme.

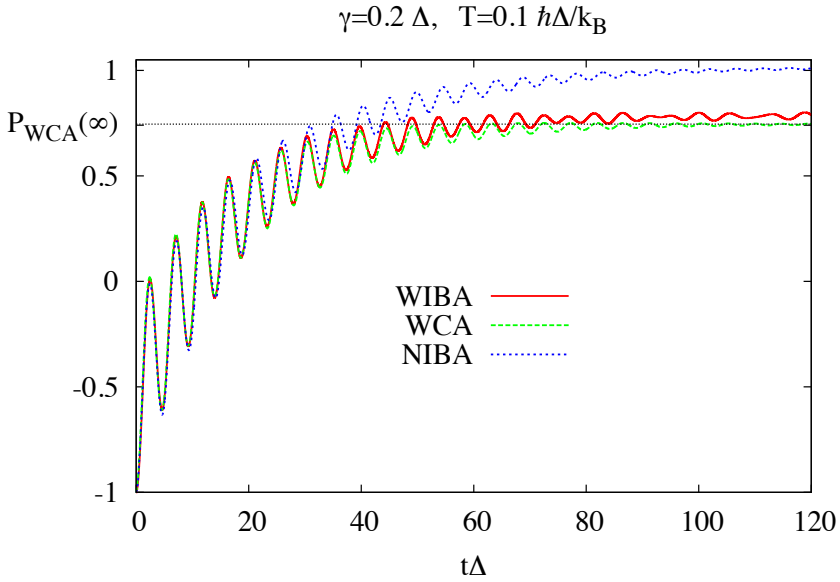

Figure 3.10: WIBA, NIBA and WCA results for the biased system ($\epsilon = 1\Delta$ and $\omega_C = 50\Delta$) in the weak to intermediate coupling $\gamma = 0.2\Delta$ and low temperature temperature $T = 0.1\hbar\Delta/k_B$. The WIBA scheme reproduces the WCA results while the NIBA predicts incorrectly localization at equilibrium.

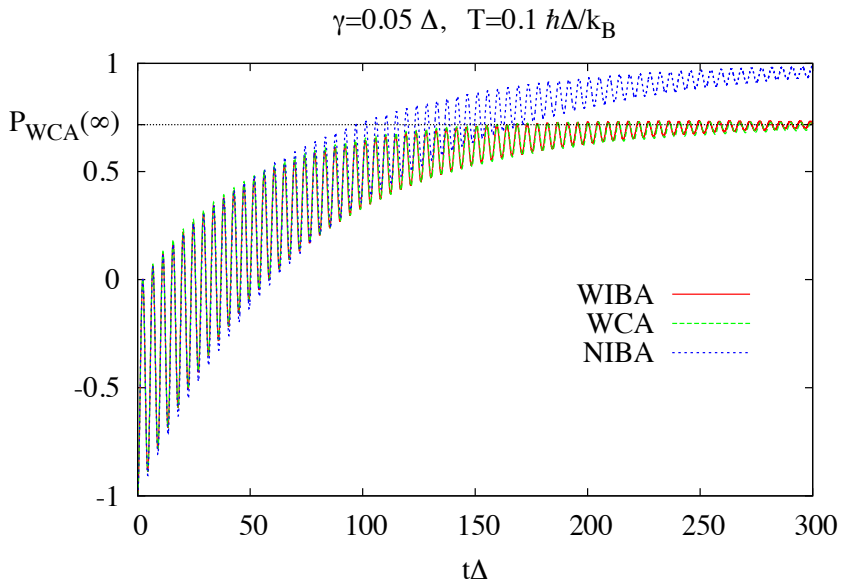

Figure 3.11: WIBA, NIBA and WCA results for the biased system ($\epsilon = 1\Delta$ and $\omega_C = 50\Delta$) in the weak coupling $\gamma = 0.05\Delta$ and low temperature temperature $T = 0.1\hbar\Delta/k_B$. The WIBA scheme reproduces exactly the WCA results. The NIBA scheme for the biased system fails in this weak coupling regime.

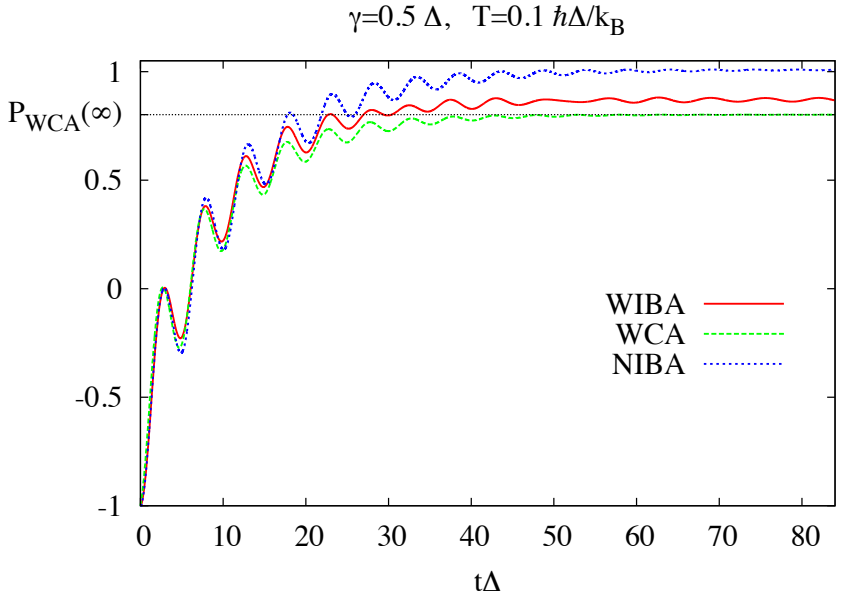

Figure 3.12: WIBA, NIBA and WCA results for the biased system ($\epsilon = 1\Delta$ and $\omega_C = 50\Delta$) in the moderate coupling $\gamma = 0.5\Delta$ and low temperature $T = 0.1\hbar\Delta/k_B$. In this intermediate coupling regime the WCA looses validity as predicts less localization than the WIBA. On the other hand the NIBA fails on the opposite direction predicting complete localization. The WIBA scheme is the most reliable in this dissipation regime.

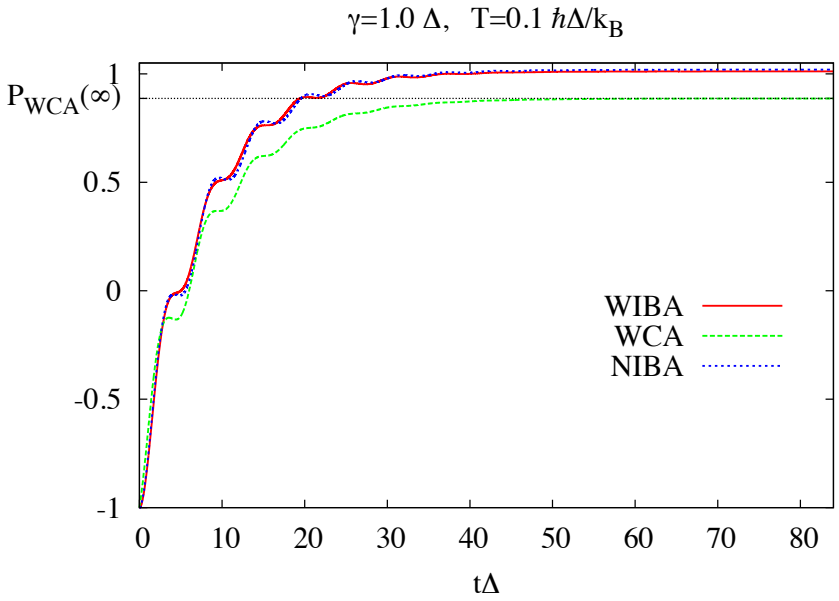

Figure 3.13: WIBA, NIBA and WCA results for the biased system ($\epsilon = 1\Delta$ and $\omega_C = 50\Delta$) in the strong coupling $\gamma = 1.0\Delta$ and low temperature $T = 0.1\hbar\Delta/k_B$. In the strong coupling regime the NIBA is valid and its results coincide with those of the WIBA scheme. The WCA completely fails since γ cannot be treated perturbatvely.

Chapter 4

The dissipative double-doublet system

[*The present chapter is published in collaboration with Prof. D. Valenti*[1]*, Prof. B. Spagnolo*[1] *and Prof. M. Grifoni*[2] [50]]

In this chapter the study of dissipative bistable quantum systems is extended beyond the TLS approximation. In the presence of strongly non linear potentials, such as those considered throughout this thesis (see Figs. 1.1, 1.4 and 3.1), the first energy levels are organized in well separated *doublets*. It follows that different time scales appear in the dynamics as energy states other than those of the first doublet are involved. Exploiting this separation in the time scales and using the techniques introduced in Chap. 3, an approximation scheme is introduced which is capable of treating the four-state system resulting from considering the first two energy doublets, in the intermediate coupling and temperature regime, where the system's dynamics displays coherent intra-well oscillations and incoherent tunneling.

If a bistable system is prepared with the particle in one of the two wells, coherent Rabi oscillations between the wells occur at very small dissipation strengths and low temperatures. On the other hand, at sufficiently large damping and/or high temperatures the dynamics is known to be incoherent. So far, the coherent to incoherent crossover has been only investigated in the so-called two-level system (TLS) approximation for the Hilbert space of the bistable system: the temperature is taken to be low enough that, to a good approximation, the system's dynamics can be restricted to the space spanned by the lowest doublet $\{|g\rangle, |e\rangle\}$ of eigenstates of the system's bare Hamiltonian (cf. Fig. 3.1). A vast literature exists [9, 33, 51, 64] which investigates the coherent to incoherent crossover for various dissipation mechanisms in great detail.

For temperatures of the order of the separation to the next lying energy levels, the TLS approximation breaks down and the multi-level nature of the bistable potential cannot be neglected. Despite its relevance for applications, the dissipative bistable dynamics in this temperature regime is so far poorly understood [65–72].

For very small damping strengths, a perturbative Bloch-Redfield approach capturing coherent intra-well and inter-well oscillations is appropriate [69, 70]. In the opposite

[1]Dipartimento di Fisica e Chimica, Università di Palermo.
[2]Theoretische Physik, Universität Regensburg, Regensburg Germany.

regime of moderate to large damping and temperatures the dynamics is fully incoherent and is well described in terms of rate equations for the populations of states localized in the wells, with rates obtained within a non-perturbative path integral approach [71]. However, the crossover regime, characterized by moderate damping and temperatures, presents an unsolved challenge. The major difficulty lies in the fact that, as the tunneling dynamics occurs on a time scale much larger than that of the intra-well dynamics, a hybrid situation can occur where quantum coherence is present at the level of intra-well motion, but is lost at longer times where tunneling processes are relevant.

In this chapter we consider a generalization of the SB model to a four level bistable system, the so-called *double-doublet system* (DDS), because its energy levels are arranged in well separated doublets due to the strong nonlinearity of the potential (see Fig. 4.1). We develop and use a novel approximation scheme, outlined in [61], which is based on a difference in time-scales between the fast intra-well motion and the slow inter-well (tunneling) dynamics and makes use of the TLS WIBA scheme (presented in Chap. 3). To take into account the different time scales of the intra- and inter-well dynamics, we include in the vibrational relaxation (VR) dynamics the long and short time correlations introduced by the Feynman-Vernon influence functional. On the other hand, only short time correlations turn out to be relevant for the tunneling process. Using this novel scheme we succeed in treating the crossover region of intermediate temperatures and damping not accessible to currently existing Bloch-Redfield-like [69, 70] or NIBA-like [71, 72] approximation schemes for multi-state systems.

At low temperature and weak damping, the resulting dynamics exhibits coherent oscillations at short times and incoherent tunneling behavior at longer times. By increasing the temperature and/or coupling strength, a crossover to a fully incoherent regime is observed, in accordance with the predictions in Ref. [71, 72].

A phase diagram in the coupling strength-temperature plane, displaying the various dynamical regimes, with the corresponding approaches or approximation schemes, gives a comprehensive account for the problem of the dissipative quantum dynamics beyond the TLS approximation.

4.0.1 The double-doublet system

The double well potential considered is modeled by the quartic polynomial in the particle position operator

$$V(\hat{q}) = \frac{M^2\omega_0^4}{64\Delta U}\hat{q}^4 - \frac{M\omega_0^2}{4}\hat{q}^2 - \epsilon\hat{q} \tag{4.1}$$

which has qualitatively the same features as that of the flux qubit in Eq. (1.7. The parameters ϵ and ΔU are the bias and the potential barrier, respectively.

The specific bistable system considered in this chapter symmetric ($\epsilon = 0$ in Eq. (4.1)) and its relevant Hilbert space spanned by the first four energy eigenstates. Since the corresponding energy levels are arranged in a pair of two well separated doublets, the system is called double-doublet system (DDS).

In Fig. 4.1 are shown the potential, the energy levels and wavefunctions $\langle q|E_i\rangle$, along with the corresponding DVR eigensystem, given by

$$\hat{q}|Q_j\rangle = Q_j|Q_j\rangle \qquad j = 1, \ldots, 4. \tag{4.2}$$

The energy doublets are characterized by internal frequency differences $\Omega_2 \ll \Omega_1 \ll \Omega_0$, where $\hbar\Omega_2 = E_2 - E_1$ and $\hbar\Omega_1 = E_4 - E_3$ are the intra-doublet (or tunneling) splittings,

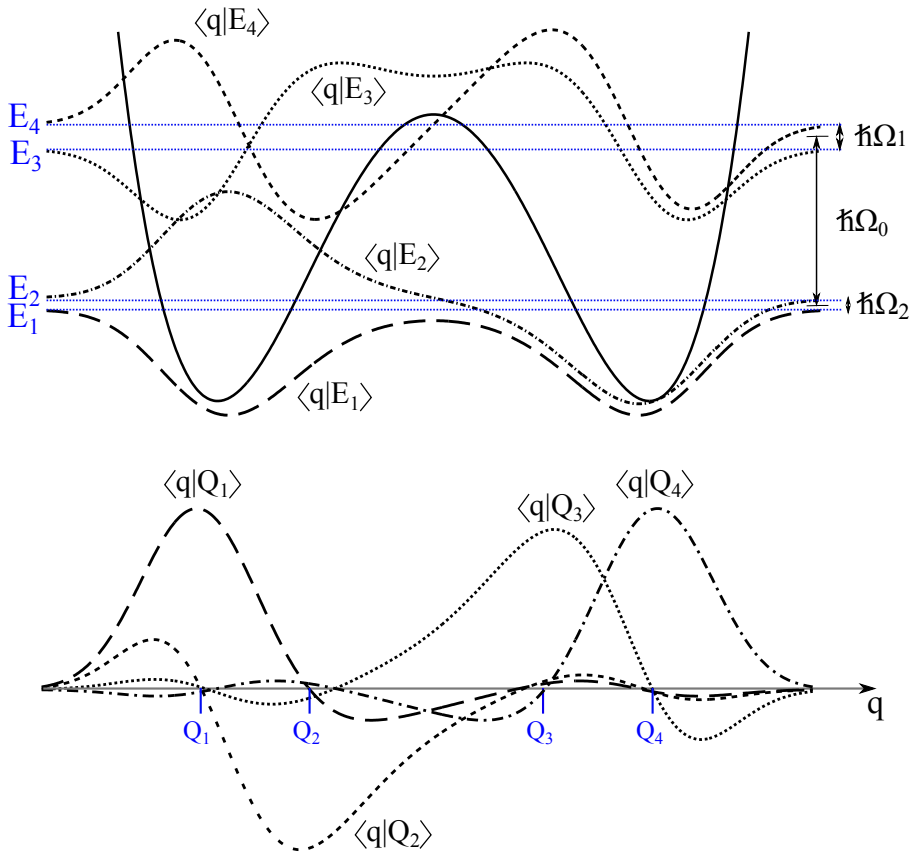

Figure 4.1: Potential V (Eq. (4.1)) with $\Delta U = 1.4\hbar\omega_0$ and $\epsilon = 0$. The minima are at $q_{L/R} \mp 3.35\sqrt{\hbar/(M\omega_0)}$. *Upper panel* - The four energy levels (horizontal lines) and the respective energy eigenfunctions. The spacing between the first two levels is exaggerated for the sake of clarity. The frequency $\Omega_0 = 0.8151\omega_0$ is the average inter-doublet frequency spacing while the tunneling frequency splittings of the higher and the lower doublet are $\Omega_1 = 0.1212\omega_0$ and $\Omega_2 = 0.0037\omega_0$, respectively. *Lower panel* - Discrete variable representation. The four position eigenvalues $\{Q_j\}$ and the corresponding eigenstates $\{|Q_j\rangle\}$. In the present problem $Q_{1/4} \sim \mp 3.51\sqrt{\hbar/(M\omega_0)}$ and $Q_{2/3} \sim \mp 1.82\sqrt{\hbar/(M\omega_0)}$.

and $\hbar\Omega_0 = (E_4 + E_3)/2 - (E_2 + E_1)/2$ is the average inter-doublet spacing, which is of the order of $\hbar\omega_0$ (the numerical values for the potential used in this work are given in the caption Fig. 4.1).

In the DVR the wave functions are peaked around the four eigenvalues $Q_1, \ldots, Q_4$ so that, for the particle, to be in the state $|Q_j\rangle$ means to be *localized* around Q_j.

It is important to notice that limiting the energy levels involved in the system dynamics to the first four is a good approximation as long as the environment is not likely to excite the particle to higher energies, i.e. as long as $k_B T/\hbar \lesssim \Omega_0$.

The passage to the DVR is performed through the diagonalization of the position operator $\hat{q}$. This operation can be carried out analytically, to a good degree of approximation, and is made more comfortable by writing the position operator in the *localized* basis of the DDS $\{|L_1\rangle, |L_2\rangle, |R_1\rangle, |R_2\rangle\}$, where

$$\begin{aligned} |L_1\rangle &= \frac{1}{\sqrt{2}}\left(|E_1\rangle - |E_2\rangle\right), \qquad |L_2\rangle = \frac{1}{\sqrt{2}}\left(|E_3\rangle - |E_4\rangle\right) \\ |R_1\rangle &= \frac{1}{\sqrt{2}}\left(|E_1\rangle + |E_2\rangle\right), \qquad |R_2\rangle = \frac{1}{\sqrt{2}}\left(|E_3\rangle + |E_4\rangle\right). \end{aligned} \tag{4.3}$$

The position operator in the localized basis reads

$$\hat{q} = \begin{pmatrix} -a_{11} & -a_{12} & 0 & b \\ -a_{12} & -a_{22} & -b & 0 \\ 0 & -b & a_{11} & a_{12} \\ b & 0 & a_{12} & a_{22} \end{pmatrix}, \qquad \text{where} \qquad \begin{aligned} a_{11} &= \langle E_1|\hat{q}|E_2\rangle \\ 2a_{12} &= \langle E_1|\hat{q}|E_4\rangle + \langle E_2|\hat{q}|E_3\rangle \\ a_{22} &= \langle E_2|\hat{q}|E_3\rangle \\ 2b &= \langle E_1|\hat{q}|E_4\rangle - \langle E_2|\hat{q}|E_3\rangle \ll a_{ij} \end{aligned} \tag{4.4}$$

The DVR is provided by the the eigensystem $\{Q_j, |Q_j\rangle\}$. To proceed analytically is simpler to take $b \sim 0$, however the parameters used for calculating the DDS dynamics in Sec. 4.3 are obtained form numerical diagonalization. The position eigenvalues are (see Fig. 4.1)

$$\begin{aligned} Q_{1,2} &= \frac{1}{2}\left(-a_{11} - a_{22} \mp \sqrt{(a_{11} - a_{22})^2 + 4a_{12}^2}\right) \\ Q_{3,4} &= \frac{1}{2}\left(a_{11} + a_{22} \mp \sqrt{(a_{11} - a_{22})^2 + 4a_{12}^2}\right). \end{aligned} \tag{4.5}$$

Note that, because of the symmetry of the potential, these eigenvalues are displaced symmetrically, i.e. $Q_{3/4} = -Q_{2/1}$. The four DVR states, expressed in terms of the energy eigenbasis $|E_1\rangle, \ldots, |E_4\rangle$, are

$$\begin{aligned} |Q_1\rangle &= \frac{v}{\sqrt{2}}\Big(|E_1\rangle - |E_2\rangle - u|E_3\rangle + u|E_4\rangle\Big) \\ |Q_2\rangle &= \frac{v}{\sqrt{2}}\Big(-u|E_1\rangle + u|E_2\rangle - |E_3\rangle + |E_4\rangle\Big) \\ |Q_3\rangle &= \frac{v}{\sqrt{2}}\Big(u|E_1\rangle + u|E_2\rangle + |E_3\rangle + |E_4\rangle\Big) \\ |Q_4\rangle &= \frac{v}{\sqrt{2}}\Big(|E_1\rangle + |E_2\rangle - u|E_3\rangle - u|E_4\rangle\Big) \end{aligned} \tag{4.6}$$

where

$$u = \frac{a_{11} + Q_1}{a_{12}} \qquad \text{and} \qquad v = \frac{1}{\sqrt{1 + u^2}}. \tag{4.7}$$

In the present problem $u \sim -0.585125$.

The transition amplitudes per unit time Δ and the bias factors ϵ, defined in Eq. (2.76) in terms of the frequency differences $\omega_{ij} = \omega_i - \omega_j$, are given by

$$\begin{aligned}
\Delta_{1,2} = \Delta_{2,1} = -\Delta_{4,3} = -\Delta_{3,4} &= v^2 u \Omega_0 \\
\Delta_{1,3} = \Delta_{3,1} = -\Delta_{2,4} = -\Delta_{4,2} &= \frac{v^2 u}{2}(\omega_{4,3} - \omega_{2,1}) \\
\Delta_{2,3} = \Delta_{3,2} &= \frac{v^2}{2}(\omega_{4,3} + u^2 \omega_{2,1}) \\
\Delta_{1,4} = \Delta_{4,1} &= \frac{v^2}{2}(u^2 \omega_{4,3} + \omega_{2,1})
\end{aligned} \tag{4.8}$$

and

$$\begin{aligned}
&\epsilon_{1,2} = \epsilon_{1,3} = \epsilon_{4,3} = \epsilon_{4,2} = -\epsilon_{2,1} = -\epsilon_{4,1} = -\epsilon_{3,4} = -\epsilon_{2,4} = v^2(u^2 - 1)\Omega_0 \\
&\epsilon_{1,4} = \epsilon_{4,1} = \epsilon_{2,3} = \epsilon_{3,2} = 0.
\end{aligned} \tag{4.9}$$

The last line derives from the symmetry of the problem. Here the two indexes are used to specify the states q_j and q'_j, whereas in Eq. (2.76) the single index specifies the transition number.

A formally exact expression for the dynamics (of the populations in a generic basis) of a multi-state system has been given in Eq. (2.73). As already noticed, because of the intricacies introduced by the Feynman-Vernon influence functional, approximate treatments are needed. Approximations which go beyond the generalized NIBA (gNIBA) proposed in Ref. [72] are discussed in Sec. 4.1. Notice that the parameters of the bistable potential are chosen as in [72], such that some of the results presented there for the incoherent regime can be used as reference.

In the DVR the double path $(q(t), q'(t))$ is no more a continuous function of time but a walk on a two-dimensional spatial grid with 4×4 grid-points. Each coordinate takes values in the set $\{Q_1, \ldots, Q_4\}$, so the path integral turns into a sum over all the possible path configurations, integrated over the transition times (as in Eq. (2.73)). An example of double path with five transitions is shown in Fig. 4.2.

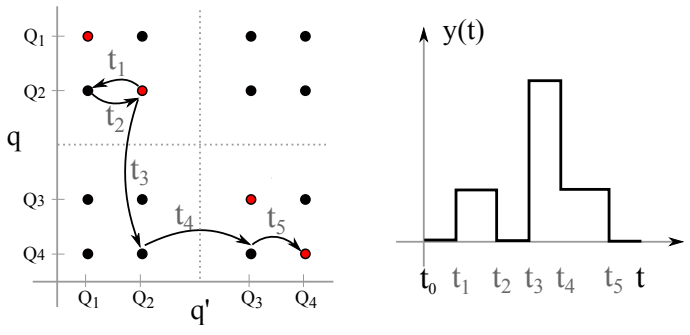

Figure 4.2: *Left panel* - Example of a double path in the DVR plane (q, q') in which the two diagonal sites (Q_2, Q_2) and (Q_4, Q_4) are connected by five transitions. When the path crosses the horizontal (vertical) dotted line the coordinate q (q') is making a tunneling transition. *Right panel* - Time resolved picture of the path in the left panel in terms of relative coordinate $y = q - q'$. The path has three sojourns and two clusters.

4.0.2 Exact free dynamics of the DDS

The calculation of the DDS dynamics in the DVR basis is not straightforward within the path integral approach described above. Nevertheless, if the system is isolated, the populations in the DVR are easily obtained by carrying out the calculations in the energy representation. Suppose the initial condition is $|\psi(0)\rangle = |Q_1\rangle$. The DVR populations, i.e. the probabilities to find the particle in the DVR states $|Q_i\rangle$ $(i = 1, \ldots, 4)$ are

$$\begin{aligned}
\rho_{11}(t) =& \frac{v^4}{2}\Big\{1 + u^4 + \cos(\omega_{21}t) + u^2\left[\cos(\omega_{31}t) + \cos(\omega_{41}t) + \cos(\omega_{32}t) + \cos(\omega_{42}t)\right] \\
&+ u^4\cos(\omega_{43}t)\Big\} \\
\rho_{22}(t) =& \frac{u^2v^4}{2}\left\{2 + \cos(\omega_{21}t) - \cos(\omega_{31}t) - \cos(\omega_{41}t) - \cos(\omega_{32}t) - \cos(\omega_{42}t) + \cos(\omega_{43}t)\right\} \\
\rho_{33}(t) =& \frac{u^2v^4}{2}\left\{2 - \cos(\omega_{21}t) - \cos(\omega_{31}t) + \cos(\omega_{41}t) + \cos(\omega_{32}t) - \cos(\omega_{42}t) - \cos(\omega_{43}t)\right\} \\
\rho_{44}(t) =& \frac{v^4}{2}\Big\{1 + u^4 - \cos(\omega_{21}t) + u^2\left[\cos(\omega_{31}t) - \cos(\omega_{41}t) - \cos(\omega_{32}t) + \cos(\omega_{42}t)\right] \\
&- u^4\cos(\omega_{43}t)\Big\},
\end{aligned} \tag{4.10}$$

where $\omega_{i,j} = \omega_i - \omega_j$.

The free DDS dynamics is shown in Fig. 4.3, where the relevant time scales are highlighted and a comparison is made with the long time free dynamics of the system in the TLS approximation.

The free dynamics displays *fast* intra-well oscillations of frequency Ω_0 and a tunneling dynamics, occurring in two distinct time scales: the shorter one is given by the higher energy doublet (frequency Ω_1, see Fig. 4.1) and the longer one, involved in the left/right population inversion, occurs on the times scale set by the frequency $\Omega_2 = (E_2 - E_1)/\hbar$. As shown in Fig. 4.3, the long time oscillations coincide with those of the system in the TLS approximation starting with the particle in the left well.

The rich dynamics described reflects the configuration of the energy levels in two well separated doublets, with different inter-doublet separation, and allows for the approximations on the Feynman-Vernon influence functional introduced in the following sections.

4.1 Approximations

We want to study the DDS dissipative dynamics in terms of the time evolution of the populations, the diagonal elements of the RDM in the DVR basis, assuming that the particle is initially in the state $|Q_1\rangle$. This amounts to calculate the propagator (see Eq. (2.25))

$$\rho_{kk}(t) = G(Q_k, Q_k, t; Q_1, Q_1, t_0), \qquad k = 1, \ldots, 4. \tag{4.11}$$

The evaluation of the propagator involves two main difficulties. The first one is that, contrary to the TLS case, the variety of possible paths of the multi-state system makes the summation difficult, if not impossible, even in the absence of coupling with the bath. This feature calls for a selection on the paths to be summed.

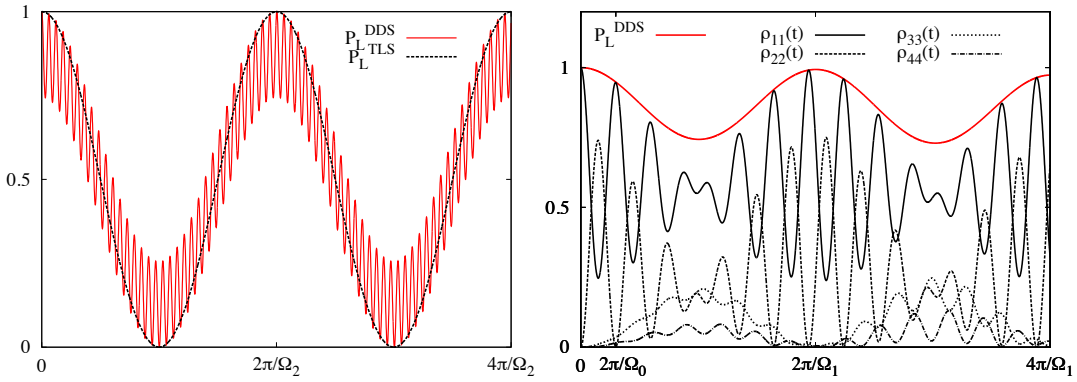

Figure 4.3: Time evolution of the populations in the DVR for the free DDS with initial condition $\rho(t_0 = 0) = |Q_1\rangle\langle Q_1|$ (analytical result). *Left panel* - Long time dynamics of the left well population $P_L = \rho_{11} + \rho_{22}$ compared to the $|L\rangle$ state population of the system in the TLS approximation. *Right panel* - Short time dynamics of the left well population of the DDS and time evolution of the single populations of the DVR basis states.

The second difficulty is constituted by the intricate set of time nonlocal correlations among the ξ_i and χ_j charges, introduced by $\mathcal{F}_{FV}$, which make the path integral expression intractable.

Hereinafter we shall use an approximation on $\mathcal{F}_{FV}$ which is based on the separation of time scales between the *intra-well* and the *inter-well* dynamics. The first one is characterized by transitions among states in the same well, called *vibrational relaxation* events (VR). The inter-well dynamics consists of transitions among states in different wells, called tunneling events (T).

In order to give a justification for this approximation we describe, in the next section, the free dynamics of the system. It shows the characteristic time scales associated with the level structure of the symmetric double well potential considered (see Fig. 4.1).

4.1.1 Selection on the paths and retained interactions

When a double path is in a diagonal configuration ($q = q'$), it is said to be in a *sojourn*. The non-diagonal configuration ($q \neq q'$) between two consecutive sojourns forms a *cluster*. The latter is a generalization of the *blip* configuration for the TLS [51]. The difference is that a blip consists, for geometrical reasons, of a single off-diagonal excursion while a cluster can be made of an arbitrary long sequence of off-diagonal transitions. In Fig. 4.2 we give an example of a path with three sojourns and two clusters, the first of which is a simple blip and the second a proper cluster with multiple off-diagonal excursions.

For Ohmic damping with exponential cutoff at a high frequency ω_C, the long time or high temperature limit ($t \gg \hbar/k_B T$) of the bath correlation function (Eq. (2.62)) is

$$Q(t) = \frac{M\gamma}{\pi\hbar}\left[\kappa t - \ln\left(\frac{2\kappa}{\omega_C}\right)\right] + i\frac{M\gamma}{2\hbar}, \tag{4.12}$$

where $\kappa = \pi k_B T/\hbar$. In this limit, the inter-cluster interactions cancel out exactly, so that the suppression of the path weight exerted through $Q'(t)$ depends on the length of the cluster. For this reason, in the presence of the dissipative Ohmic environment considered

here, the contribution of paths with long off-diagonal excursions is suppressed. Thus, the main contribution to the sum (2.73) is given by those path returning in a sojourn after a single off-diagonal excursion.

The first approximation we do is to consider only this class of paths. Following the TLS convention, we call the off-diagonal configurations *vibrational relaxation*-blips (VR-blips), if q and q' belong to the same well, and *tunneling*-blips (T-blips), if q and q' belong to different wells.

The second approximation consists in neglecting, among the interactions induced by $\mathcal{F}_{FV}$, i) all the interactions between couples of T-blips, ii) those between a T-blip and a VR-blip and iii) the interactions between two non-consecutive VR-blips. This approximation is justified by the long time scale of the tunneling dynamics, i.e. by the fact that, on the average, tunneling events are rare, because the transition amplitude per unit time associated with them is small in comparison with that of a VR event. Since in a typical path the T-blips are well separated in time, their ξ and χ charges interact through the long time limit of the bath correlation function, meaning that the total interaction sums up to zero, as stated above.

Moreover, a tunneling blip is strongly suppressed by the environment, since $\xi_j \xi_{j-1} = -(q_j - q'_j)^2$ in Eq. (2.72) is large if q and q' are in different wells. The resulting picture, for a typical path among those retained in the summation, is that of a sequences of frequent VR-blips, which we call **VR-blip chain**, interrupted by T-blips, as sketched in Fig. 4.4. Notice that, inside a VR-blip chain, the interactions are retained.

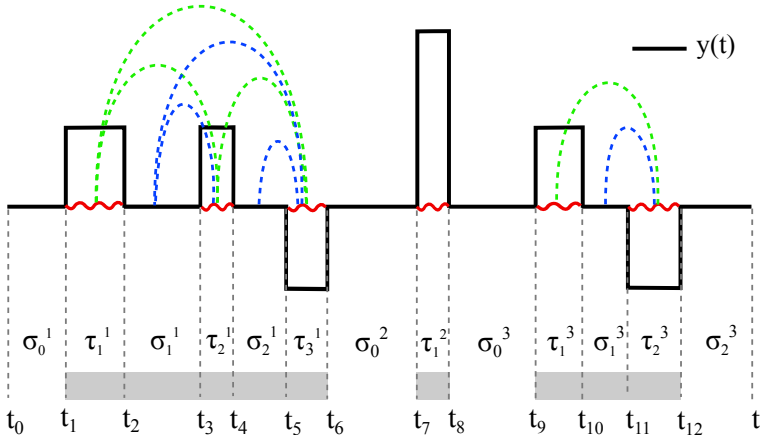

Figure 4.4: A path made by two VR-blip chains separated by a T-blip. The transition times and the blip/sojourn times are indicated. The shaded areas on the lower part of the figure represent the time intervals inside which the correlations are retained according to the approximations discussed in Sec. 4.1.1. Specifically, according to the VR-WIBA scheme introduced in Sec. 4.1.2, the intra-VR-blip and intra-T-blip interactions (solid wavy lines) are taken at all order in γ while the inter-VR-blip and VR-blip-sojourn interactions (dashed lines) are taken to the first order in γ.

Under these two approximations the system decouples into a set of six TLSs. Any double path can be seen as a sequence of arbitrarily long, non-interacting paths inside the two dimensional sublattices in Fig. 4.5, each of which represents a different TLS characterized by its own bias factor, tunneling element and distance between the spatial coordinates.

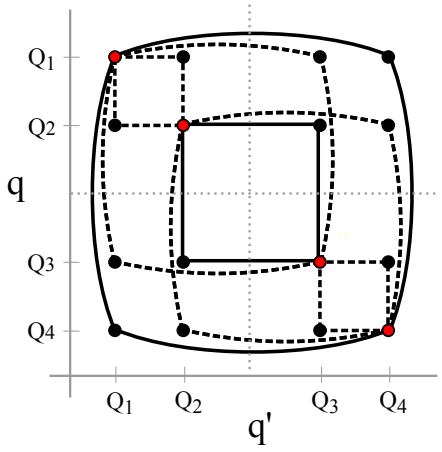

Figure 4.5: With the limitations on the allowed paths and the separation of the intra- and inter-well dynamics, the motion of the system in the 4×4 grid of spatial positions decouples into a sequence of arbitrarily long paths inside the six two-dimensional square sublattices in the figure, each one representing a different TLS. The dashed squares indicate the TLSs with nonzero effective bias while the solid squares indicate symmetric TLSs.

4.1.2 Weakly-interacting VR-blip approximation

The approximations done still allow for the treatment of the VR-blip chains, i.e. the motion of the TLSs formed by the couples of states inside each well, to arbitrary accuracy.

Again, also for an intra-well TLS, an exact treatment is impossible due to the intricacies brought by $\mathcal{F}_{FV}$. It is therefore necessary to make further approximations on the nonlocal interactions inside the VR-blip chains.

At high temperatures, in the limits of the DDS description, the long time limit of $Q(t)$ (see Eq. (4.12)) is attained at short times. If the linearized form is attained on time scales of the order of magnitude of the average separation between two VR-blips, they can be considered noninteracting objects. This amounts to retain only the local in time effects introduced by $\mathcal{F}_{FV}$. The resulting scheme for the intra-well dynamics is the well known NIBA. Within the NIBA for the VR-blip chains every blip is noninteracting with any other. The resulting overall scheme is the multi-level generalization of the NIBA, which can be called generalized non-interacting blip approximation (**gNIBA**)[3].

At lower temperature the gNIBA breaks down because the inter-blip interactions are not removed completely inside a VR-blip chain. However, due to the long timescale of the inter-well dynamics, the isolation of the T-blips is still valid if the cutoff operated by $\mathcal{F}_{FV}$ occurs on the time scale Ω_1^{-1} of the fast tunneling dynamics.

To account for inter-blip correlations in the VR dynamics, we adapt to our purposes a scheme for the TLS, called *weakly interacting blip approximation* (WIBA) [59], which interpolates between strong and weak damping regimes. The scheme retains, to the first order in γ, the nonlocal part of the interactions among the VR-blips and, to all orders, the interactions inside the VR-blips. We name the resulting overall scheme for the DDS **VR-WIBA**.

[3]This scheme corresponds to the generalized non-interacting cluster approximation (gNICA) at the leading order in the Δ factors [72].

From what stated above two considerations can be made about the validity of our VR-WIBA approximation scheme. The first is that the region of the parameter space in which the VR-WIBA is valid includes that of the gNIBA because the isolation of any blip implies the separation among T-blips and VR-blip chains. The second comment is that, while the validity of the gNIBA is established by the temperature and depends weakly on the damping, in determining the validity of the VR-WIBA both temperature and damping play an important role.

In the Sec. 4.2 we discuss in more detail the validity domains and in Sec. 4.3 we show and compare their results for the dissipative DDS dynamics.

4.1.3 VR-WIBA generalized master equation

By properly taking into account the above approximations every double path can be considered as a sequence of non-interacting paths along the two 2×2 sublattices in Fig 4.5. A sublattice is identified by the coordinates of its two diagonal sites (red dots in the figure). Suppose a sublattice has diagonl sites (q_A, q_A) and (q_B, q_B). Then the path inside this sublattice is mapped onto the motion of the TLS $\{|q_A\rangle, |q_B\rangle\}$. Every TLS path has, by definition, an even number of transitions, since it starts and ends in a diagonal configuration, so the whole path has an even number $2n$ of transitions (see Fig. (4.5)). We can therefore factorize the amplitude $A(t_0, \ldots, t_{2n}, t) = \mathcal{A}(q)\mathcal{A}^*(q')\mathcal{F}_{FV}(x, y)$ into the product of the amplitudes A_j associated to the paths into the TLSs. The initial and final states are fixed: $q_0 = Q_1$ and $q_n = Q_k$.

From inspection of Eq. (2.73) (see also Fig. 4.4) we see that the amplitudes don't depend on the last sojourn time.

Moreover we neglect, in each of the amplitudes A_j, the interactions involving the first sojourn time (this is justified by the fact that the VR-blip chains and the T-blips are well separated, which implies a long first sojourn time).

If a path switches sublattice M times, with $2k_j$ transitions in the j-th sublattice and $\sum_{j=1}^{N} k_j = n$, we have

$$A(t_1, t_2 \ldots, t_{2n-1}, t_{2n}) = \prod_{j=1}^{M} A_j(\tau_1^j, \sigma_1^j, \ldots, \sigma_{k_j-1}^j, \tau_{k_j}^j), \tag{4.13}$$

where $\tau_j = t_{2j} - t_{2j-1}$ are the blip times and $\sigma_j = t_{2j+1} - t_{2j}$ the sojourn times.

The population $\rho_{kk}(t)$ of the state $|Q_k\rangle$ at time t, given the initial condition $\rho(t_0) = |Q_1\rangle\langle Q_1|$ (see Eq. (4.11)), is

$$\rho_{kk}(t) = \delta_{Q_k Q_1} + \sum_{n=1}^{\infty} \int_{t_0}^{t} \mathcal{D}_{2n}\{t_j\} A(t_0, t_1, \ldots, t_{2n}, t). \tag{4.14}$$

Due to the fact that the amplitudes in this sum over the paths factorize as in Eq. (4.13), the Laplace transform of $\rho_{kk}(t)$ reads

$$\rho_{kk}(\lambda) = \frac{\delta_{Q_k Q_1}}{\lambda} + \frac{1}{\lambda} \sum_{M=1}^{\infty} \sum_{\{q_j\}=Q_1}^{Q_4} \prod_{j=1}^{M} \frac{\hat{K}_{q_{j-1}q_j}(\lambda)}{\lambda}, \tag{4.15}$$

where, for $q_j \neq q_{j-1}$, the functions $\hat{K}_{q_{j-1}q_j}(\lambda)$ are the Laplace transforms of the TLS kernel $K_{q_{j-1}q_j}(\tau)$ in the master equation for the populations of the TLS $\{|q_{j-1}\rangle, |q_j\rangle\}$ (see Appendix C).

We now switch to vector notation. We define the four-dimensional vector $\vec{\rho}(\lambda)$, whose components are the Laplace transform $\rho_{kk}(\lambda)$ of the four populations. Defining also the 4×4 matrix $\hat{\mathcal{K}}(\lambda)$, whose elements are the functions $\hat{K}_{q_j q_{j-1}}(\lambda)$, Eq. (4.15) reads

$$\begin{aligned}\vec{\rho}(\lambda) =& \frac{\vec{\rho}(t_0)}{\lambda} + \frac{1}{\lambda}\sum_{M=1}^{\infty}\left[\frac{\hat{\mathcal{K}}(\lambda)}{\lambda}\right]^N \vec{\rho}(t_0) \\ =& \frac{1}{\lambda}\sum_{N=0}^{\infty}\left[\frac{\hat{\mathcal{K}}(\lambda)}{\lambda}\right]^N \vec{\rho}(t_0) \\ =& \left[\lambda\mathbb{I} - \hat{\mathcal{K}}(\lambda)\right]^{-1}\vec{\rho}(t_0).\end{aligned} \tag{4.16}$$

Transforming back to the time domain we obtain the following generalized master equation (GME)

$$\dot{\vec{\rho}}(t) = \int_{t_0}^{t} dt' \mathcal{K}(t-t')\vec{\rho}(t'),$$

where $\mathcal{K}(t) = \mathcal{L}^{-1}\{\hat{\mathcal{K}}(\lambda)\}$. Restoring the index notation, we find equivalently

$$\dot{\rho}_{kk}(t) = \sum_{j=1}^{4}\int_{t_0}^{t} dt' K_{kj}(t-t')\rho_{jj}(t'). \tag{4.17}$$

The diagonal elements of the kernel matrix $\mathcal{K}(t)$ are given by the probability conservation

$$K_{jj}(t) = -\sum_{i(\neq j)=1}^{4} K_{ij}(t).$$

The non-diagonal elements have been defined as the TLS kernels corresponding to the motion into the sublattices. These elements of the kernel matrix are taken within different approximation schemes, according to the populations they connect in the GME. Specifically, on the basis of the approximations made, they are classified as follows

- If the DVR states k and j belong to different wells, i.e.

  $$(k,j) = (1,3),(3,1),(1,4),(4,1),(2,3),(3,2),(2,4),(4,2),$$

  the corresponding kernel is a NIBA kernel $K_{kj}^{N}(t)$.

- If the DVR states k and j belong to the same well, i.e

  $$(k,j) = (1,2),(2,1),(3,4),(4,3),$$

  the nonlocal correlations can be, in principle, taken into account to any accuracy. We use the WIBA scheme for these intra-well kernels. In this scheme they consist of a NIBA plus a beyond-NIBA part

  $$K_{kj}^{W}(t) = K_{kj}^{N}(t) + K_{kj}^{BN}(t).$$

  If we set to zero the beyond-NIBA correction in these *intra-well kernels* we obtain the gNIBA scheme for the DDS discussed in [71].

The explicit expressions for the kernels are given in Appendix E.

4.2 Dynamical regimes and validity of the approximation schemes: phase diagram

While the dynamics of a TLS can occur in the coherent or incoherent tunneling regime, for the DDS there's a richer variety of dynamical regimes, due to the different energy scales involved in the problem.

Looking at the free DDS dynamics depicted in Fig. 4.3, we recognize three characteristic frequencies: $\Omega_2 \ll \Omega_1 \ll \Omega_0$. As discussed in Sec. 4.0.2, this is reflected by the presence of a slow tunneling dynamics, occurring at the time scale Ω_2^{-1}, a fast tunneling dynamics with frequency Ω_1 and the intra-well dynamics, which occurs on the shortest time scale Ω_0^{-1}. In the dissipative case the different oscillatory behaviors undergo damping/temperature dependent frequency shifts and are progressively suppressed at different dissipation regimes.

At intermediate damping and temperature the dynamical regimes are controlled by the behavior of the effective TLSs introduced in Sec. 4.1, as the natural description for the system passes from the energy representation to the localized one given by the DVR. It is thus suggestive to use the machinery existing for the spin-boson problem to give an indication of the boundaries between different dynamical regimes in the parameter space.

As discussed in Sec. 4.1.1, each effective TLS, denoted by $\{|Q_i\rangle, |Q_j\rangle\}$, has its tunneling element Δ_{ij}, bias ϵ_{ij} and characteristic distance $q_{ij} = Q_i - Q_j$. It follows that at fixed γ, the effective coupling K_{ij} to which a TLS is subject can be more or less strong, depending on its parameters. The effective damping strength, or Kondo parameter, for the TLS $\{|Q_i\rangle, |Q_j\rangle\}$ is defined by

$$K_{ij} = M\gamma q_{ij}^2/(2\pi\hbar). \tag{4.18}$$

For a real symmetric TLS at $T = 0$, the value $K = 1/2$ corresponds to the transition from the coherent to the incoherent behavior, while at $K = 1$ the *localization* occurs, consisting in the complete inhibition of the tunneling, with the consequence that the particle doesn't leave the well where it was prepared. The coherent-to-incoherent transition temperature T^* as a function of the effective damping for the symmetric TLS is given by [9]

$$T^*(K) = \left(\frac{(2\pi)^K}{\pi K}\right)^{1/(1-K)} \frac{\hbar\Delta_r}{k_B}, \tag{4.19}$$

where $\Delta_r = \Delta(\Delta/\omega_c)^{K/(1-K)}$ $(K < 1)$ is the renormalized tunneling element.

We exploit the decoupling of the DDS into effective TLSs, in conjunction with numerical tests, to identify the following dynamical regimes in the (γ, T)-space for the DDS: (a) - completely coherent regime, with coherent tunneling at both the slow (Ω_2^{-1}) and the fast (Ω_1^{-1}) tunneling time scales and coherent intra-well oscillations (Ω_0^{-1}); (b) - coherence at the fast tunneling time scale Ω_1^{-1}, with oscillations of the left/right well populations around a slow incoherent relaxation behavior and coherent intra-well dynamics; (c) - crossover regime, where the coherence is only at the level of intra-well motion (on the time scale Ω_0^{-1}); (d) incoherent regime, where the four populations relax incoherently to their equilibrium values.

The regions in the parameter space corresponding to the above mentioned dynamical regimes and the validity areas of the approximation schemes used to treat the DDS are depicted in the phase diagram of Fig. 4.6.

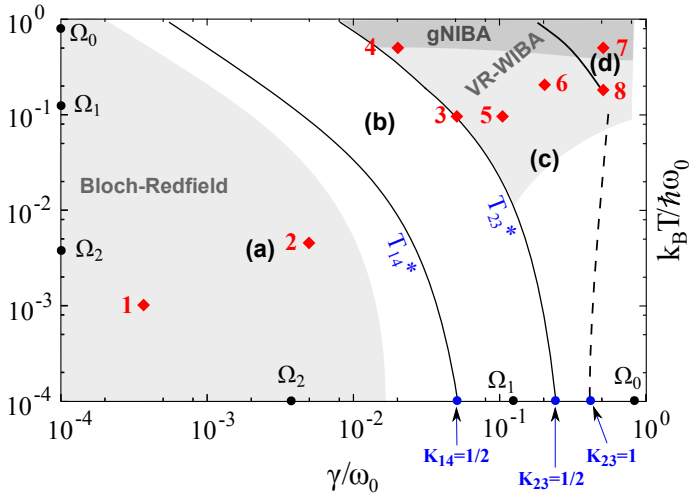

Figure 4.6: Phase-space diagram in the dimensionless coupling-temperature space. The dynamical regions, separated by solid lines, are: (a) complete coherence, (b) coherent regime, (c) crossover regime and (d) incoherent regime. The dashed line is an extrapolation to finite temperatures of the localization regime predicted for the effective symmetric TLS $\{|Q_2\rangle, |Q_3\rangle\}$ at $T = 0$. The shaded areas indicate the validity domains of the approximation schemes used. The WR-WIBA reduces to the gNIBA at high temperatures, so the domain of the first scheme includes that of the latter. The characteristic frequencies Ω_i of the DDS, reported in both axes in units of ω_0, serve as reference to establish the effective dissipation regimes. The diamonds refer to the parameters chosen to obtain the results presented in Sec. 4.3.

The completely coherent regime (Region (a) on the phase diagram) is established by considering T_{14}^*, the coherent-to-incoherent transition temperature as a function of the effective coupling for the effective TLS $\{|Q_1\rangle, |Q_4\rangle\}$ (cf. Eq. (4.19)). The boundary between Regions (a) and (b), given by T_{14}^*, determines the suppression of the slow oscillatory behavior of $P_L = \rho_{11} + \rho_{22}$, while both the intermediate tunneling oscillations and the fast intra-well dynamics survive.

In the part of Region (a) where the perturbative in the coupling treatment is appropriate, the Bloch-Redifield master equation describes correctly the dynamics of the DDS. The master equation has, for the coherences in the energy representation, the solution (see Appendix D)

$$\rho_{nm}^E(t) = e^{-i\omega_{nm}t} e^{-\mathcal{L}_{nm,nm}t} \rho_{nm}^E(t_0). \tag{4.20}$$

To determine the domain of validity of the Bloch-Redfield approach we compare the dephasing coefficient $\mathcal{L}_{12,12}$ with the frequency $\omega_{21} \equiv \Omega_2 = \omega_2 - \omega_1$ imposing $\mathcal{L}_{12,12} \leq \omega_{21}$. The result is the shaded area on the left part of the phase diagram. However, the extension of this validity domain may be overestimated, having neglected the frequency shifts in the evaluation of the Bloch-Redifield tensor (see. Eq. D.5). The weak coupling approximation fails near the boundary between (a) and (b) where the long time oscillations of P_L turn into incoherent relaxation.

Region (b) of the diagram, characterized by stronger damping and/or higher temperature, is outside the validity domain of the Bloch-Redfield approach. Nevertheless we can use the weak coupling estimates for the asymptotic values of the populations on the basis of the following argument. Whenever the relaxation to the equilibrium occurs, the asymp-

totic values of the left- and right-well populations are $P_L(\infty) = P_R(\infty) = 1/2$, due to the symmetry of the system. This means that we can obtain the single populations $\rho_{ii}(\infty)$, focusing on the intra-well biased TLSs $\{|Q_1\rangle, |Q_2\rangle\}$ and $\{|Q_3\rangle, |Q_4\rangle\}$. They are characterized by effective tunneling elements $|\Delta_{12}| \simeq 0.35\omega_0$ and effective biases $|\epsilon_{12}| \simeq 0.40\omega_0$. For these intra-well TLSs the effective damping $K_{12/34}$ is still weak and we can use the expressions given by the WCA [9] for the asymptotic populations of the intra-well TLSs states

$$\rho_{33/44}(\infty) = \frac{1}{4} \mp \frac{\epsilon}{4\Delta_b} \tanh\left(\frac{\hbar\Delta_b}{2k_BT}\right), \tag{4.21}$$

where $\Delta_b = \sqrt{\Delta_{12}^2 + \epsilon_{12}^2}$. By the symmetry of the problem we have $\rho_{22/11}(\infty) = \rho_{33/44}(\infty)$.

The boundary between the Regions (b) and (c) indicates the passage to the crossover regime in which the tunneling is incoherent. The right boundary to the area (b) is obtained considering the coherent-to-incoherent transition temperature T_{23}^* as a function of K_{23} for the symmetric TLS $\{|Q_2\rangle, |Q_3\rangle\}$.

The boundary between the coherent and the crossover regimes delimits also the validity of the approximation lying at the basis of the factorization of the DDS amplitudes into uncorrelated amplitudes relative to TLS paths. Indeed in the crossover regime, where the tunneling is incoherent, the contribution of the clusters in the sum over the paths is negligible so that the limitation made on the contributing paths holds.

Since the two intra-well TLSs have an effective bias, they can be treated according to the NIBA only in the high temperature/strong coupling regime (on the frequency scale Ω_0 of the intra-well motion) [9].

Treating the intra-well dynamics within the NIBA amounts to use the gNIBA scheme for the complete DDS and we can conclude that the gNIBA reproduces correctly the dynamics inside the darker shaded area in the uppermost part of the diagram.

The WIBA scheme applied to the intra-well TLSs extends the path integral approach for the DDS to low temperatures in a quite large damping range. The WIBA correctly predicts both the transient behavior and the asymptotic populations for the TLS whenever the intra-blip correlation can be neglected (high temperature at any coupling) or treated to the first order (from low to high temperature at weak coupling) [59]. Thus the validity area of the VR-WIBA includes that of the gNIBa and covers the upper-right shaded region in the phase diagram.

The dissipation regime inaccessible to the WIBA for a biased TLS, and consequently to the VR-WIBA for the DDS, is the low temperature/intermediate-to-strong coupling, where the inter-blip correlations are non suppressed by the bath and the coupling is not sufficiently weak to justify their treatment to the first order in γ. This corresponds to the lower-right part of the diagram where the dashed line at strong damping indicates an extrapolation to finite temperatures of the localization regime occurring at $T = 0$ for the symmetric effective TLS $\{Q_2, Q_3\}$. The extrapolation is made observing that, in this region of the parameter space, the effective tunneling elements of the inter-well effective TLSs vanish [9], so that the DDS is not expected to undergo the tunneling dynamics, irrespective of the initial condition.

4.3 Results for the DDS dynamics

4.3.1 Parameters and units

We scale all the parameters with ω_0, the natural oscillation frequency around the minima of the potential described in Eq. (4.1). We use the Ohmic bath spectral density function with exponential cutoff $J(\omega) = M\gamma\omega \exp(-\omega/\omega_C)$. The cutoff frequency is set to $\omega_C = 50\omega_0$. The potential is the same as in Fig. 4.1, with parameters $\epsilon = 0$ and $\Delta U = 1.4\hbar\omega_0$. In what follows $t_0 = 0$ and the initial condition is $\rho(0) = |Q_1\rangle\langle Q_1|$.

4.3.2 Dissipative DDS dynamics

In this section we show the time evolution of the populations in the DVR basis $|Q_1\rangle, \ldots, |Q_4\rangle$, at the parameter space points indicated in the phase diagram (Fig. 4.6).

In the Region (a) of the phase diagram (completely coherent dynamical regime) we give the dynamics at two phase space points. The first one (Fig. 4.7), at very low T and γ, is well within the applicability domain of the Bloch-Redfield master equation. The dynamics of the left/right well populations, $P_{L/R}$, of the DDS shows a slow damped oscillatory behavior of frequency Ω_2 with superposed small oscillations of frequency Ω_1 featured also in the free dynamics (see Fig 4.3). The short time behavior of the single populations is shown in the lower panels and resembles the free case, with fast oscillations of frequency Ω_0 and an oscillatory envelope of frequency Ω_1. This is because, at short times, the effect of the environment is not visible in this dissipation regime. We remark that in this dissipation regime the fast intra-well oscillations are a result of the initial condition (cf. Sec. 4.0.2).

The second dynamics is shown in Fig. 4.8 and corresponds to point 2 in the diagram. It is in the same dynamical regime as the first. The populations show the same qualitative feature as in the free case even if the damping of the fast tunneling oscillations is now visible.

The third point in the diagram is in the crossover regime at weak coupling and intermediate temperature (with respect to Ω_0). Here the coherence is only in the intra-well motion. In this dissipation regime the WCA completely fails as $\gamma \sim \Omega_1$, so the time evolution of the populations is calculated within the path integral approach in the gNIBA and in the novel VR-WIBA scheme.

The results are given in Fig. 4.9 and show that the gNIBA fails as expected from the discussion in Sec. 4.2. Indeed the point 3 in the phase diagram is outside the regime of validity of the gNIBA because the temperature is not sufficiently high to justify NIBA in the biased intra-well TLS.

The next time evolution is provided at point 4 in the diagram of Fig. 4.6, i.e. at weak damping and high temperature with respect to the intra-well frequency. Contrary to the previous case, here both the VR-WIBA and the gNIBA are expected to give the correct prediction. The results for the two schemes at this point of the parameter space coincide, as shown in Fig. 4.10.

The point 5 in the phase diagram is inside the crossover region at intermediate damping and temperature with respect to Ω_0. The gNIBA and VR-WIBA dynamics are shown in Fig. 4.11. Similarly to the case 3, the gNIBA fails and the VR-WIBA is expected to give the correct predictions. Interestingly, even if the damping is larger than that at point 3 in the phase diagram, the gNIBA prediction in this case is even worse than in Fig. 4.9,

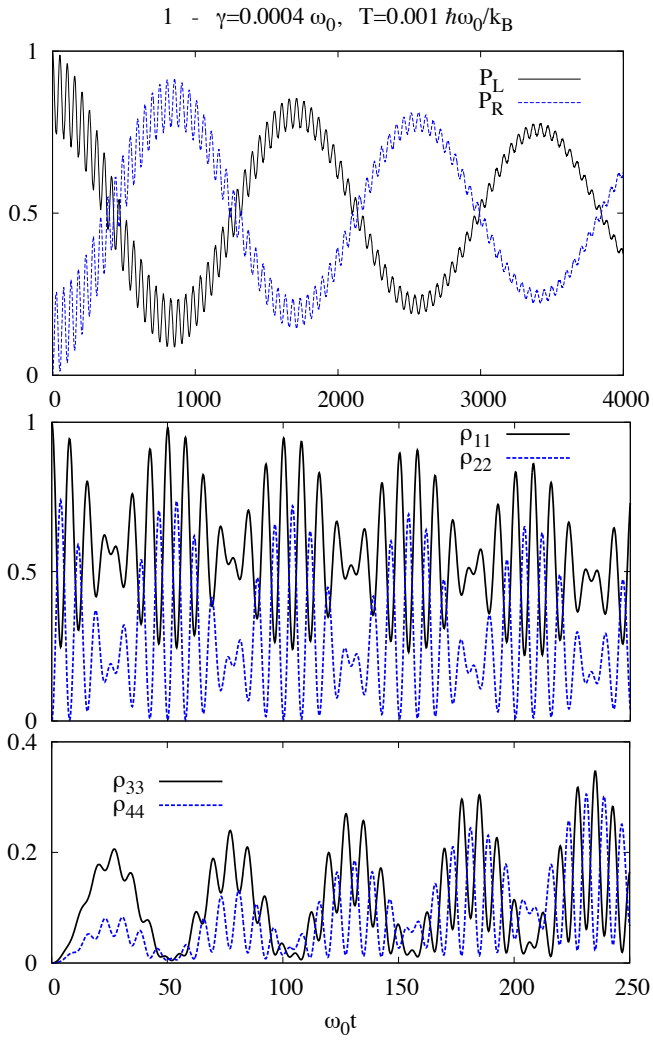

Figure 4.7: Completely coherent dynamics of the DDS at very weak damping and low temperature (point 1 in the phase diagram). Results obtained within the Bloch-Redfield master equation. *Uppermost panel* - Time evolution of the left/right well populations of the DDS. The long time behavior of $P_{L/R} = \rho_{11/33} + \rho_{22/44}$ is characterized by weakly damped oscillations of frequency Ω_2 and fast oscillations (of frequency Ω_1) around the long time envelope. Both these features are related to the tunneling dynamics. *Lowest panels* - Time evolution of the four populations in the DVR basis. The short time behavior of the DDS in this dissipation regime is very similar to the free case (see Fig 4.3).

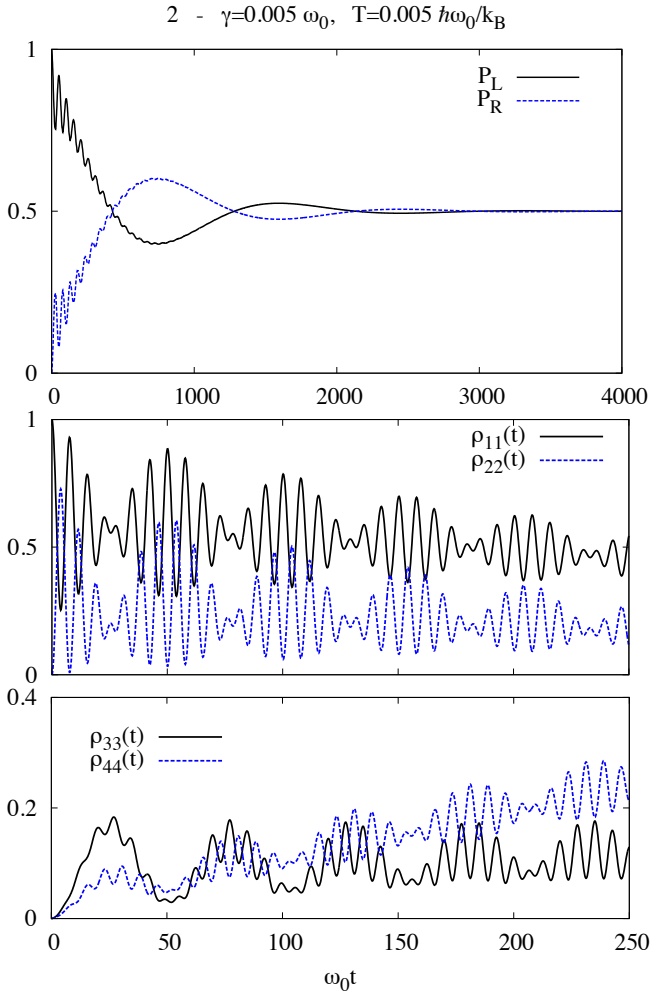

Figure 4.8: *Uppermost panel* - Time evolution of the left/right well populations of the DDS ($P_{L/R} = \rho_{11/33} + \rho_{22/44}$) for γ and T at point 2 in the phase diagram. The long time oscillations are more damped with respect to the case in the uppermost panel of Fig. 4.7. *Lowest panels* - Short time dynamics (with respect to Ω_2^{-1}) of the individual DDS populations. As in Fig. 4.7, the time evolutions display qualitatively the same features found in the free case (right panel of Fig. 4.3) but the damping is now visible at this short time scale.

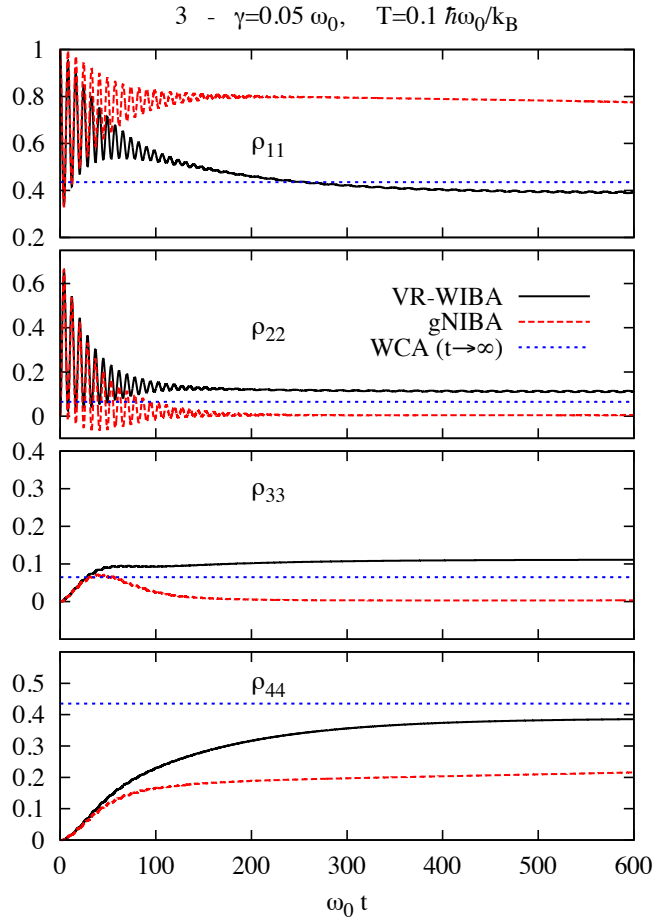

Figure 4.9: Weak damping and low to intermediate temperature with respect to the intra-well frequency (point 3 in the phase diagram). Comparison between the VR-WIBA and the gNIBA results for the time evolution of the populations in the crossover dynamical regime (Region (*c*) in Fig. 4.6). As expected, the gNIBA gives incorrect predictions of both the transient and the stationary, while the VR-WIBA is expected to give the correct results. The configuration at equilibrium, as given by the WCA (Eq. (4.21)), is shown for comparison.

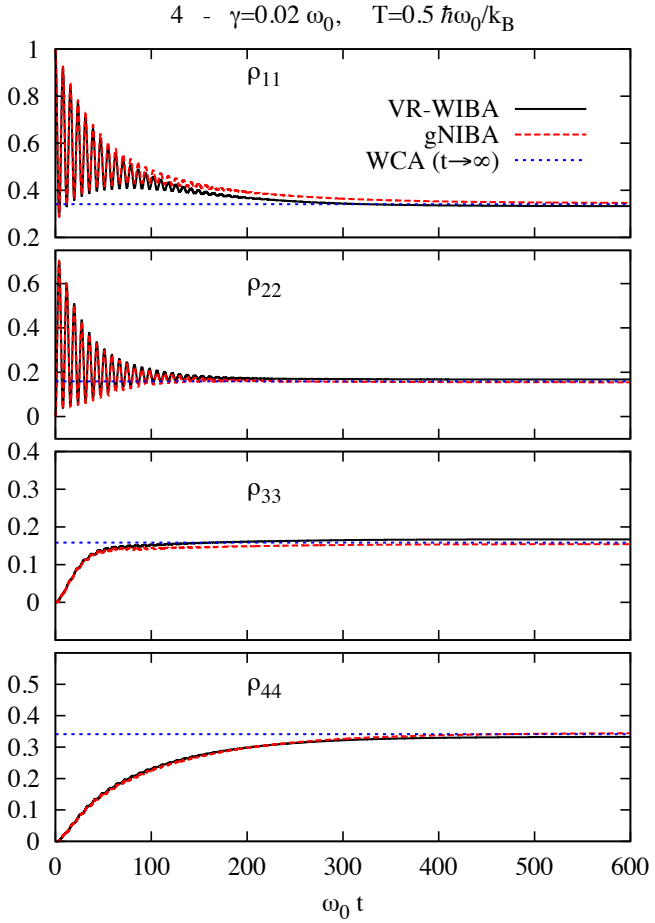

Figure 4.10: Weak damping and high temperature with respect to the the intra-well frequency (point 4 in the phase diagram). Comparison between the VR-WIBA and the gNIBA results for the time evolution of the populations in the crossover dynamical regime (Region (c)). The results in the two scheme coincide and reproduce the correct stationary configuration, provided by the WCA (Eq. (4.21)). This example shows that the gNIBA scheme is reliable also at weak damping, provided that the temperature is high enough, according to the domain of validity established in Sec. 4.2.

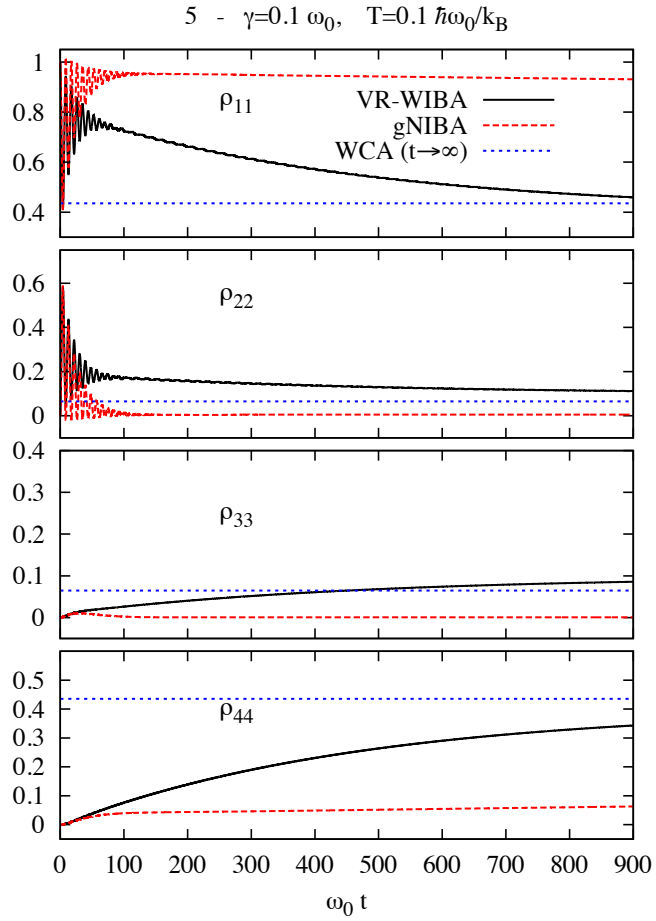

Figure 4.11: Intermediate damping and temperature with respect to the intra-well frequency (point 5 in the phase diagram). Comparison between the VR-WIBA and the gNIBA results for the time evolution of the populations in the crossover dynamical regime (Region (*c*)). As in Fig. 4.9 the gNIBA fails and the VR-WIBA is expected to be valid. The blue dashed lines are WCA prediction for the equilibrium values of the populations.

as it predicts localization. This is because the beyond-NIBA correction in the intra-well kernels on the GME is proportional (at appropriate damping) to the damping itself (see Appendix **??**).

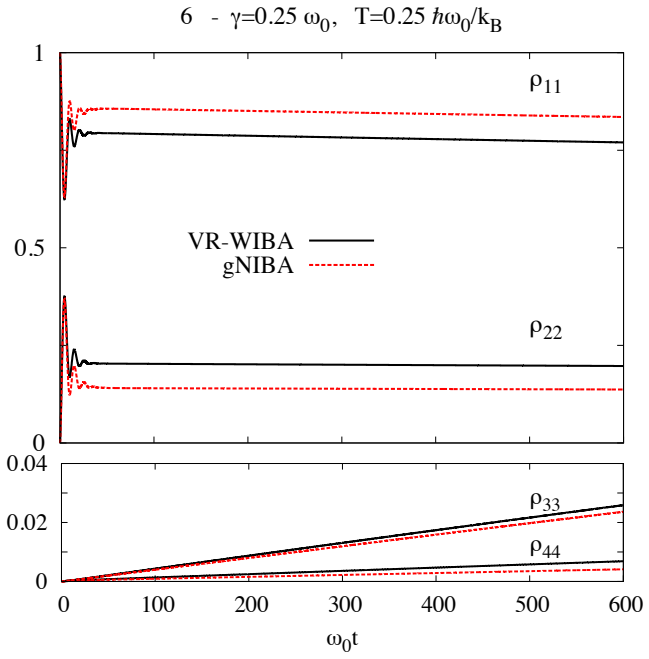

Figure 4.12: Strong damping and intermediate to high temperature with respect to the intra-well frequency (point 6 in the phase diagram). Comparison between the VR-WIBA and the gNIBA results for the time evolution of the populations in the strong coupling part of the crossover dynamical regime (Region (*c*)). The gNIBA and VR-WIBA results disagree as the coordinates of point 6 in the diagram are outside the gNIBA validity domain.

The sixth point in the diagram is in the strong coupling and intermediate to high temperature regime with respect to the intra-well TLS parameters. The dynamical regime is the crossover (Region (*c*)) with strongly damped intra-well oscillations and slow incoherent tunneling relaxation. Again, the gNIBA results differ from those of the VR-WIBA, which confirms that also in this coupling regime the gNIBA is valid only at high temperatures.

The last two points (7 and 8 in the diagram of Fig. 4.6) are in the incoherent regime (Region (*d*)). The gNIBA describes well the incoherent relaxation at strong damping and high temperature, as shown in Fig. 4.13. In the strong coupling regime at intermediate temperatures (point 8) the gNIBA fails. The VR-WIBA is expected to give better results even if the treatment of the inter-blip interactions to the first order is questionable at this level of coupling with the environment. The comparison of the WIBA with numerically exact approaches (QUAPI [73]) for the asymmetric TLS, in the strong dissipation regime, proves that the WIBA attains a good performance also outside the weak coupling limit at finite temperature [59].

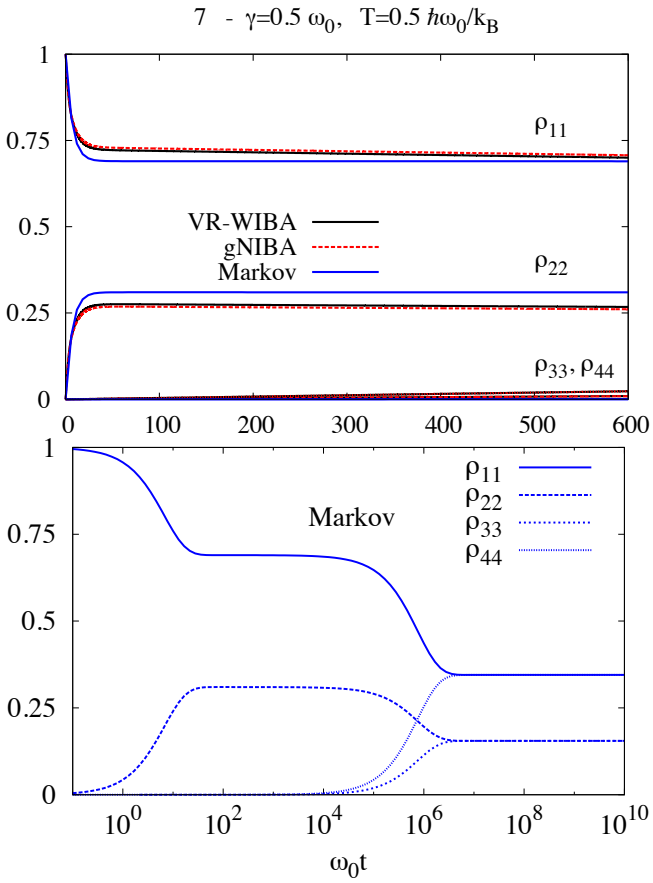

Figure 4.13: Incoherent dynamics at strong damping and high temperature (point 7 in the phase diagram). This dissipation regime is in the overlap of the validity domains of VR-WIBA and gNIBA. As expected, the results in the two schemes agree. *Upper panel* - Short time dynamics within the two approximation schemes; comparison with the Markov approximated gNIBA master equation (see Chap. 5). *Lower panel* - Long time dynamics (time in log scale) calculated by the gNIBA Markovian master equation.

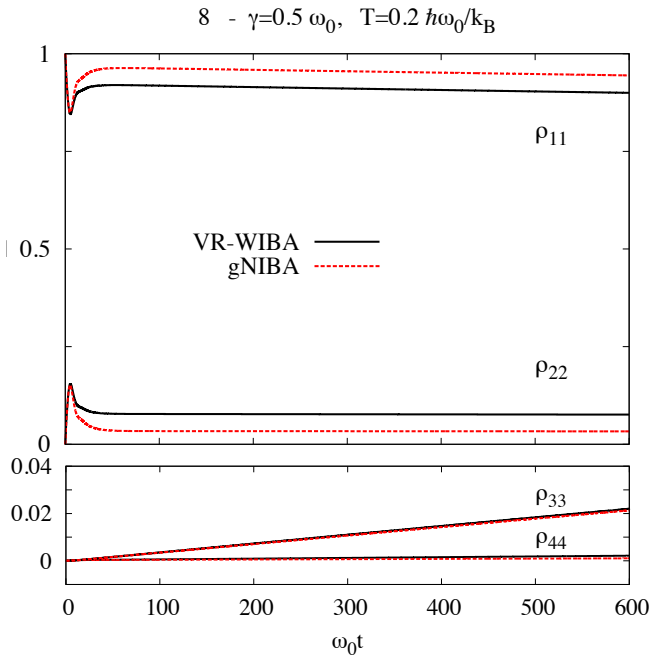

Figure 4.14: Strong damping and intermediate temperature (point 8 in the phase diagram). This regime is outside the reach of the gNIBA scheme, as shown in Fig. 4.6. Nevertheless the gNIBA predictions are in qualitative agreement with those of the VR-WIBA.

4.4 Conclusions

In this chapter we give a comprehensive account of the dissipative dynamics of the double-doublet system in an Ohmic environment with a high frequency cutoff, using a novel approximation scheme based on a real-time path integral approach, the VR-WIBA.

By taking into account the nonlocal inter-blip correlations at the level of the intra-well dynamics, this scheme contains and extends the domain of validity of the generalized NIBA and succeeds in describing the crossover dynamical regime occurring at intermediate temperatures for a broad range of damping. The crossover regime is characterized by coherence at the level of intra-well motion and incoherent tunneling dynamics and is, to a large extent, inaccessible to previous approximation schemes.

At weak damping and low temperatures we use a Born-Markov approximated master equation technique to account for the coherent oscillatory behavior of the intra-well and tunneling dynamics. This approach is also used to check the VR-WIBA predictions for the stationary configuration where the damping is large respect to the tunneling frequency but still weak with respect to the intra-well characteristic frequency.

The combined use of the master equation and path integral techniques, within our novel scheme, accounts for the dissipative dynamics of the DDS in a large region of the parameter space where the four-state truncation of the Hilbert space is justified. To show this we establish a phase diagram which describes the dynamics corresponding to the various dissipation regimes and the domains of validity of the techniques used in this work. We provide several examples of DDS dynamics in each of the accessible dynamical regimes in the phase diagram, ranging from the weak coupling/low temperature to the

strong coupling/high temperature regime.

Two final remarks are in order. Even if the calculations presented in this work are performed for an unbiased double well potential, the applicability of the VR-WIBA is not limited to the symmetric case. Indeed a static bias can be taken into account as long as the dynamical time scales of the intra- and inter-well dynamics remain well separated. In terms of energy levels this means that the inter-doublet energy separation should be much larger than the intra-doublet separation. This condition is not very restrictive as it is fulfilled for any bias for which the two energy doublets are below the top of the potential barrier.

Finally, the generalization of the VR-WIBA to broadband sub-Ohmic or super-Ohmic environments is possible, although care must be taken in establishing, from time to time, the validity of the approximations discussed throughout this chapter.

Chapter 5

Strong coupling regime: driven multi-state systems and metastability

[*Part of the present chapter is going to be published in collaboration with Prof. D. Valenti*[1]*, Dr. P. Caldara and Prof. B. Spagnolo*[1]]

In this chapter, following Ref. [72], we consider the general case of a D-state bistable quantum system (with $D \geq 4$), possibly subject to a (high-frequency) sinusoidal driving, in the strong coupling regime. Using the analytic technique of the strong coupling Markov-approximated master equation, the transient dynamics occurs as an incoherent relaxation towards an equilibrium state which depends on the driving parameters as well as on the damping regime. Along with the time evolution a systematic study is performed in the driving parameters space (amplitude and frequency) to give an account for the stationary configuration and time scales of the relaxation in different (strong coupling) dissipation regimes [74].

The same technique is used to study the problem of the escape from a metastable state (static case) in the quantum regime. By an analysis of a suitably defined escape time, a non monotonic behavior with respect to the damping and temperature is found, which resembles the well known phenomenon, in the classical context, of the *noise enhanced stability*.

5.1 Master equation for the driven multi-state system within the gNIBA

In the presence of a sinusoidally varying bias the bare system Hamiltonian $\hat{H}_S$ in Caldeira-Leggett Hamiltonian (1.11) acquires a time dependence

$$\hat{H}_S(t) = \frac{\hat{p}^2}{2M} + \frac{M^2\omega_0^4}{64\Delta U}\hat{q}^4 - \frac{M\omega_0^2}{4}\hat{q}^2 - \hat{q}\epsilon(t). \tag{5.1}$$

[1]Dipartimento di Fisica e Chimica, Università di Palermo.

The time dependent bias is defined by

$$\epsilon(t) = \epsilon + A\sin(\Omega t), \tag{5.2}$$

where we assume $\Omega \gg \omega_0$. The general expression for the propagator for a D-state non-driven system, given in Eq. (2.73), with the time dependent Hamiltonian, turns into

$$G(q_k, q_k, t; q_0, q_0', t_0) = \sum_{N=0}^{\infty} \int_{t_0}^{t} \mathcal{D}_N\{t_j\} B_0(t_1, t_0) \prod_{j=1}^{N} (-i)\, \Delta_j B_j(t_{j+1}, t_j) \mathcal{F}_{FV} \tag{5.3}$$

The bias factors, defined in Eq. (2.75) for the non-driven system, now do not depend anymore on the time differences $t_{j+1} - t_j$, but take on the form

$$\begin{aligned} B_j(t_{j+1}, t_j) =& \exp\left(-i \int_{t_j}^{t_{j+1}} dt' \epsilon_j(t')\right) \\ =& \exp\left[-i\epsilon_j(t_{j+1} - t_j)\right] \\ & \times \exp\left[-i \frac{2\Delta q_j A}{\Omega} \left(\sin\frac{\Omega}{2}(t_{j+1} + t_j) \sin\frac{\Omega}{2}(t_{j+1} - t_j)\right)\right], \end{aligned} \tag{5.4}$$

where $\Delta q_j = q_j - q_j'$ is the difference between the left and right coordinates at the j-th transition.

Having assumed a fast driving it is reasonable [72] to average over a driving period with respect to the variable $\tilde{t} = t_{j+1} + t_j$, so as to restore the time-convolution character of Eq. (2.73) in the propagator (5.3), allowing for the simple derivation of the GME given in Sec. 4.1.3. The averaged bias factors read

$$\begin{aligned} \bar{B}_j(t_{j+1} - t_j) =& \frac{\Omega}{2\pi} \int_{-\Omega/4\pi}^{\Omega/4\pi} d\tilde{t} B_j(\tilde{t}_j, t_{j+1} - t_j) \\ =& \exp\left[-i\epsilon_j(t_{j+1} - t_j)\right] J_0\left(2\Delta q_j \frac{A}{\Omega} \sin\frac{\Omega}{2}(t_{j+1} - t_j)\right), \end{aligned} \tag{5.5}$$

where J_0 is the zero-th order Bessel function of the first kind.

By this procedure and assuming to be within the validity of the gNIBA (see Sec. 4.1), it is possible to derive the generalized master equation for the populations in the DVR for the D-state system along the same lines as done for the non-driven case in Sec. 4.1.3. The GME for the D-state system reads

$$\dot{\rho}_{kk}(t) = \sum_{j=1}^{D} \int_{t_0}^{t} dt' K_{kj}^{gN}(t - t') \rho_{jj}(t'), \tag{5.6}$$

where the gNIBA kernels with averaged bias factors read (see Sec. 4.1.3 and Appendix E)

$$\begin{aligned} K_{kj}^{gN}(t) =& 2\Delta_{kj}^2 e^{-q_{kj}^2 Q'(t)} J_0\left(\frac{2q_{kj}A}{\Omega} \sin\frac{\Omega t}{2}\right) \cos\left(\epsilon_{kj} t + q_{kj}^2 Q''(t)\right) \qquad (j \neq k) \\ K_{kk}^{gN}(t) =& -\sum_i K_{ik}^{gN}(t). \end{aligned} \tag{5.7}$$

Here we have used

$$\begin{aligned}\Delta_{kj} &= \frac{1}{\hbar}\langle q_k|\hat{H}_S|q_j\rangle \\ \epsilon_{kj} &= \frac{1}{\hbar}\Big(\langle q_k|\hat{H}_S|q_k\rangle - \langle q_j|\hat{H}_S|q_j\rangle\Big) \\ q_{kj} &= q_k - q_j,\end{aligned} \tag{5.8}$$

where $\hat{H}_S$ is the *static* part of the system Hamiltonian in Eq. (5.1).

At strong damping, in the incoherent regime, the populations evolve on time scales larger than the time intervals over which the gNIBA kernels are substantially different from zero. The characteristic time over which they vanish is dictated by the smallest q_{ij} and by γ and T in Q', at the exponent in Eq. (5.7). This observation allows to approximate the gNIBA GME (5.6) into the Markovian master equation

$$\dot{\rho}_{kk}(t) = \sum_{j=1}^{D} \Gamma_{ij}\rho_{jj}(t), \tag{5.9}$$

where

$$\Gamma_{ij} = \int_0^\infty dt K_{kj}^{gN}(t). \tag{5.10}$$

The Markov-approximated maser equation (5.9) admits the analytical solution

$$\rho_{kk}(t) = \sum_{ij=1}^{D} S_{ki}S_{ij}^{-1}e^{\Lambda_i(t-t_0)}\rho_{jj}(t_0). \tag{5.11}$$

The rates Λ_i are the eigenvalues of the rate matrix Γ and S is the transformation matrix which diagonalizes Γ. The probability conservation implies that the smallest in absolute value of the Λ's, say Λ_1, is zero (the others have negative non zero values) so that the asymptotic value of ρ_{kk} is obtained as

$$\rho_{kk}(\infty) = \sum_{j=1}^{D} S_{k1}S_{1j}^{-1}\rho_{jj}(t_0). \tag{5.12}$$

The smallest, in absolute value, of the Λ's gives the so-called *quantum relaxation rate* ($|\Lambda_{\rm relax}|$) whose inverse, $\tau_{\rm relax}$, gives the time scale of the relation to the equilibrium configuration [72].

5.2 Driven dissipative multi-state dynamics

In the following discussion the environment is assumed to be Ohmic ($J(\omega) = M\gamma\omega$, with a high-frequency cut-off) and the static potential of Hamiltonian (5.1) considered is depicted in Fig. 5.1. The potential barrier is $\Delta U = 1.4\hbar\omega_0$ and the static bias (Eq. (5.2)) $\epsilon = 0.15\sqrt{M\hbar\omega_0^3}$. We show the time evolution of the populations $\rho_{\mu\mu}(t)$ in the DVR in different driving regimes as well as the asymptotic population of the metastable well and the relaxation times as functions of the diving parameters. Everything is evaluated for $\gamma = 0.1\omega_0$ and $0.3\omega_0$ and $T = 0.1\hbar\omega_0/k_B$ and $0.14\hbar\omega_0/k_B$, in regimes in which quantum tunneling through the potential barrier is an active mechanism of population transfer from one well to the other.

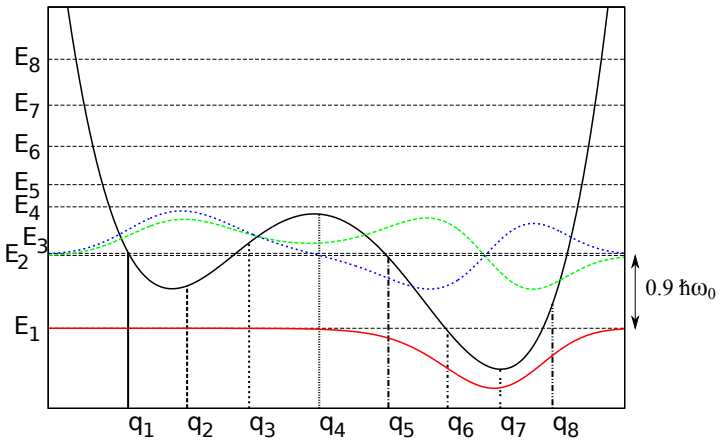

Figure 5.1: Static potential (barrier height $\Delta U = 1.4\hbar\omega_0$ and static bias $\epsilon = 0.15\sqrt{M\hbar\omega_0^3}$) and first three energy eigenfunctions. The horizontal lines are the first eight energy levels and the vertical lines the position eigenvalues in the DVR. The distance between the minima is $\sim 6.5\sqrt{\hbar/(M\omega_0)}$

Within the present choices for the environmental parameters, it is a good approximation to assume that no energy levels higher than the first eight are involved in the dynamics, even in the presence of external driving. The resulting unequally spaced grid of positions in the DVR is depicted in Fig. (5.1) together with the potential profile and the first two energy eigenvalues in units of $\hbar\omega_0$.

The system-plus-environment initial condition is of the factorized kind of Eq. (2.41), with the system in the state

$$\rho(t_0) = |q_4\rangle\langle q_4|. \tag{5.13}$$

Notice that in the static case, since $T \ll \omega_0$, a description in terms of fewer states is sufficient, provided that the initial condition doesn't involve higher energy states. Our preparation (5.13) actually involves all of the eight states, being a state *localized* around the top of the potential barrier.

5.2.1 Results I: Dynamics

For each of the four combinations (γ, T), three different driving regimes are studied, namely: (i) non-driven, (ii) driven off-resonance and (iii) resonantly driven ($\Omega \simeq E_2 - E_1$). At the resonance the oscillating bias induces transitions among states localized in different wells, in particular $|q_7\rangle \to |q_2\rangle$. Indeed, for this configuration of the potential $|q_7\rangle \sim |E_1\rangle$ and $|q_2\rangle \sim (|E_2\rangle + |E_3\rangle)/\sqrt{2}$ as can be seen in Fig. 5.1. This is at the basis of the striking difference in the stationary configuration of the populations between the static and the resonantly driven case.

The results for the dynamics of the eight populations in the three driving regimes are shown in Figs. 5.2 and 5.3. Each time evolution is plotted up to time $t = 100\tau_{\rm relax}$, where $\tau_{\rm relax}$ is the relaxation time defined in Sec. 5.1. By comparing the truncation times of two plots one gets an indication of the relative magnitude of $\tau_{\rm relax}$ (which depends on both the driving and the dissipation regime) for the two configurations considered. A more

systematic study of the relaxation time as function of the driving parameters is done in Sec. 5.2.2.

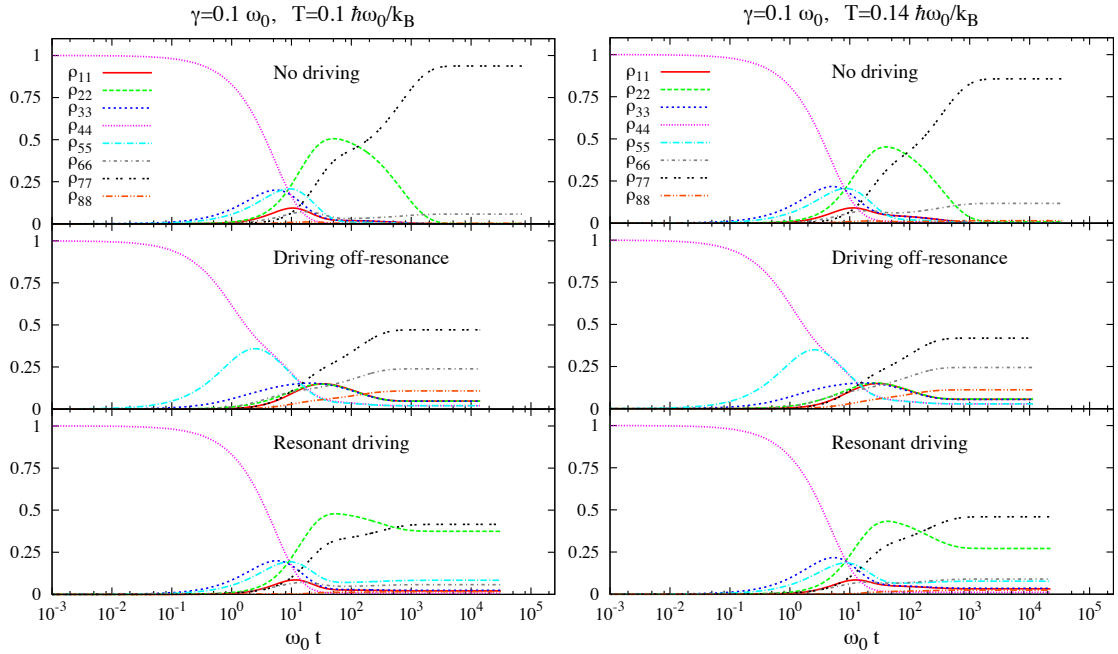

Figure 5.2: Populations in the DVR as functions of time (in units of ω_0^{-1}) for $\gamma = 0.1\omega_0$. The driving amplitude is set to $A = 0.2\sqrt{M\hbar\omega_0^3}$ and the frequencies are $\Omega = 0.35\omega_0$ (off-resonant driving, middle panels) and $\Omega = 0.87\omega_0$ (resonant driving, lowest panels). *Left* - $T = 0.1\hbar\omega_0/k_B$. *Right* - $T = 0.14\hbar\omega_0/k_B$. The off-resonant driving suppresses the peak in ρ_{22} during the transient and populates the right well states at the stationary. The driving resonance gives a noticeable stationary population of the left well. At the higher temperature a speed-up of the transient dynamics occurs together with a reduction of the stationary $|q_2\rangle$ population in the resonantly driven regime.

A general feature of the transient is the presence of peaks in the populations of the metastable well states ($|q_1\rangle$, $|q_2\rangle$ and $|q_3\rangle$) whose height is sensitive to the driving force, being largest in the non-driven case, and smallest with off-resonant driving. Notice that, in the driven case far from resonance, these peaks are almost suppressed. Another general related feature is that the external driving, especially in the off-resonant case, shortens the transient times. This is clearly visible in the results of Sec. 5.2.2.

This behavior is given by the interplay among driving parameters (A and Ω) and distances q_{ij} present in the argument of the Bessel function in Eq. (5.7). These parameters determine the time integrals of the kernels giving the rates Γ.

The off-resonant driving suppresses the rates involved in the tunneling dynamics and enhances the vibrational relaxation inside the right well. As a consequence the stationary state is reached faster and the asymptotic configuration displays a spread in the population among the states in the right well.

On the other hand, the driving at the resonance ($\Omega \simeq E_2 - E_1 \simeq \omega_0$) induces transitions between $|q_2\rangle$ and $|q_7\rangle$, and an asymptotic population of the state ρ_{22} (in the metastable well) which is substantially different from zero, as shown in Fig. 5.2. By slightly increasing

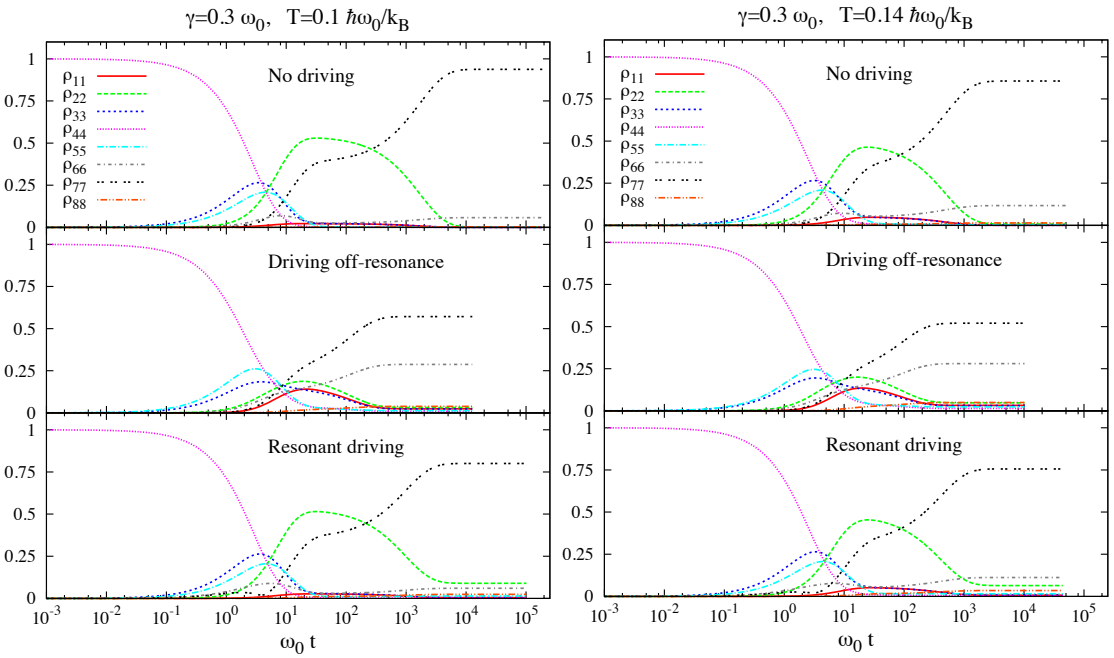

Figure 5.3: Populations in the DVR as functions of time (in units of ω_0^{-1}) for $\gamma = 0.3\omega_0$. The driving amplitude is set to $A = 0.2\sqrt{M\hbar\omega_0^3}$ and the frequencies are $\Omega = 0.35\omega_0$ (off-resonant driving, middle panels) and $\Omega = 0.87\omega_0$ (resonant driving, lowest panels). *Left* - $T = 0.1\hbar\omega_0/k_B$. *Right* - $T = 0.14\hbar\omega_0/k_B$. The qualitative features of the dynamics for the two temperature considered are similar to those in Fig. 5.2 ($\gamma = 0.1\omega_0$). The main differences are that, at this stronger damping regime, the relaxation in slower and the system relaxes almost completely into the right (lower) well, even in the presence of resonant driving.

the temperature, the relaxation times are shortened in all the driving regimes, and the asymptotic value of ρ_{22} in the resonant case decreases (see Figs. 5.2 and 5.3).

In passing to the stronger coupling regime ($\gamma = 0.3\omega_0$, Fig. 5.3), two new features appear: a noticeable slowing down of the evolutions and an almost complete relaxation towards the lower well, even with driving at the resonance. This is because the damping inhibits transitions among far away lying states. As in the $\gamma = 0.1\omega_0$ case, an increase in the temperature enhances the relaxation, making $\tau_{\rm relax}$ smaller.

5.2.2 Results II: Stationary left well population and relaxation times

In this section we show the results for the asymptotic value of the population of the metastable (left) well, defined as the sum of the asymptotic populations of the DVR states belonging to the left well

$$P_L(\infty) = \rho_{11}(\infty) + \rho_{22}(\infty) + \rho_{33}(\infty),$$

with $\rho_{kk}(\infty)$ defined in Eq. (5.12). We also consider the relaxation time $\tau_{\rm relax}$, defined in Sec. 5.1. Both these quantities are plotted as functions of the amplitude A and frequency Ω of the high-frequency oscillating bias, in the same four damping/temperature parameters as considered in Sec. 5.2.1.

We observe a strong non-monotonic behavior of both $P_L(\infty)$ and $\tau_{\rm relax}$ with respect to Ω. Specifically, all the $P_L(\infty)$ plots display peaks in the lower part of the frequency domain, whose magnitude is sensitive to the damping constant, being larger at lower damping (compare Figs. 5.4 and 5.5 with Figs. 5.6 and 5.7, upper panels). For $\gamma = 0.1\omega_0$ peaks are also present in the higher frequencies domain, noticeably at the resonance, while for $\gamma = 0.3\omega_0$ these peaks are strongly suppressed, even at the resonance.

As noticed in Sec. 5.2.1, this is because the driving couples far away lying states and the transfer of population between these states is inhibited by the exponential cut off in the kernels (5.7), which is larger at stronger damping.

At the lower damping $\gamma = 0.1\omega_0$, the plot of $P_L(\infty)$ displays several peaks, corresponding to the level structure of the static potential in Fig. 5.1. We note also that, in all of the four dissipation regimes considered, if the system is driven at very high frequency its behavior is the same as in the non-driven case. The same happens for $\tau_{\rm relax}$.

Finally, for both the values of γ at the higher temperature, a non-zero asymptotic P_L is present for $A = 0$ (static potential). This is due to the fact that the system eventually reaches a γ-dependent state of equilibrium with the environment at temperature T: at high temperature states of energy higher than that of the first few are thermally populated.

In the lower panels of Figs. 5.4-5.7, we show the relaxation time in the four regimes considered. The key feature is that at low driving frequency, around $\Omega = 0.3$, the driving enhances the relaxation, as already pointed out in sec. 5.2.1, in all of the dissipation regimes. A relevant feature, already pointed out in Sec. 5.2.1, is that $\tau_{\rm relax}$, in the stronger damping regime, has roughly twice the value taken at $\gamma = 0.1\omega_0$.

On the other hand, the slight increase in temperature has the opposite effect of reducing considerably the relaxation time at both the damping regimes considered.

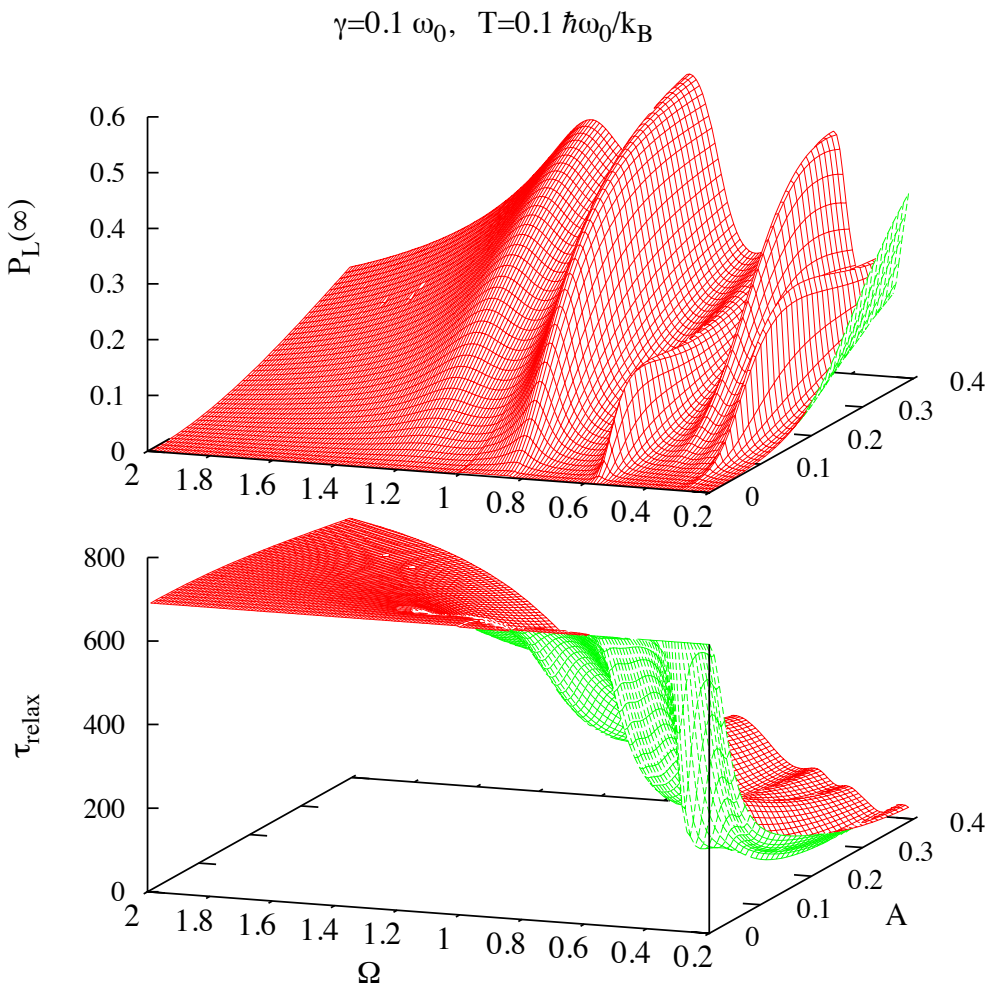

Figure 5.4: Asymptotic left well population $P_L(\infty)$ (upper panel) and relaxation time $\tau_{\rm relax}$ (in units of ω_0^{-1}, lower panel) as functions of the driving amplitude A (in units of $\sqrt{M\hbar\omega_0^3}$) and frequency Ω (in units of ω_0). Damping constant and temperature are $\gamma = 0.1\omega_0$ and $T = 0.1\hbar\omega_0/k_B$, respectively.

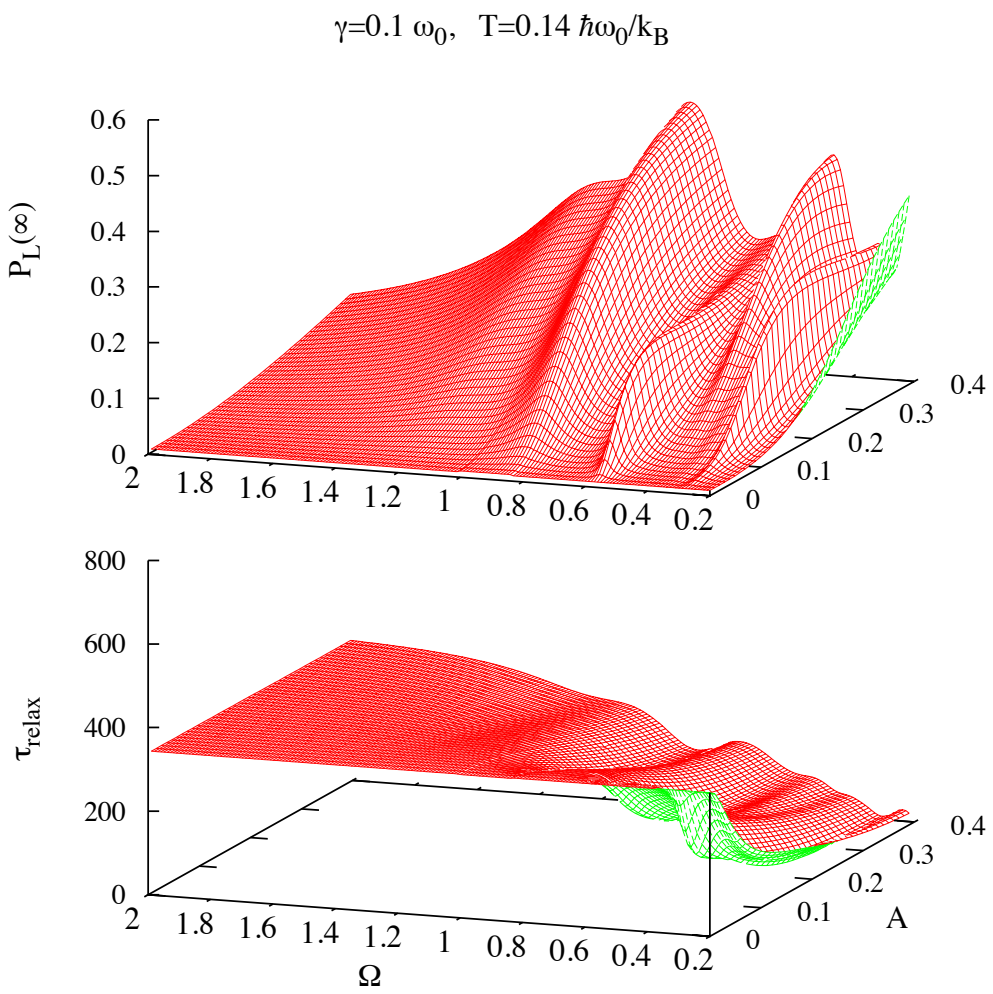

Figure 5.5: Asymptotic left well population $P_L(\infty)$ (upper panel) and relaxation time $\tau_{\rm relax}$ (in units of ω_0^{-1}, lower panel) as functions of the driving amplitude A (in units of $\sqrt{M\hbar\omega_0^3}$) and frequency Ω (in units of ω_0). Damping constant and temperature are $\gamma = 0.1\omega_0$ and $T = 0.14\hbar\omega_0/k_B$, respectively.

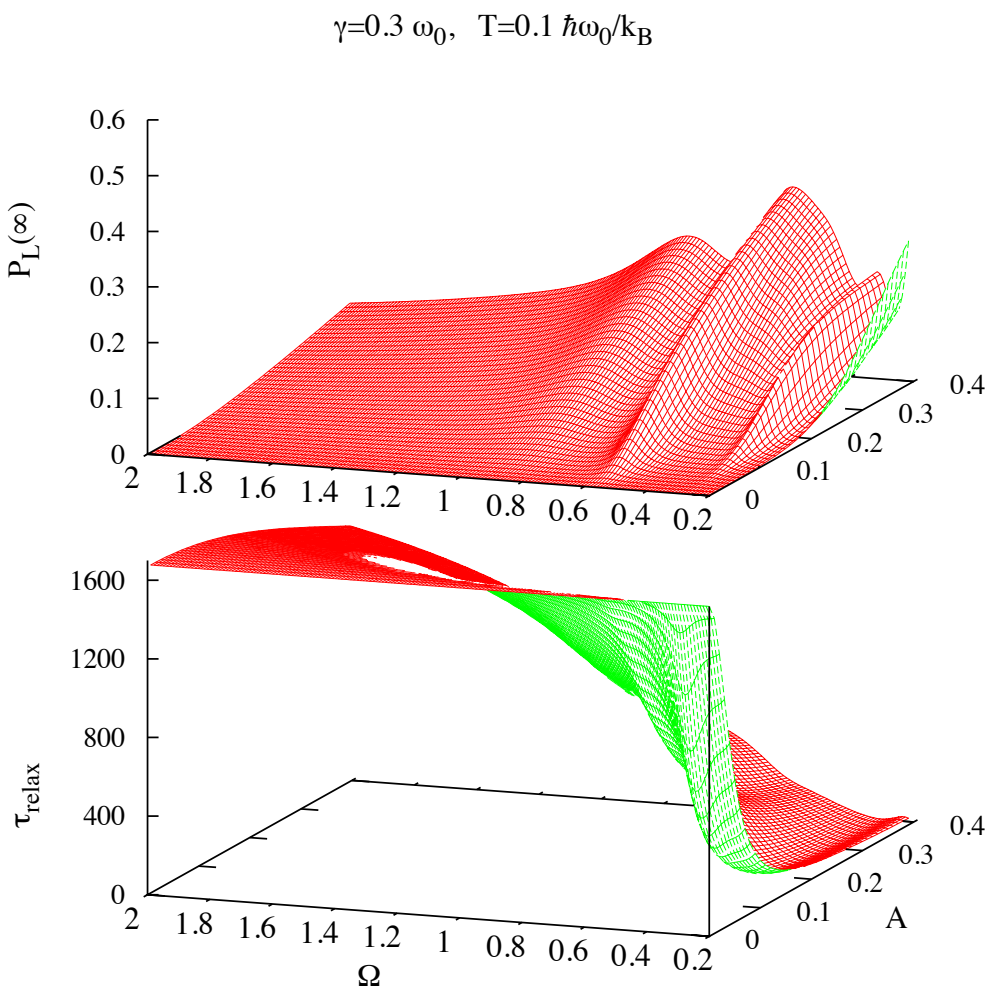

Figure 5.6: Asymptotic left well population $P_L(\infty)$ (upper panel) and relaxation time $\tau_{\rm relax}$ (in units of ω_0^{-1}, lower panel) as functions of the driving amplitude A (in units of $\sqrt{M\hbar\omega_0^3}$) and frequency Ω (in units of ω_0). Damping constant and temperature are $\gamma = 0.3\omega_0$ and $T = 0.1\hbar\omega_0/k_B$, respectively.

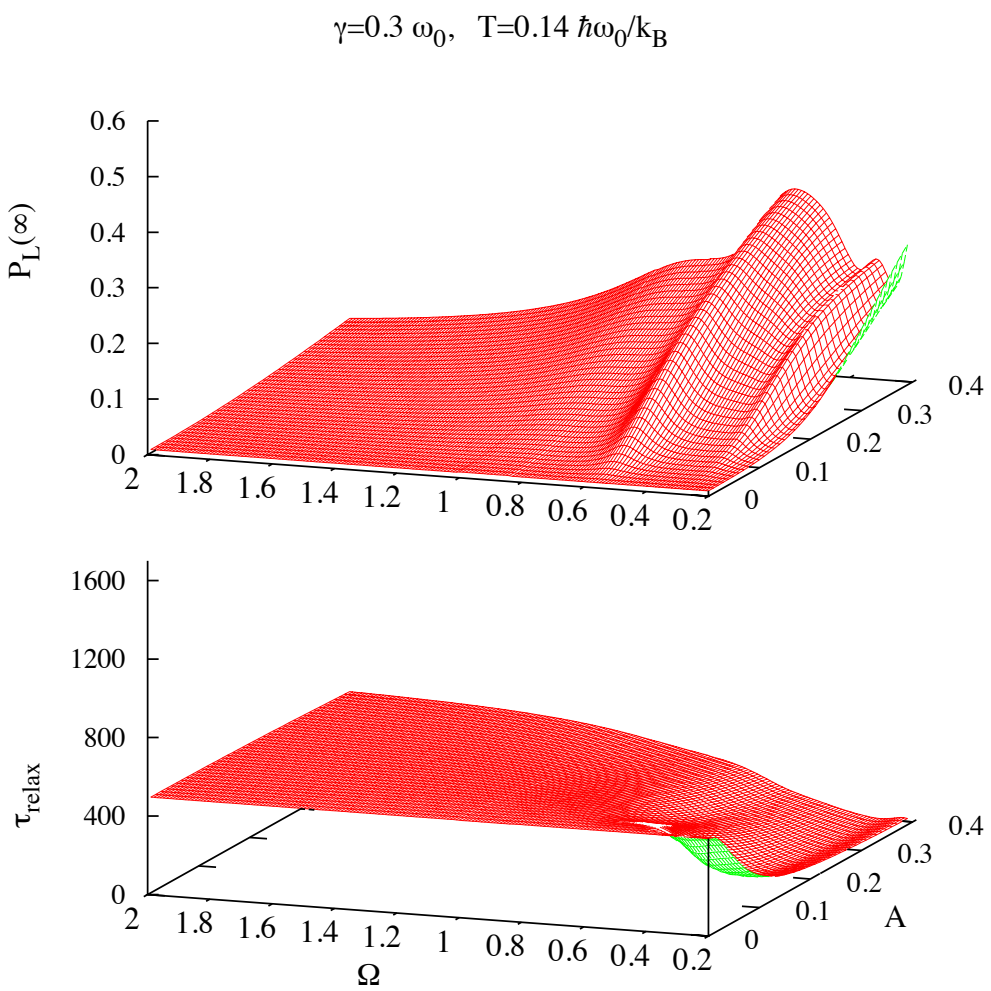

Figure 5.7: Asymptotic left well population $P_L(\infty)$ (upper panel) and relaxation time $\tau_{\rm relax}$ (in units of ω_0^{-1}, lower panel) as functions of the driving amplitude A (in units of $\sqrt{M\hbar\omega_0^3}$) and frequency Ω (in units of ω_0). Damping constant and temperature are $\gamma = 0.3\omega_0$ and $T = 0.14\hbar\omega_0/k_B$, respectively.

5.3 Metastability in the strong coupling regime

Recently, the role of dissipation on the dynamics of quantum systems has been the subject of renewed interest [75, 76].

The presence of a dissipative environment indeed influences significantly the escape from a quantum metastable state. This is a general problem, of interest in many areas of physics, whenever a sudden change in the state of a system occurs on time scales small with respect to the typical times of the systems dynamics.

The archetypical model describing the escape process is that of a particle subject to a cubic or asymmetric bistable potential and linearly coupled to a heat bath of quantum harmonic oscillators [9, 40, 77]. In such a system the decay from the metastable state occurs on time scales that depend on the friction and temperature. Various physical systems such as magnetization in solid state systems [37, 78], proton transfer in chemical reactions [79] and superconducting devices [24, 30] can be described within this framework.

Calculations of the decay rates, using a cubic potential, have been performed in Refs. [43, 80] using functional integral techniques. In Ref. [43], starting with the particle at the bottom of the metastable well, it has been shown that the decay rate decreases monotonically as the damping increases and grows with the bath temperature. Similarly, by using a master equation technique, a monotonic increase of the escape rate, with respect to the temperature, is found in Ref. [81] for a Gaussian wave packet initially in the metastable well of a biased quartic potential.

Stabilization of a quantum metastable state by an external time-periodic driving, in absence of environment, was obtained in Ref. [82]. Moreover, suppression of activated escape from a metastable state by increasing the temperature was found in a time-periodically driven quantum dissipative system [83].

Common wisdom is that environmental fluctuations always enhance the escape from a quantum metastable state. A critical issue of great importance is: can the dissipation enhance the stability of a quantum metastable state?

To answer this question we follow the time evolution of the populations of spatially localized states in a strongly asymmetric bistable system, starting from a nonequilibrium initial condition. This choice allows us to observe how, increasing the damping, the relaxation process towards the stable well goes from a population transfer in which the metastable well is temporarily populated, to a mechanism of direct transfer to the stable state. This stabilization effect is related to that due to the suppression of tunneling by dissipation in quantum regime [40, 43]. As a result we find that dissipation can enhance the stability of the quantum metastable state. Indeed, we observe that the escape dynamics is characterized by a nonmonotonic behavior, with a maximum, as a function of the damping strength: there is an optimal value of the damping strength which maximizes the escape time, producing a *stabilizing* effect in the quantum system. This result, which resembles the phenomenon known, in the classical context, as noise enhanced stability (NES) of metastable states [84–87], sheds new light on the role of the environmental fluctuations in stabilizing quantum metastable systems. We also find that the behavior of the escape time versus the temperature is nonmonotonic with a minimum. Therefore as the temperature increases, an enhancement of the escape time is observed, increasing the stability of the quantum metastable state.

5.3.1 Model

We consider the static biased bistable potential

$$V(\hat{q}) = \frac{M^2\omega_0^4}{64\Delta U}\hat{q}^4 - \frac{M\omega_0^2}{4}\hat{q}^2 - \hat{q}\epsilon, \tag{5.14}$$

where ϵ is taken large enough to mimic the cubic potential, which is the archetypal potential to model metastable systems.

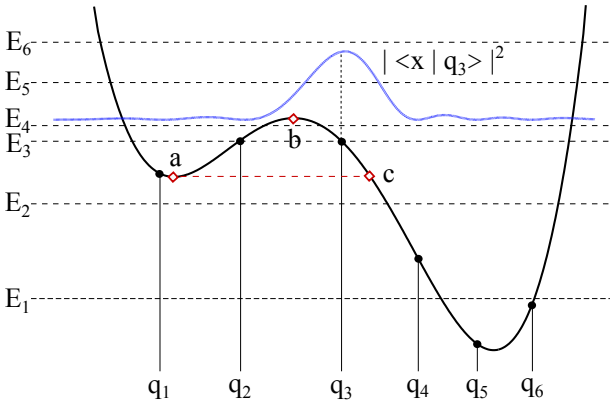

Figure 5.8: Potential profile $V(q)$ (Eq. (5.14)) for $\Delta U = 1.4\hbar\omega_0$ and $\epsilon = 0.27\sqrt{M\hbar\omega_0^3}$. Horizontal lines: the first 6 energy levels. Vertical lines: the position eigenvalues in the DVR. The dashed curve is the initial probability distribution $|\Psi(x,0)|^2$. For the tunneling splitting we have $\Delta E_{4,3} = E_4 - E_3 = 0.2\hbar\omega_0$ while $E_2 - E_1 = 0.985\hbar\omega_0$.

As in the previous section, the oscillators bath is assumed to have the Ohmic spectral density $J(\omega) = M\gamma\omega$, with a cut-off at a frequency much larger than any other involved.

In the quantum regime, given our choice for the particle's initial preparation and the bath temperature (see Sec. 5.3.2), it is appropriate to assume that the dynamics is practically confined among the first 6 levels of the potential shown in Fig. 5.8. In this reduced Hilbert space, the particle's reduced dynamics is described in terms of the *localized* basis of the position eigenstates $\{|q_1\rangle, \ldots, |q_6\rangle\}$, where $\hat{q}|q_i\rangle = q_i|q_i\rangle$, giving the discrete variable representation (DVR, see Sec. 2.5).

5.3.2 Escape time

In the following we focus on the particle's transient dynamics, as given by the solution (5.11) of the master equation (5.9), starting from the nonequilibrium initial condition

$$\rho(0) = |q_3\rangle\langle q_3|, \tag{5.15}$$

i.e. with the particle's probability density initially peaked on the right of the potential barrier, in the interval (q_b, q_c) (see Fig. 5.8). This may be experimentally attained by preparing the particle in the ground state of an appropriate harmonic well centered at the desired position, and then relaxing the harmonic potential [88].

Before giving the definition of escape time in the present context, we define the population of the lower (right side) well as the cumulative population of the three DVR states

from $|q_4\rangle$ to $|q_6\rangle$, that is

$$P_{\text{right}}(t) = \sum_{\mu=4}^{6} \rho_{\mu\mu}(t), \tag{5.16}$$

which is a discretized version of the probability of penetration of the wave packet through the barrier [81]. During the transient dynamics the populations of the metastable states ($|q_1\rangle$ and $|q_2\rangle$) reach a maximum. Afterwards, by tunneling through the potential barrier, the population of the metastable well decays, finally settling down to a stationary value dependent on the temperature.

We consider large asymmetry of the potential, low temperatures with respect to the barrier height, and damping regimes ranging from moderate to strong ($\gamma \gtrsim \omega_0$). Given the above conditions, the relaxation occurs in the incoherent regime, with no oscillations in the populations. As a consequence we may consider the particle irreversibly escaped from the metastable state once $P_{\text{right}}(t)$ has reached a certain threshold value that we set to $P_{\text{right}}(\tau) = 0.95$.

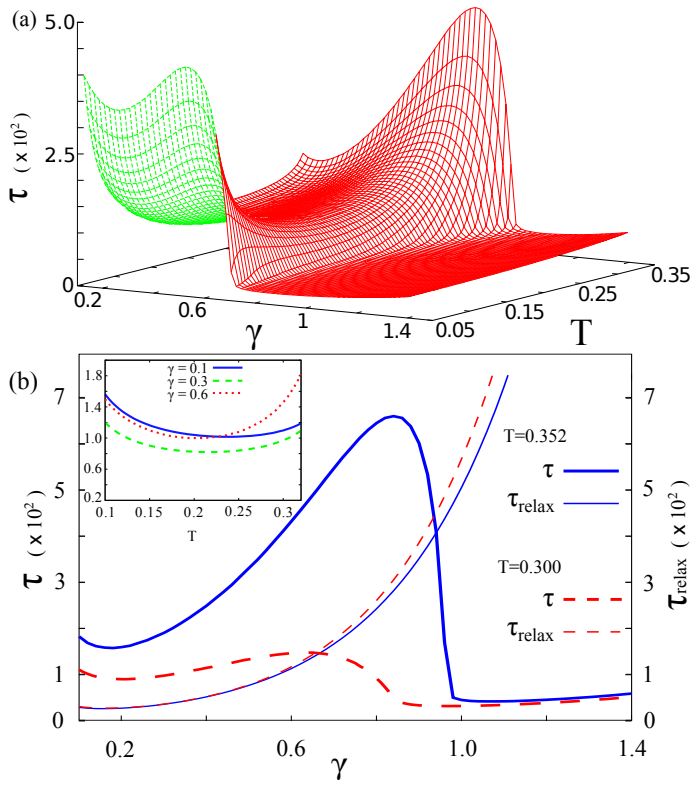

Figure 5.9: Escape time τ, in units of ω_0^{-1}, for the initial condition $\rho(0) = |q_3\rangle\langle q_3|$ (see Eq. (5.15)). (a) τ and τ_{relax} as a function of both damping γ and bath's temperature T. (b) τ as a function of γ for different temperatures. Inset - escape time vs temperature at fixed values of γ. The variables γ and T are given in units of ω_0 and $\hbar\omega_0/k_B$, respectively.

5.3.3 Results

We observe a nonmonotonic behavior of τ with respect to both γ and T . In Fig. 5.9 it is shown the presence of a peak in τ vs γ, whose height and position depend on the temperature.

A comparison between τ and $\tau_{\rm relax}$ versus γ indicates that the two quantities exhibit roughly the same behavior until the peak in τ is reached (see Fig. 5.9b). At higher γ, while $\tau_{\rm relax}$ keeps increasing monotonically, τ has a sudden fall off at a critical value γ_c, dependent on the temperature (for example $\gamma_c \simeq 0.98$ at $T = 0.352$).

This critical value corresponds to a dynamical regime in which the population transfer from the initial state to the states of the metastable well is inhibited and there is a direct transfer to the states of the lower right well. In this regime the probability to find the particle in the metastable state is practically zero throughout the entire dynamics. Indeed, while $\tau_{\rm relax}$ is the time needed for the system to reach the equilibrium in the double well potential, the escape time is a relevant quantity for the transient dynamics, involving the crossing of the potential barrier and the depletion of the metastable well. Therefore, our analysis applies to the general problem of the escape from a metastable well, starting from a nonequilibrium condition.

The nonmonotonic behavior of τ vs γ can be interpreted as the quantum counterpart of the NES phenomenon observed in classical systems, and may be called quantum noise enhanced stability (QNES).

Another interesting feature is the presence of a slow monotonic increase of τ for $\gamma > \gamma_c$, which leads to the quantum Zeno effect [89].

The behavior of τ vs the temperature is characterized by a minimum as $k_B T$ approaches the tunneling splitting $\Delta E_{4,3} = E_4 - E_3$ (see Fig. 5.8). This is the signature of the *thermally activated tunneling*, an experimentally well established phenomenon [90]. This is better shown in the inset of Fig. 5.9b.

Finally we wish to point out that our results are robust against the variation of the potential asymmetry, threshold value and initial conditions (initial DVR states within the interval (q_b, q_c), see Figs. 5.8 and 5.10).

To exemplify this robustness, we give here the results for another potential profile and a different initial condition (see Fig. 5.10).

The definition of τ is the same as for the previous case i.e. $P_{\rm right}(\tau) = 0.95$. In this situation however, due to the different number of energy levels considered, the right well population is defined as $P_{\rm right}(t) = \sum_{\mu=5}^{8} \rho_{\mu\mu}(t)$.

The escape time displays qualitatively the same features as for the first configuration, even if now the initial wave packet is centered close to the top of the potential barrier. In particular τ has a nonmonotonic behavior as a function of both γ and T. The minimum of τ vs T is at $T \simeq 0.27/k_B$, which is the average value of the three tunneling splittings $\Delta E_{7,6}, \Delta E_{6,5}$, and $\Delta E_{5,4}$ (see Fig. 5.10a). Moreover, for $\gamma > \gamma_c$, we observe a monotonic increasing behavior of τ leading to the quantum Zeno effect.

5.4 Conclusions

In this chapter the analysis of the dissipative bistable system, carried out for the two-level system in Chap. 3 and for the double-doublet system in Chap. 4, was generalized to a multi-state system with an arbitrary number of states and possibly subject to a

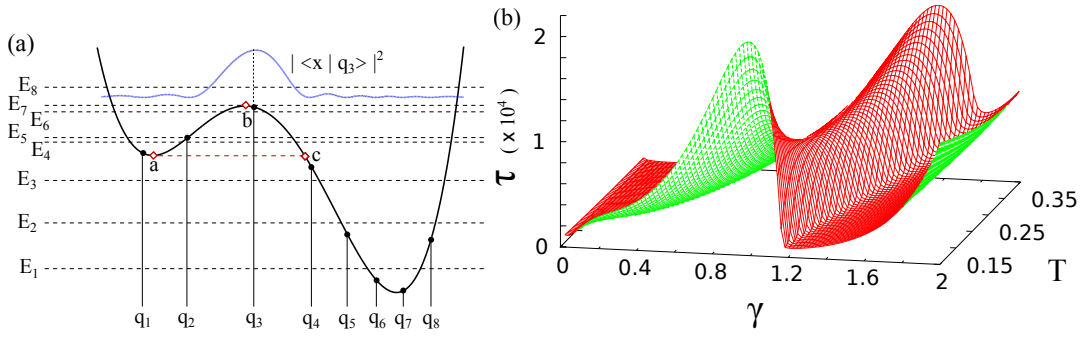

Figure 5.10: (a) Potential profile $V(q)$ (see Eq. (5.14)) for $\Delta U = 2.5\hbar\omega_0$ and $\epsilon = 0.35\sqrt{M\hbar\omega_0^3}$. Horizontal lines: the first 8 energy levels. Vertical lines: position eigenvalues in the DVR. The dashed curve is the initial probability distribution $|\Psi(x,0)|^2$. Here $\Delta E_{7,6} = 0.14\hbar\omega_0$, $\Delta E_{6,5} = 0.58\hbar\omega_0$, $\Delta E_{5,4} = 0.1\hbar\omega_0$. (b) Escape time τ, in units of ω_0^{-1}, for the initial condition shown in panel (a).

periodically varying bias. This general case was treated exclusively in the strong coupling regime, where the analytical technique of the master equation derived within the path integral approach is available.

The first part of the chapter was devoted to the study of the driven dynamics starting from a nonequilibrium initial condition. The time evolution and the stationary values of the populations in the discrete variable representation were studied, along with the characteristic time scales of the dynamics. In particular the interplay between the dissipation and the driving was systematically investigated.

A strong non-monotonicity with respect to the driving frequency was found in the metastable well population at equilibrium, which is characterized by the presence of resonant peaks. This means that, at appropriate frequency, the probability to find the particle in the metastable well is noticeably different from zero. On the other hand, a strong damping enhances the relaxation towards the lower well. The analysis, carried out at two temperatures, showed also that the relaxation times are smaller at higher temperature.

In the second part of the chapter considered the static case of a strongly asymmetric potential was considered, which mimic the situation encountered in escape problems in classical and quantum mechanics. We showed that in nonequilibrium dynamics the escape time from a quantum metastable state exhibits a nonmonotonic behavior as a function of both the damping, with a maximum (QNES), and temperature, with a minimum at the resonance with the tunneling splitting (see Figs. 5.8 and 5.10).

We also observed stabilization of the quantum metastable state due to the dissipation and its interplay with the temperature. Moreover, a suppression of the activated escape was obtained by increasing the temperature. The stabilization phenomenon associated to the model considered is within the reach of existing experimental technologies such as superconducting qubits [88] and optical trapping [91].

Chapter 6

Conclusions

In this thesis the path integral approach is used to study the dissipative dynamics of the bistable quantum system. The open quantum system, consisting in a particle subject to a double well potential, is assumed to interact with an environment of bosonic modes, according to the celebrated Caldeira-Leggett model [40]. This Hamiltonian model allows for a microscopical derivation of the dissipation, which emerges as the environmental degrees of freedom are traced out and a description in terms of reduced density matrix is given for the open system.

If the coupling is weak, perturbative techniques based on the Born-Markov approximation are appropriate for predicting the time evolution of the system's reduced density matrix. However, as the coupling with the environment cannot be treated as a perturbation, the inherently non-perturbatively path integral has to be used, which allows in principle to deal with every coupling regime.

The strong nonlinearity of the potential causes the energy levels below the barrier top to form doublets with large inter-doublet spacing with respect to the intra-doublet separation. As a consequence, if the temperature is much lower than the inter-doublet energy difference and the particle is initially in a superposition of the first two energy states, a description in terms of an effective two-level system is appropriate. This regime is experimentally attained, for example, in the superconducting qubits operating at temperature in the mK scale. The model describing the two-level system linearly coupled to the bosonic environment takes the name of *spin-boson* model [51]. The spin-boson model has been, and still is, extensively studied using a variety of techniques, including the path integral [9, 51] and related stochastic [54] and numerically exact methods [53, 92], or the numerical renormalization group [93, 94]. Present-day path integral approaches, based on suitable approximation schemes, are capable to investigate the spin-boson problem virtually in every regime of dissipation, corresponding to dynamical regimes ranging from the coherent regime to incoherent relaxation to equilibrium, both in the symmetric and the biased case.

However, if the initial condition involves higher energy levels or the temperature is of the order of the inter-doublet energy separation, the two-level system approximation is no more tenable. Considering the successive energy states entails the introduction of multiple dynamical time scales, due to the nonlinearity of the potential, as mentioned above. Moreover the description in terms of sum over paths, which, for a finite-dimensional Hilbert space, consists in sequences of transitions among localized states, gets dramatically more involved as the dimension of the problem exceeds two.

This is reflected by the fact that, up to now, investigations of multi-state dissipative

systems are confined to the opposite regimes of weak and strong coupling [69–71], describing coherent dynamics and incoherent relaxation. The crossover region, absent in the spin-boson problem, characterized by the simultaneous presence of long time incoherent relaxation associated to the tunneling and coherent oscillations at the level of the intra-well motion remained poorly understood.

In Chap. 3 of the present work the path integral approach was applied to the spin-boson problem, in its various approximation limits, covering the corresponding dissipation regimes. Specifically the non-interacting blip approximation (NIBA [9]), an approximation scheme which discards the time non-local interactions inside the double-paths of the reduced density matrix, was illustrated together with the weakly-interacting blip approximation (WIBA [59]) scheme, treating the time non-local interactions to the first order in the coupling and the local ones to all orders. Finally the weak coupling approximation (WCA [9, 62]) was introduced as a perturbative limit of the WIBA.

The techniques described for the spin-boson model were then applied to the so-called double-doublet system (DDS), the four level generalization of the two-level system, characterized by two well separated energy doublets, producing a rich dynamics which has three, well separated time scales. The crossover regime for the (DDS) is investigated using a novel approximation scheme which exploits the separation of the time scales of the system dynamics. In particular the NIBA scheme is applied to the tunneling dynamics and the WIBA to the intra-well motion (vibrational reaxation). The resulting novel scheme, called vibrational relaxation weakly-interacting blip approximation (VR-WIBA, outlined in Ref [61]) describes successfully the fast intra-well oscillations and the incoherent tunneling relaxation of the crossover regime. Moreover it reduces to the gNIBA (the multi-states generalization of the NIBA [72]) in the strong coupling limit. These path integral approximation schemes, in conjunction with the Bloch-Redifield (weak coupling) master equation approach, cover almost entirely the coupling-temperature parameter space of the problem and allowed for the realization of a phase space diagram in which the various dynamical regimes are described, together with the domain of applicability of the above mentioned approximation. The phase-space diagram for the DDS is the main result of Chap. 4.

The part of the parameter space of the DDS which remains outside the reach of the novel approximation scheme is that in which coherence is still present at the level of both the fast tunneling dynamics (involving the higher doublet) and intra-well motion, while the slow tunneling dynamics has turned into incoherent relaxation. In the corresponding dissipation regime the coupling is too strong to allow for weak coupling description (such as the Bloch-Redfield) and, on the other hand, is still too weak for the DDS to separate into a set of effective two-level systems to be treated within the NIBA or the WIBA. The difficulty in this case is not given by the intricate time non-local correlations introduced by the environment, but it is due to the fact that the so-called clusters (complicated path configurations) start to contribute, in the sum over the paths, as the coupling is weak or the temperature is low. Further investigations are needed to find a technique which fully exploits the approximations on the environmental influence on the path's amplitudes, without neglecting classes of intricate path configurations.

In Chap. 5 a systematic study of the multi-state dynamics (for an asymmetric eight-level system) in the presence of time dependent bias was performed. The interplay between a high-frequency driving and the dissipative environment in the strong coupling regime was illustrated using a Markov approximated master equation technique [72]. It was found that the resonant driving (of the order of the natural oscillation frequency of the wells)

increases the population of the metastable well at the stationary. A plot of the overall metastable well population at the stationary versus the driving amplitude and frequency shows several resonant peaks as a function of the driving frequency. Moreover the effect of increasing the coupling is to enhance the relaxation towards the lower well. Finally an increase of the temperature enhances the relaxation in the sense that the equilibrium configuration is reached within a shorter time.

In the second part of Chap. 5 a study on the escape problem in the strong coupling regime was carried out using the same analytical technique as that used in the first part of the chapter. The escape from a metastable well, starting from a nonequilibrium initial condition has been extensively investigated in the classical context [84–87], where the counterintuitive phenomenon of an enhacement of the lifetime of a metastable state at appropriate noise intensity occurs. This effect is called noise enhanced stability (NES). Considering the dynamics of the particle starting in a localized nonequilibrium state, in a strongly biased (static) potential, and introducing a suitable definition of escape time in the quantum context, we obtained a result which can be considered a quantum version of the NES. Specifically we found a non-monotonicity of the escape time with respect to both the damping strength (a peak followed by a rapid fall-off of the escape time at a critical damping strength) and the temperature (a resonant minimum). The finding that the environment can have a positive role in the enhancement of the lifetime of a metastable quantum state is the main result of Chap. 5.

The study of multi-state bistable systems in the general case of arbitrary bias and number of levels within the path integral technique is at present limited to the strong coupling regime. This is because, at low temperature/weak coupling the clusters start to contribute and the path integral becomes intractable, as already pointed out for the DDS. However in general, contrary to the DDS case, one cannot rely on a sharp separation of the time scales of the dynamics. For this reason it may be useful to find a weak coupling path integral scheme for the DDS, to be possibly suitable for further approximations or to be used for dealing with some other specific multi-state system in the weak or, at least, intermediate coupling regime.

Acknowledgments

Per avermi sempre sostenuto, grazie ai miei genitori Grazia e Maurizio e a mia sorella Laura.

Grazie a Claudio per la sua generosa e paziente amicizia e per essere stato un ottimo compagno di stanza, in Dipartimento, e di viaggio in giro per l'Italia e l'Europa.

In questi tre anni ho avuto la fortuna di conoscere persone meravigliose e di visitare città stupende. Grazie a Bratek e Maja per l'amicizia e per avermi ospitato nella loro incantata Cracovia. Grazie alle colleghe ed amiche Anna, Irina ed Ekaterina per le tante allegre gite e serate in giro.

Grazie alla Prof. Milena Grifoni per aver generosamente contribuito in modo determinante alla mia formazione e per avermi ospitato nella magnifica Ratisbona.

Un ringraziamento speciale al mio tutor, il Dott. Davide Valenti, per essere stato sempre presente e incondizionatamente disponibile ad aiutarmi in ogni problema scientifico o pratico incontrato nel corso del Dottorato e inoltre per avermi spronato e incoraggiato.

Grazie al Prof. Bernardo Spagnolo per avermi dato la possibilità di vivere tutte le bellissime esperienze, scientifiche ma anche umane, fatte durante il Dottorato e per avermi mostrato, attraverso l'esempio, l'umiltà e l'entusiasmo nella dedizione al lavoro.

Appendix A

Numerical scheme for the GME

The following numerical schemes are applied independently of the particular approximation used for the kernels of the generalized master equation.

GME for the TLS

We use a simple implicit scheme for integrating the GME for the population difference

$$\dot{P}(t) = \int_0^t dt' \left[K^{(+)}(t,t')P(t') + K^{(-)}(t,t') \right]. \tag{A.1}$$

We denote the time dependencies by discrete indexes: $P_i \equiv P(i\Delta t)$ and $K_{i,j} \equiv K(i\Delta t, j\Delta t)$. Using the forward finite difference for the derivative and the trapezoid rule for the integral, Eq. (A.1) becomes

$$\begin{aligned}\frac{1}{\Delta t}\left(P_{i+1} - P_i\right) =& \Delta t \sum_{j=1}^{i} \left[K^{(+)}_{i+1,j} P_j + K^{(-)}_{i+1,j} \right] \\ &+ \frac{\Delta t}{2} \left[K^{(+)}_{i+1,0} P_0 + K^{(-)}_{i+1,0} + K^{(+)}_{i+1,i+1} P_{i+1} + K^{(-)}_{i+1,i+1} \right],\end{aligned}$$

so that we can express the population difference at time $(i+1)\Delta t$ in terms of the same quantity at previous times

$$\begin{aligned}P_{i+1} = \left(1 - \frac{(\Delta t)^2}{2} K^{(+)}_{i+1,i+1}\right)^{-1} \Bigg[& P_i + \frac{(\Delta t)^2}{2} \left(K^{(+)}_{i+1,0} P_0 + K^{(-)}_{i+1,0} + K^{(-)}_{i+1,i+1} \right) \\ & + (\Delta t)^2 \sum_{j=1}^{i} \left(K^{(+)}_{i+1,j} P_j + K^{(-)}_{i+1,j} \right) \Bigg].\end{aligned}$$

GME for multi-state systems

We integrate the master equation for the populations of the M-state system ($M \geq 2$) using a generalization of the method employed for the TLS population difference. In this case however, the implicit method requires a matrix inversion at every time step. The master

equation reads

$$\dot{\rho}_{\mu,\mu}(t) = \sum_{\nu=1}^{M} \int_0^t dt' K_{\mu\nu}(t,t')\rho_{\nu\nu}(t').$$

Using vector notation

$$\dot{\vec{\rho}}(t) = \int_0^t dt' \mathbf{K}(t,t')\vec{\rho}(t'), \tag{A.2}$$

where $\mathbf{K}$ is the $M \times M$ kernel matrix and $\vec{\rho} = (\rho_{11}, \ldots, \rho_{MM})$ is the M-dimensional population vector.

As for the TLS, we use forward finite difference, trapezoid rule and discrete time indexes. Thus Eq. (A.2) becomes

$$\frac{1}{\Delta t}\left(\vec{\rho}_{i+1} - \vec{\rho}_i\right) = \Delta t \sum_{j=1}^{i} \mathbf{K}_{i+1,j}\vec{\rho}_j + \frac{\Delta t}{2}\left[\mathbf{K}_{i+1,0}\vec{\rho}_0 + \mathbf{K}_{i+1,i+1}\vec{\rho}_{i+1}\right],$$

The solution at time $(i+1)\Delta t$ in terms of the populations at previous times is

$$\vec{\rho}_{i+1} = \mathbf{M}_{i+1}^{-1}\vec{C}_i,$$

where

$$\mathbf{M}_{i+1} = \mathbf{1} - \frac{(\Delta t)^2}{2}\mathbf{K}_{i+1,i+1}$$

$$\vec{C}_i = \vec{\rho}_i + \frac{(\Delta t)^2}{2}\mathbf{K}_{i+1,0}\vec{\rho}_0 + (\Delta t)^2 \sum_{j=1}^{i} \mathbf{K}_{i+1,j}\vec{\rho}_j.$$

Appendix B

$n = 2$ influence functions

Exact $n = 2$ symmetric influence function

$$\begin{aligned}\sum_{\xi_1,\xi_2=\pm1} B_2^{(s)} F_2^{(+)} =& \exp(-S(\tau_1) - S(\tau_2)) \cos(X_{2,1}) \\ &\times \Big[\cosh(\Lambda_{2,1}) \cos(X_{1,0}) \cos(X_{2,0}) \cos(\epsilon\tau_1) \cos(\epsilon\tau_2) \\ &+ \sinh(\Lambda_{2,1}) \cos(X_{1,0}) \cos(X_{2,0}) \sin(\epsilon\tau_1) \sin(\epsilon\tau_2) \\ &+ \sinh(\Lambda_{2,1}) \sin(X_{1,0}) \sin(X_{2,0}) \cos(\epsilon\tau_1) \cos(\epsilon\tau_2) \\ &+ \cosh(\Lambda_{2,1}) \sin(X_{1,0}) \sin(X_{2,0}) \sin(\epsilon\tau_1) \sin(\epsilon\tau_2) \Big].\end{aligned}$$

Approximated form ($\Lambda_{2,1}$ and $X_{2,0}$ to first order in γ)

$$\begin{aligned}\sum_{\xi_1,\xi_2=\pm1} B_2^{(s)} F_2^{(+)} \simeq& \exp(-S(\tau_1) - S(\tau_2)) \cos(X_{2,1}) \\ &\times \Big[\cos(X_{1,0}) \cos(\epsilon\tau_1) \cos(\epsilon\tau_2) \\ &+ \Lambda_{2,1} \cos(X_{1,0}) \sin(\epsilon\tau_1) \sin(\epsilon\tau_2) \\ &+ X_{2,0} \sin(X_{1,0}) \sin(\epsilon\tau_1) \sin(\epsilon\tau_2) \Big].\end{aligned}$$

Irreducible approximated symmetric influence function

$$\begin{aligned}\sum_{\xi_1,\xi_2=\pm1} \tilde{B}_2^{(s)} \tilde{F}_2^{(+)} \simeq& \exp(-S(\tau_1) - S(\tau_2)) \cos(X_{2,1}) \\ &\times \Big[\Lambda_{2,1} \cos(X_{1,0}) \sin(\epsilon\tau_1) \sin(\epsilon\tau_2) \\ &+ X_{2,0} \sin(X_{1,0}) \sin(\epsilon\tau_1) \sin(\epsilon\tau_2) \Big].\end{aligned}$$

Exact $n = 2$ antisymmetric influence function

$$\begin{aligned}\sum_{\xi_1,\xi_2=\pm1} B_2^{(a)} F_2^{(-)} &= \exp(-S(\tau_1) - S(\tau_2)) \cos(X_{2,1}) \\ &\times \Big[\cosh(\Lambda_{2,1}) \sin(X_{1,0}) \cos(X_{2,0}) \sin(\epsilon\tau_1) \cos(\epsilon\tau_2) \\ &+ \cosh(\Lambda_{2,1}) \cos(X_{1,0}) \sin(X_{2,0}) \cos(\epsilon\tau_1) \sin(\epsilon\tau_2) \\ &- \sinh(\Lambda_{2,1}) \cos(X_{1,0}) \sin(X_{2,0}) \sin(\epsilon\tau_1) \cos(\epsilon\tau_2) \\ &- \sinh(\Lambda_{2,1}) \sin(X_{1,0}) \cos(X_{2,0}) \cos(\epsilon\tau_1) \sin(\epsilon\tau_2) \Big].\end{aligned}$$

Approximated form ($\Lambda_{2,1}$ and $X_{2,0}$ to first order in γ)

$$\begin{aligned}\sum_{\xi_1,\xi_2=\pm1} B_2^{(a)} F_2^{(-)} &\simeq \exp(-S(\tau_1) - S(\tau_2)) \cos(X_{2,1}) \\ &\times \Big[\sin(X_{1,0}) \sin(\epsilon\tau_1) \cos(\epsilon\tau_2) \\ &+ X_{2,0} \cos(X_{1,0}) \cos(\epsilon\tau_1) \sin(\epsilon\tau_2) \\ &- \Lambda_{2,1} \sin(X_{1,0}) \cos(\epsilon\tau_1) \sin(\epsilon\tau_2) \Big].\end{aligned}$$

Irreducible approximated antisymmetric influence function

$$\begin{aligned}\sum_{\xi_1,\xi_2=\pm1} \tilde{B}_2^{(s)} \tilde{F}_2^{(+)} &\simeq \exp(-S(\tau_1) - S(\tau_2)) \cos(X_{2,1}) \\ &\times \Big[X_{2,0} \cos(X_{1,0}) \cos(\epsilon\tau_1) \sin(\epsilon\tau_2) \\ &- \Lambda_{2,1} \sin(X_{1,0}) \cos(\epsilon\tau_1) \sin(\epsilon\tau_2) \Big].\end{aligned}$$

For $n > 2$ it is convenent to expand the $b - b$ and $b - s$ terms to the 1^{st} order in γ, then to get rid of all the possible reducible contributions and finally sum over the ξ's.

Appendix C

Propagator in Laplace space

First we give the expressions for the blip times τ and the sojourn times σ

$$\tau_j = t_{2j} - t_{2j-1}$$
$$\sigma_j = t_{2j+1} - t_{2j}.$$

The approximation on the paths made in Sec. 4.1.1 implies that, if $\rho(t_0) = |Q_j\rangle\langle Q_j|$, then each path contributing to the population $\rho_{kk}(t)$ has an even number $2n$ of transitions. Consider the series of integrals

$$\int_{t_0}^{t} dt_{2n} \int_{t_0}^{t_{2n}} dt_{2n-1} \dots \int_{t_0}^{t_3} dt_2 \int_{t_0}^{t_2} dt_1. \tag{C.1}$$

Using repeatedly the integral interchange rule

$$\int_{t_0}^{t_{j+1}} dt_j \int_{t_0}^{t_j} dt_{j-1} = \int_{t_0}^{t_{j+1}} dt_{j-1} \int_{t_{j-1}}^{t_{j+1}} dt_j, \tag{C.2}$$

we can put Eq. (C.1) in the form

$$\begin{aligned}
&\int_{t_0}^{t} dt_1 \int_{t_1}^{t} dt_2 \int_{t_2}^{t} dt_3 \dots \int_{t_{2n-2}}^{t} dt_{2n-1} \int_{t_{2n-1}}^{t} dt_{2n} \\
&\quad = \int_0^{\bar{t}} d\sigma_0 \int_0^{\bar{t}-\sigma_0} d\tau_1 \int_0^{\bar{t}-\tau_1-\sigma_0} d\sigma_1 \dots \\
&\qquad \times \int_0^{\bar{t}-\dots-\tau_{n-1}} d\sigma_{n-1} \int_0^{\bar{t}-\dots-\sigma_{n-1}} d\tau_n.
\end{aligned}$$

Notice that there is no integration over the last sojourn time, since it is fixed by the length of the interval $\bar{t} = t - t_0$.

In passing to the Laplace space we note that $\bar{t} = \sigma_n + \tau_n + \dots + \tau_1 + \sigma_0$. Using repeatedly the rule $\int_0^\infty dt \int_0^t dt' = \int_0^\infty dt' \int_{t'}^\infty dt$, we obtain

$$\begin{aligned}
&\mathcal{L}_{\bar{t}} \int_0^{\bar{t}} d\sigma_0 \dots \int_0^{\bar{t}-\dots-\sigma_{n-1}} d\tau_n \\
&\quad = \int_0^\infty d\bar{t} e^{-\lambda \bar{t}} \int_0^{\bar{t}} d\sigma_0 \dots \int_0^{\bar{t}-\dots-\sigma_{n-1}} d\tau_n \\
&\quad = \int_0^\infty d\sigma_n e^{-\lambda\sigma_n} \int_0^\infty d\tau_n e^{-\lambda\tau_n} \dots \int_0^\infty d\sigma_0 e^{-\lambda\sigma_0}.
\end{aligned} \tag{C.3}$$

Suppose that a path of the DDS with $2n$ transitions starts in the diagonal state (q_0, q_0) and ends in the diagonal state (q, q). Suppose moreover that the path changes sublattice M times. Specifically it passes from (q_0, q_0) to (q_1, q_1) making $2k_1$ transitions in the first sublattice, then passes from (q_1, q_1) to (q_2, q_2) making $2k_2$ transitions in the second sublattice and so on, with $n = \sum_{j=1}^{N} k_j$. Notice that the starting and arrival sites of the sub-paths need not to be different. Due to the approximations made in Sec. 4.1, the amplitude A for this path factorizes as

$$A(\tau_1, \sigma_1 \ldots, \sigma_{n-1}, \tau_n) = \prod_{j=1}^{M} A_j(\tau_1^j, \sigma_1^j, \ldots, \sigma_{k_j-1}^j, \tau_{k_j}^j).$$

Here τ_i^j (σ_i^j) is the i-th blip (sojourn) in the j-th sublattice (see Fig. 4.4 and 4.5). Therefore the Laplace transform of the multiple integral of the amplitude A is

$$\mathcal{L}_{\bar{t}} \int_0^{\bar{t}} d\sigma_0 \ldots \int_0^{\bar{t}-\cdots-\sigma_{n-1}} d\tau_n A(\tau_1, \ldots, \tau_n) = \frac{1}{\lambda} \prod_{j=1}^{M} \frac{\hat{f}_j(\lambda)}{\lambda}, \tag{C.4}$$

where

$$\begin{aligned} \frac{\hat{f}_j(\lambda)}{\lambda} =& \int_0^{\infty} d\tau_{k_j}^j e^{-\lambda \tau_{k_j}^j} \ldots \int_0^{\infty} d\sigma_0^j e^{-\lambda \sigma_0^j} A_j(\tau_1^j, \ldots, \tau_{k_j}^j) \\ =& \mathcal{L}_T \int_0^{T} d\tau_1^j \ldots \int_0^{T-\cdots-\sigma_{k_j-1}^j} d\tau_{k_j}^j A_j(\tau_1^j, \ldots, \tau_{k_j}^j), \end{aligned}$$

with σ_0^j playing the role of σ_n in Eq. (C.3): the integral over the sojourn times results in the $1/\lambda$ factors because none of the amplitudes depend on the initial or final sojourn time.

The full propagator from (q_0, q_0) to (q, q) is the sum over the paths

$$G(q, q, t; q_0, q_0, t_0) = \delta_{qq_0} + \sum_{n=1}^{\infty} \int_{t_0}^{t} \mathcal{D}_{2n}\{t_j\} A(t_0, \ldots, t). \tag{C.5}$$

Exploiting the factorization of the amplitudes in this sum and extending the reasoning made above for a single amplitude, the Laplace transform of the propagator is

$$G(q, q; q_0, q_0; \lambda) = \frac{\delta_{qq_0}}{\lambda} + \frac{1}{\lambda} \sum_{M=1}^{\infty} \sum_{\{q_j\}=Q_1}^{Q_4} \prod_{j=1}^{M} \frac{\hat{K}_{q_{j-1}q_j}(\lambda)}{\lambda} \tag{C.6}$$

where, if $q_j \neq q_{j-1}$, the function $\hat{K}_{q_{j-1}q_j}(\lambda)$ is the Laplace transform of

$$\begin{aligned} K_{j,j-1}(t - t') =& \sum_{k_j=1}^{\infty} \int_{t'}^{t} dt_{2k_j-1} \ldots \int_{t'}^{t} dt_2 \\ & \times \sum_{\text{paths}_{2k_j}} A_j^{q_{j-1}, q_j}(t, t_{2k_j-1} \ldots, t'). \end{aligned}$$

This, in turn, is the kernel that connects the populations of the states $|q_{j-1}\rangle$ and $|q_j\rangle$ in the integro-differential equation [9, 60]

$$\dot{\rho}_{q_j q_j}(t) = \sum_{l=q_{j-1}}^{q_j} \int_{t_0}^{t_{2k}} dt_1 K_{q_j, l}(t - t') \rho_{ll}(t')$$

for the populations of the TLS $\{|q_{j-1}\rangle, |q_j\rangle\}$ corresponding to the j-th sublattice $\{q_{j-1}, q_j\}$.

Appendix D

Bloch-Redfield master equation

The energy representation of the DDS is given by the four energy eigenstates $|\mu\rangle$ satisfying the equations

$$\hat{H}_S|n\rangle = \hbar\omega_n|n\rangle \qquad (n = 1, \ldots, 4).$$

We define

$$\omega_{nm} = \omega_n - \omega_m \qquad \text{and} \qquad q_{nm} = \langle n|\hat{q}|m\rangle.$$

In the energy representation, to the first order in the coupling and under the assumption that the memory time of the bath is short compared to the characteristic times in the evolution of the density matrix (Markov approximation), the following master equation can be derived [52] from the microscopical model given in Sec. 1.2

$$\dot{\rho}^E_{nm}(t) = -i\omega_{nm}\rho^E_{nm}(t) + \sum_{k,l} \mathcal{L}_{nm,kl}\rho^E_{kl}(t). \tag{D.1}$$

This is the *Bloch-Redfield master equation*. The Bloch-Redfield tensor is

$$\begin{aligned}\mathcal{L}_{nm,kl} = {} & q_{nk}\left(Q_{lm} + P_{lm}\right) + q_{lm}\left(Q_{nk} - P_{nk}\right) \\ & - \sum_j \left[\delta_{kn}q_{jm}\left(Q_{lj} + P_{lj}\right) + \delta_{lm}q_{nj}\left(Q_{jk} - P_{jk}\right)\right]\end{aligned} \tag{D.2}$$

where

$$\begin{aligned}Q_{nm} = q_{nm}\int_0^\infty d\tau \int_0^\infty d\omega \frac{J(\omega)}{\pi\hbar} \\ \times \coth\left(\frac{\beta\hbar\omega}{2}\right)\cos(\omega\tau)e^{-i\omega_{nm}\tau}\end{aligned} \tag{D.3}$$

and

$$P_{nm} = q_{nm}\omega_{nm}\int_0^\infty d\tau \int_0^\infty d\omega \frac{J(\omega)}{\omega\pi\hbar}\cos(\omega\tau)e^{-i\omega_{nm}\tau}. \tag{D.4}$$

To perform the integral over τ we use

$$\int_0^\infty d\tau e^{i\tilde{\omega}\tau} = \pi\delta(\tilde{\omega}) + i\mathcal{P}\frac{1}{\tilde{\omega}}. \tag{D.5}$$

Neglecting the principal value, which gives a frequency shift, we have

$$Q_{nm} = q_{nm}\frac{J(|\omega_{nm}|)}{2\hbar}\coth\left(\frac{\beta\hbar|\omega_{nm}|}{2}\right) \tag{D.6}$$

and

$$P_{nm} = \frac{q_{nm}\omega_{nm}}{2\hbar}\frac{J(|\omega_{nm}|)}{|\omega_{nm}|}. \tag{D.7}$$

We notice that for $\omega_{nm} > 0$

$$Q_{nm} - P_{nm} = Q_{mn} + P_{mn} = q_{nm}\frac{J(|\omega_{nm}|)}{\hbar}n_\beta(\omega_{nm})$$

while, for $\omega_{nm} < 0$,

$$Q_{nm} - P_{nm} = Q_{mn} + P_{mn} = q_{nm}\frac{J(|\omega_{nm}|)}{\hbar}\left(n_\beta(|\omega_{nm}|) + 1\right).$$

Here $n_\beta(\omega_{nm})$ is the expectation value of the number of bath excitations of energy $\hbar\omega_{nm}$ at temperature $T = (k_B\beta)^{-1}$.

Analytic solution in the full secular approximation

Setting $\rho^E_{nm}(t) = e^{-i\omega_{nm}(t-t_0)}\sigma_{nm}(t)$, Eq. (D.1) becomes

$$\dot{\sigma}_{nm}(t) = \sum_{kl}\mathcal{L}_{nm,kl}\Omega_{nm,kl}(t)\sigma_{kl}(t), \tag{D.8}$$

where $\Omega_{nm,kl}(t) = \exp\left[i(\omega_{nm} - \omega_{kl})(t - t_0)\right]$. We have $\sigma(t_0) = \rho(t_0)$.

The *full secular approximation* (FSA) consists in neglecting the terms in the master equation for which $\omega_{\mu\nu} - \omega_{\kappa\lambda} \neq 0$. Mathematically this condition reads

$$\Omega_{\mu\nu\kappa\lambda}(t) \to \left(\delta_{\kappa\mu}\delta_{\lambda\nu} + \delta_{\kappa\lambda}\delta_{\mu\nu}\right)\Omega_{\mu\nu\kappa\lambda}(t).$$

In the FSA the equations for the diagonal elements decouple from those for the non-diagonal elements of σ.

Specifically, the dynamics of $\sigma(t)$ is given by a master equation for the diagonal elements and a set of independent equations for the *non-diagonal* elements. The master equation for the diagonal elements reads

$$\dot{\sigma}_{nn}(t) = \sum_{k}\mathcal{L}_{nn,kk}\sigma_{kk}(t), \tag{D.9}$$

where, for $n \neq k$,

$$\mathcal{L}_{nn,kk} = q_{nk}\left(Q_{kn} + P_{km}\right) + q_{kn}\left(Q_{nk} - P_{nk}\right)$$

and $\mathcal{L}_{n,n} = -\sum_k \mathcal{L}_{k,n}$.

The solution of Eq. (D.9) is

$$\sigma_{nn}(t) = \sum_{ij} S_{ni}e^{\lambda_i(t-t_0)}(S^{-1})_{ij}\sigma_{jj}(t_0),$$

where S is the transformation that diagonalizes the matrix $L_{nk} = \mathcal{L}_{nn,kk}$ and λ_i are the eigenvalues. From the definition of $\sigma(t)$ we have $\rho^E_{nn}(t) = \sigma_{nn}(t)$.

The uncoupled equations for the non-diagonal elements of $\sigma(t)$ are

$$\dot{\sigma}_{nm}(t) = -\mathcal{L}_{nm,nm}\sigma_{nm}(t) \tag{D.10}$$

with

$$\begin{aligned}\mathcal{L}_{nm,nm} =&(q_{nn} - q_{mm})\left[Q_{nn} - P_{nn} - (Q_{mm} + P_{mm})\right] \\ &+ \sum_{j\neq m} q_{jm}(Q_{mj} + P_{mj}) + \sum_{j\neq n} q_{nj}(Q_{jn} - P_{jn}).\end{aligned}$$

In our specific problem, due to the symmetry of the potential, the diagonal matrix elements q_{ii} of the position operator in the energy representation vanish.

The solutions of Eq. (D.10) are

$$\sigma_{nm}(t) = e^{-\mathcal{L}_{nm,nm}(t-t_0)}\sigma_{nm}(t_0),$$

so that the non-diagonal elements of the density matrix in the energy representation are

$$\rho^E_{nm}(t) = e^{-i\omega_{nm}(t-t_0)}e^{-\mathcal{L}_{nm,nm}(t-t_0)}\rho^E_{nm}(t_0).$$

Once the solution for $\rho(t)$ in the energy basis $\{|n\rangle\}$ is known, to pass to the DVR basis $\{|q_j\rangle\}$ it is sufficient to perform the transformation

$$\rho^{DVR}_{nm}(t) = \sum_{ij} T_{ni}\rho^E_{ij}(t)T^\dagger_{jm},$$

where $T_{ij} = \langle i|q_j\rangle$.

Appendix E

VR-WIBA kernels

The gNIBA kernels connecting the populations of the states $|q_k\rangle$ and $|q_j\rangle$ in Eq. (4.17) are the modified versions of the TLS NIBA kernels

$$K_{kj}^{gN}(t) = 2\Delta_{kj}^2 e^{-q_{kj}^2 Q'(t)} \cos\left(\epsilon_{kj} t + q_{kj}^2 Q''(t)\right) \tag{E.1}$$

where

$$\begin{aligned}
\Delta_{kj} &= \frac{1}{\hbar}\langle q_k|\hat{H}_S|q_j\rangle \\
\epsilon_{kj} &= \frac{1}{\hbar}\left(\langle q_k|\hat{H}_S|q_k\rangle - \langle q_j|\hat{H}_S|q_j\rangle\right) \\
q_{kj}^2 &= (q_k - q_j)^2.
\end{aligned}$$

In the VR-WIBA scheme we use these expressions only if q_k and q_j belong to different wells.

If q_k and q_j belong to the same well, we use the modified TLS WIBA kernels (see Ref. [59]) $K_{kj}^{VRW}(t) = K_{kj}^{gN}(t) + K_{kj}^{BgN}(t)$. The beyond-gNIBA correction is

$$\begin{aligned}
K_{kj}^{BgN}(t) =& 8\Delta_{kj}^4 \int_0^t d\tau \int_0^{t-\tau} d\tau' e^{-q_{kj}^2 Q'(\tau) - q_{kj}^2 Q'(\tau')} \\
&\times \sin(\epsilon_{kj}\tau') \cos(q_{kj}^2 Q''(\tau')) p_{kj}(t-\tau-\tau') \\
&\times [q_{kj}^2 X(t,\tau') \cos(\epsilon_{kj}\tau + q_{kj}^2 Q''(\tau)) \\
&- q_{kj}^2 \Lambda(t,\tau',\tau) \sin(\epsilon_{kj}\tau + q_{kj}^2 Q''(\tau))],
\end{aligned} \tag{E.2}$$

where

$$\Lambda(t,\tau',\tau) = Q'(t) + Q'(t-\tau'-\tau) - Q'(t-\tau) - Q'(t-\tau')$$

and

$$X(t,\tau') = Q''(t) - Q''(t-\tau').$$

In the calculations the function $Q'(t)$ and $Q''(t)$ are taken in the form of Eq. (2.62).

The functions p_{kj} obey the equations

$$\dot{p}_{kj}(t) = \int_0^t dt' K_{kj}^{N,(+)}(t-t') p_{kj}(t')$$

with initial condition $p_{kj}(0) = 1$ and kernel

$$K_{kj}^{N,(+)}(\tau) = -4\Delta_{kj}^2 e^{-q_{kj}^2 Q'(\tau)} \cos(\epsilon_{kj}\tau) \cos(q_{kj}^2 Q''(\tau)).$$

Note that, by the symmetry of the problem, the four functions p_{12}, p_{21}, p_{34} and p_{43} are the same for the symmetric DDS.

Bibliography

[1] C. W. Gardiner, *Handbook of stochastic methods for Physics, Chemistry, and the Natural Sciences* (Springer, 2004, 3rd Ed.).

[2] J. Preskill, "Lecture notes for ph219/cs219: Quantum information and computation chapter 2," http://www.theory.caltech.edu/~preskill/ph219/chap2_13.pdf, accessed: 2014-11-28.

[3] W. H. Zurek, Phys. Rev. D **24**, 1516 (1981).

[4] W. H. Zurek, S. Habib, and J. P. Paz, Phys. Rev. Lett. **70**, 1187 (1993).

[5] W. H. Zurek, Rev. Mod. Phys. **75**, 715 (2003).

[6] M. A. Schlosshauer, *Decoherence: and the quantum-to-classical transition* (Springer, 2007).

[7] T. Dittrich, P. Hänggi, G.-L. Ingold, B. Kramer, G. Schön, and W. Zwerger, *Quantum transport and dissipation*, Vol. 3 (Wiley-Vch Weinheim, 1998).

[8] P. Hänggi and G.-L. Ingold, Chaos **15** (2005).

[9] U. Weiss, *Quantum Dissipative Systems* (World Scientific, Singapore, 2012, 4th Ed.).

[10] M. A. Nielsen and I. L. Chuang, *Quantum computation and quantum information* (Cambridge university press, 2010).

[11] G. Falci and E. Paladino, Int. J. Quantum Inf. **12**, 1430003 (2014).

[12] P. W. Shor, in *Foundations of Computer Science, 1994 Proceedings., 35th Annual Symposium on* (IEEE, 1994) pp. 124–134.

[13] D. P. DiVincenzo, Science **270**, 255 (1995).

[14] T. D. Ladd *et al.*, Nature **464**, 45 (2010).

[15] N. A. Gershenfeld and I. L. Chuang, Science **275**, 350 (1997).

[16] C. Negrevergne *et al.*, Phys. Rev. Lett. **96**, 170501 (2006).

[17] M. Steffen *et al.*, IBM J. Res. & Dev. **55**, 13 (2011).

[18] R. Blatt and D. Wineland, Nature **453**, 1008 (2008).

[19] D. Loss and D. P. DiVincenzo, Phys. Rev. A **57**, 120 (1998).

[20] J. M. Raimond, M. Brune, and S. Haroche, Rev. Mod. Phys. **73**, 565 (2001).

[21] E. Knill, R. Laflamme, and G. J. Milburn, Nature **409**, 46 (2001).

[22] L. B. Ioffe *et al.*, Nature **398**, 679 (1999).

[23] J. Mooij *et al.*, Science **285**, 1036 (1999).

[24] Y. Nakamura, Y. Pashkin, and J. Tsai, Nature **398**, 786 (1999).

[25] C. Van der Wal *et al.*, Science **290**, 773 (2000).

[26] J. Friedman, V. Patel, W. Chen, S. Tolpygo, and J. Lukens, Nature **406**, 43 (2000).

[27] D. Vion *et al.*, Science **296**, 886 (2002).

[28] J. M. Martinis, S. Nam, J. Aumentado, and C. Urbina, Phys. Rev. Lett. **89**, 117901 (2002).

[29] J. Clarke and F. K. Wilhelm, Nature **453**, 1031 (2008).

[30] M. H. Devoret and R. J. Schoelkopf, Science **339**, 1169 (2013).

[31] J. You and F. Nori, Nature **474**, 589 (2011).

[32] G. Ithier *et al.*, Phys. Rev. B **72**, 134519 (2005).

[33] E. Paladino, Y. M. Galperin, G. Falci, and B. L. Altshuler, Rev. Mod. Phys. **86**, 361 (2014).

[34] L. Thomas *et al.*, Nature **383**, 145 (1996).

[35] G. Christou, D. Gatteschi, D. N. Hendrickson, and R. Sessoli, Mrs Bulletin **25**, 66 (2000).

[36] J. R. Friedman and M. P. Sarachik, Annu. Rev. Condens. Matter Phys. **1**, 109 (2010).

[37] M. N. Leuenberger and D. Loss, Nature **410**, 789 (2001).

[38] L. Bogani and W. Wernsdorfer, Nature materials **7**, 179 (2008).

[39] S. Takahashi *et al.*, Phys. Rev. Lett. **102**, 087603 (2009).

[40] A. O. Caldeira and A. J. Leggett, Phys. Rev. Lett. **46**, 211 (1981).

[41] A. O. Caldeira and A. J. Leggett, Physica A **121**, 587 (1983).

[42] H. P. Breuer and F. Petruccione, *The theory of open quantum systems* (Oxford University Press, 2002).

[43] H. Grabert, P. Olschowski, and U. Weiss, Phys. Rev. B **36**, 1931 (1987).

[44] H. Grabert, P. Schramm, and G.-L. Ingold, Phys. Rep. **168**, 115 (1988).

[45] H. Carmichael, *An open systems approach to Quantum Optics*, Vol. 18 (Springer, 1993).

[46] A. Altland and B. D. Simons, *Condensed matter field theory* (Cambridge University Press, 2010).

[47] T. Brandes, "Lecture notes: Statistische mechanik 1 - computergestützte methoden," http://www.itp.tu-berlin.de/menue/lehre/lv/ss_2007/wahlpflichtveranstaltungen/stat-i-ss070/, accessed: 2014-12-05.

[48] J. Hausinger, *Quantum Dissipation in Flux Qubits*, Master thesis, Universität Regensburg (2007).

[49] L. S. Schulman, *Techniques and Applications of Path Integration* (Wiley, 1981).

[50] L. Magazzù, D. Valenti, B. Spagnolo, and M. Grifoni, arXiv:1412.7467v1 (2014).

[51] A. J. Leggett *et al.*, Rev. Mod. Phys. **59**, 1 (1987).

[52] K. Blum, *Density matrix theory and applications*, Vol. 64 (Springer, 2012).

[53] N. Makri and D. Makarov, J. Chem. Phys. **102**, 4600 (1995).

[54] J. T. Stockburger and H. Grabert, Phys. Rev. Lett. **88**, 170407 (2002).

[55] W. Koch, F. Großmann, J. T. Stockburger, and J. Ankerhold, Phys. Rev. Lett. **100**, 230402 (2008).

[56] P. P. Orth, A. Imambekov, and K. Le Hur, Phys. Rev. B **87**, 014305 (2013).

[57] R. P. Feynman and F. Vernon Jr, Ann. Phys. **24**, 118 (1963).

[58] R. Görlich, M. Sassetti, and U. Weiss, EPL (Europhysics Letters) **10**, 507 (1989).

[59] F. Nesi, E. Paladino, M. Thorwart, and M. Grifoni, Phys. Rev. B **76**, 155323 (2007).

[60] M. Grifoni, M. Sassetti, and U. Weiss, Phys. Rev. E **53**, R2033 (1996).

[61] F. Nesi, *Characterization of a qubit in presence of dissipation and external driving*, Phd thesis, Universität Regensburg (2007).

[62] L. Hartmann, I. Goychuk, M. Grifoni, and P. Hänggi, Phys. Rev. E **61**, R4687 (2000).

[63] U. Weiss and M. Wollensak, Phys. Rev. Lett. **62**, 1663 (1989).

[64] A. Leggett *et al.*, Rev. Mod. Phys. **67**, 725 (1995).

[65] H. Dekker, Physica A: Statistical Mechanics and its Applications **175**, 485 (1991).

[66] H. Dekker, Physica A: Statistical Mechanics and its Applications **176**, 220 (1991).

[67] H. Dekker, Physica A: Statistical Mechanics and its Applications **179**, 81 (1991).

[68] R. I. Cukier, M. Morillo, K. Chun, and N. O. Birge, Phys. Rev. B **51**, 13767 (1995).

[69] M. Morillo, C. Denk, and R. Cukier, Chem. Phys **212**, 157 (1996), rate Processes with Kinetic Parameters Distributed over Time and Space.

[70] R. Cukier, C. Denk, and M. Morillo, Chem. Phys **217**, 179 (1997), dynamics of Driven Quantum Systems.

[71] M. Thorwart, M. Grifoni, and P. Hänggi, Phys. Rev. Lett. **85**, 860 (2000).

[72] M. Thorwart, M. Grifoni, and P. Hänggi, Ann. Phys. **293**, 15 (2001).

[73] D. E. Makarov and N. Makri, Phys. Rev. B **52**, R2257 (1995).

[74] L. Magazzù, D. Valenti, P. Caldara, A. La Cognata, B. Spagnolo, and G. Falci, Acta Phys. Pol. B **44**, 1185 (2013).

[75] D. Kast and J. Ankerhold, Phys. Rev. Lett. **110**, 010402 (2013).

[76] S. Bera *et al.*, Phys. Rev. B **89**, 121108 (2014).

[77] M. Grifoni and P. Hänggi, Physics Reports **304**, 229 (1998).

[78] D. Gatteschi and R. Sessoli, Angew. Chem. Int. Ed. **42**, 268 (2003).

[79] H. Naundorf, K. Sundermann, and O. Kühn, Chem. Phys **240**, 163 (1999).

[80] I. Affleck, Phys. Rev. Lett. **46**, 388 (1981).

[81] V. Sargsyan, Y. Palchikov, Z. Kanokov, G. Adamian, and N. Antonenko, Phys. Rev. A **75**, 062115 (2007).

[82] C.-L. Ho and C.-C. Lee, Phys. Rev. A **71**, 012102 (2005).

[83] A. Shit, S. Chattopadhyay, and J. R. Chaudhuri, The Journal of Physical Chemistry A **117**, 8576 (2013).

[84] R. Mantegna and B. Spagnolo, Phys. Rev. Lett. **76**, 563 (1996).

[85] N. Agudov and B. Spagnolo, Phys. Rev. E **64**, 035102 (2001).

[86] A. Dubkov, N. Agudov, and B. Spagnolo, Phys. Rev. E **69**, 061103 (2004).

[87] A. Fiasconaro, B. Spagnolo, and S. Boccaletti, Phys. Rev. E **72**, 061110 (2005).

[88] F. Chiarello, E. Paladino, M. G. Castellano, C. Cosmelli, A. D'Arrigo, G. Torrioli, and G. Falci, New Journal of Physics **14**, 023031 (2012).

[89] P. Facchi *et al.*, Phys. Rev. A **71**, 022302 (2005).

[90] J. R. Friedman, M. P. Sarachik, J. Tejada, and R. Ziolo, Phys. Rev. Lett. **76**, 3830 (1996).

[91] P. Korda, M. Taylor, and D. Grier, Phys. Rev. Lett. **89**, 128301 (2002).

[92] D. Makarov and N. Makri, Chem. Phys. Lett. **221**, 482 (1994).

[93] R. Bulla, N.-H. Tong, and M. Vojta, Phys. Rev. Lett. **91**, 170601 (2003).

[94] R. Bulla, T. Costi, and T. Pruschke, Rev. Mod. Phys. **80**, 395 (2008).